THE ROLE OF TUNDRA VEGETATION IN THE ARCTIC WATER CYCLE

By

Jason A. Clark, B.A., M.S.

A Dissertation Submitted in Partial Fulfillment of the Requirements

for the Degree of

Doctor of Philosophy

in

Ecology: Interdisciplinary Program

University of Alaska Fairbanks

December 2019

APPROVED:

Ken Tape, Committee Chair
William Schnabel, Committee Member
Eugénie Euskirchen, Committee Member
Roger Ruess, Committee Member
Robert Perkins, Chair
Department of Civil and Environmental Engineering
William Schnabel, Dean
College of Engineering and Mines
Michael Castellini, *Interim Dean of the Graduate School*

Abstract

Vegetation plays many roles in arctic ecosystems, and the role of vegetation in linking the terrestrial system to the atmosphere through evapotranspiration is likely important. Through the acquisition and use of water, vegetation cycles water back to the atmosphere and modifies the local environment. Evapotranspiration is the collective term used to describe the transfer of water from vascular plants (transpiration) and non-vascular plants and surfaces (evaporation) to the atmosphere. Evapotranspiration is known to return large portions of the annual precipitation back to the atmosphere, and it is thus a major component of the terrestrial arctic hydrologic budget. However, the relative contributions of dominant arctic vegetation types to total evapotranspiration is unknown. This dissertation addresses the role of vegetation in the tundra water cycle in three chapters: (1) woody shrub stem water content and storage, (2) woody shrub transpiration, and (3) partitioning ecosystem evapotranspiration into major vegetation components. In Chapter 1 I present a method to continuously monitor arctic shrub water content. The water content of three species (*Salix alaxensis*, *Salix pulchra*, *Betula nana*) was measured over two years to quantify seasonal patterns of stem water content. I found that spring uptake of snowmelt water and stem water storage was minimal relative to the precipitation and evapotranspiration water fluxes. In Chapter 2, I focused on water fluxes by measuring shrub transpiration at two contrasting sites in the arctic tundra of northern Alaska to provide a fundamental understanding of water and energy fluxes. The two sites contrasted moist acidic shrub tundra with a riparian tall shrub community having greater shrub density and biomass. The much greater total shrub transpiration at the riparian site reflected the 12-fold difference in leaf area between the sites. I developed a statistical model using vapor pressure deficit, net radiation, and leaf area, which explained >80% of the variation in hourly shrub transpiration. Transpiration was approximately 10% of summer evapotranspiration in the tundra shrub community and a possible majority of summer evapotranspiration in the riparian shrub community. At the tundra shrub site, the other plant species in that watershed apparently accounted for a much larger proportion of evapotranspiration than the measured shrubs. In Chapter 3, I therefore measured partitioned evapotranspiration from dominant vegetation types in a small arctic watershed. I used weighing micro-lysimeters to isolate evapotranspiration contributions from moss, sedge tussocks, and mixed vascular plant assemblages. I found that mosses and sedge tussocks are the major constituents of overall evapotranspiration, with the

mixed vascular plants making up a minor component. The potential shrub transpiration contribution to overall evapotranspiration covers a huge range and depends on leaf area. Predicted increases in shrub abundance and biomass due to climate change are likely to alter components of the arctic hydrologic budget. The thermal and hydraulic properties of the moss and organic layer regulate energy fluxes, permafrost stability, and future hydrologic function in the arctic tundra. Shifts in the composition and cover of mosses and vascular plants will not only alter tundra evapotranspiration dynamics, but will also affect the significant role that mosses, their thick organic layers, and vascular plants play in the thermodynamics of arctic soils and in the resilience of permafrost.

Table of Contents

Page

Abstract iii

Table of Contents v

List of Figures vii

List of Tables viii

Acknowledgements x

General Introduction 1

References 5

Chapter 1: Deciduous Shrub Stem Water Storage in Arctic Alaska 7

1.1 Abstract 7

1.2 Introduction 7

1.3 Methods 8

1.4 Results 13

1.5 Discussion 17

1.6 References 19

Chapter 2: Transpiration and Environmental Controls in Arctic Tundra Shrub Communities 21

2.1 Abstract 21

2.2 Introduction 21

2.3 Methods 23

2.4 Results 28

2.5 Discussion 38

2.6 Conclusion 45

2.7 References 46

Chapter 3: Weighing Micro-Lysimeters Used to Quantify Dominant Vegetation Contributions to Evapotranspiration in the Arctic 58

3.1 Abstract 58

3.2 Introduction 59

3.3 Methods 61

3.4 Results 67

3.5 Discussion 71
3.6 References 79
General Conclusion 86
References 89

List of Figures

Page

Figure 0.1: Conceptual diagram of Arctic water pools and measurement of shrub stem water content (S) using time-domain reflectometry (TDR) 2

Figure 0.2: Conceptual diagram of Arctic water fluxes (evapotranspiration) from dominant vegetation types including lysimeter and sap flow measurement methods 4

Figure 1.1: Installation of TDR probe on shrub stem for stem water content measurement using a small saw to create grooves in the stem (a) and using silicone tape to hold stainless steel TDR probes in place (b) 9

Figure 1.2: Example TDR waveform (black line) and its first derivative (red line) showing water content induced change in signal impedance, and points (P1, P2, P3) for calculating apparent probe length (*La*) and dielectric constant (*Ka*) 10

Figure 1.3: Location of study sites (a) in arctic Alaska, USA, and photographs showing vegetation at the tundra shrub site (b: 68.62°N, 149.32°W) and riparian shrub site (c: 68.47°N, 149.55°W) 12

Figure 1.4: Example shrub stem drying curve and corresponding measures of dielectric constant used for calibrating VWC to TDR measurements 14

Figure 1.5: Calibration lines for each of the three shrub species 15

Figure 1.6: Air temperature, leaf area index, precipitation, soil moisture and stem moisture for the riparian and tundra site for 2016 and 2017 16

Figure 1.7: Estimated shrub stem water storage for riparian and tundra shrubs 17

Figure 2.1: Location of study sites (a) in arctic Alaska, USA, and photographs showing vegetation at the tundra shrub site (b: 68.62°N, 149.32°W) and riparian shrub site (c: 68.47°N, 149.55°W) 24

Figure 2.2: Daily meteorology and leaf area index (LAI) from riparian shrub and tundra shrub sites for 2016 and 2017 30

Figure 2.3: Daily soil moisture (% volumetric water content) and temperature data from riparian shrub and tundra shrub sites for 2016 and 2017 32

Figure 2.4: Daily shrub transpiration from the (a) riparian shrub and (b) tundra shrub site for 2016 and 2017 33
Figure 2.5: One-week subset of hourly (a) sap flow (F), (b) vapor pressure deficit (D), and (c) net radiation (Rn) data from the riparian shrub site and tundra shrub site 35
Figure 2.6: Observed T and predicted $\hat{T}$ rate from model for (a) riparian shrub in 2016, (b) tundra shrub in 2016, (c) riparian shrub in 2017, and (d) tundra shrub in 2017 37
Figure 2.7: Parameters for shrub transpiration model at (a) the riparian shrub site and (b) the tundra shrub site for each time period 38
Figure 2.8: Comparison of ET measurements for Imnavait Creek watershed (Euskirchen et al., 2012; Kane et al., 2004) and sap flow derived T from woody shrubs (this study) 40
Figure 2.9: Sensitivity of predicted $\hat{T}$ to covariates (D, Rn, LA) for the riparian shrub site in 2017 42
Figure 2.10: Sensitivity of predicted $\hat{T}$ to covariates (D, Rn, LA) for the tundra shrub site in 2017 43
Figure 3.1: Alaska and inset map of spatial distribution of lysimeters in Imnaviat Research Watershed 61
Figure 3.2: Micro-lysimeters with mixed tundra vegetation (a) and moss only (b) 62
Figure 3.3: (a) Schematic of micro-lysimeter (not to scale) 63
Figure 3.4: Example of AWAT filter applied to lysimeter data for period of strong ET (a), 16mm rain event (b), and strong wind period (c; mean wind speed: 6.8m/s) 68
Figure 3.5: Examples of lysimeters recording (a) a daytime evapotranspiration event, and (b) a precipitation event 69
Figure 3.6: Boxplot of hourly ET rates by month 70
Figure 3.7: Average cumulative ET (solid lines) and P (dashed lines) recorded on lysimeters (n=54) by vegetation type (colors) 71
Figure 3.8: Comparison of summer (June, July, August) ET measurements for Imnavait Creek watershed (Euskirchen et al., 2012; Kane et al., 2004, Ch. 2) and lysimeter-derived ET (this study, denoted by *) 72

Figure 4.1: Conceptual diagram depicting findings of this dissertation and measurement methods. 87

List of Tables

Page

Table 1.1: Shrub stem density and stem water storage 17
Table 2.1: Environmental variables (mean and SD) for the riparian and tundra shrub sites in 2017 summer (June-August) 55
Table 2.2: Summary of measured sap flow for the riparian and tundra shrub sites in 2016 and 2017 55
Table 2.3: Riparian shrub model parameter estimates 56
Table 2.4: Tundra shrub model parameter estimates 56
Table 2.5: Summer (June-August) environmental variable means by season (early, mid, late) 57
Table 3.1: AWAT filter parameters 77
Table 3.2: Lysimeter ET components, recording period, hourly rates, and seasonal total ET 77
Table 3.3: Rain gauge and lysimeter recording period, measured P and accuracy 78

Acknowledgments

I acknowledge financial support for this dissertation from the National Science Foundation (NSF Arctic Natural Sciences award number 1418123). Additional financial support was provided by a fellowship from the Graduate School of the University of Alaska and the National Institutes of Water Research. My committee provided academic support and provided valuable comments. I am deeply appreciative of the supportive and helpful efforts of my advisor, Ken Tape, over the past 4 years. I also wish to thank Sara and JB Wilbur for the general support.

General Introduction

Many of the environmental shifts observed and predicted in the Arctic are related to components of the water cycle. Changes in the amount and timing of precipitation, in addition to changes in proportioning of snow and rain and snow cover duration, affect the *influx* of water to terrestrial system. Conversely, environmental parameters such as changes to thaw and freeze dates, growing season length, temperature, and humidity, cloudiness, permafrost thaw, and vegetation communities affect the *efflux* of water from the terrestrial system to the atmosphere and ocean.

The Arctic water cycle is complex and characterized by feedback mechanisms, and accounting of dominant water fluxes can yield important insights into the system as whole, as well as future changes. This dissertation clarifies the role of arctic vegetation in the water cycle. It focuses on the role of woody shrubs in storing and using snowmelt water (Ch. 1), the role of woody shrubs in transferring water to the atmosphere through transpiration (Ch. 2), and the role of dominant tundra vegetation types in transferring water to the atmosphere through transpiration and evaporation (Ch. 3).

To discuss the role of woody shrubs in storing snowmelt water, it is helpful to conceptualize the arctic freshwater cycle as a model of pools and fluxes (Fig. 1). The atmosphere, soil, surface water bodies, glaciers, ice sheets, snow, and vegetation all contain pools of water. Some pools are relatively stable, fluxing water to other pools at relatively low rates on the order of years to millennia (i.e. continental ice sheets or deep aquifers), while other pools are more dynamic and volatile, quickly expanding and contracting on the order of days to weeks (i.e. snowpack during spring melt or flood in rivers). Like many other arctic processes, the pool of water in arctic vegetation is highly seasonal.

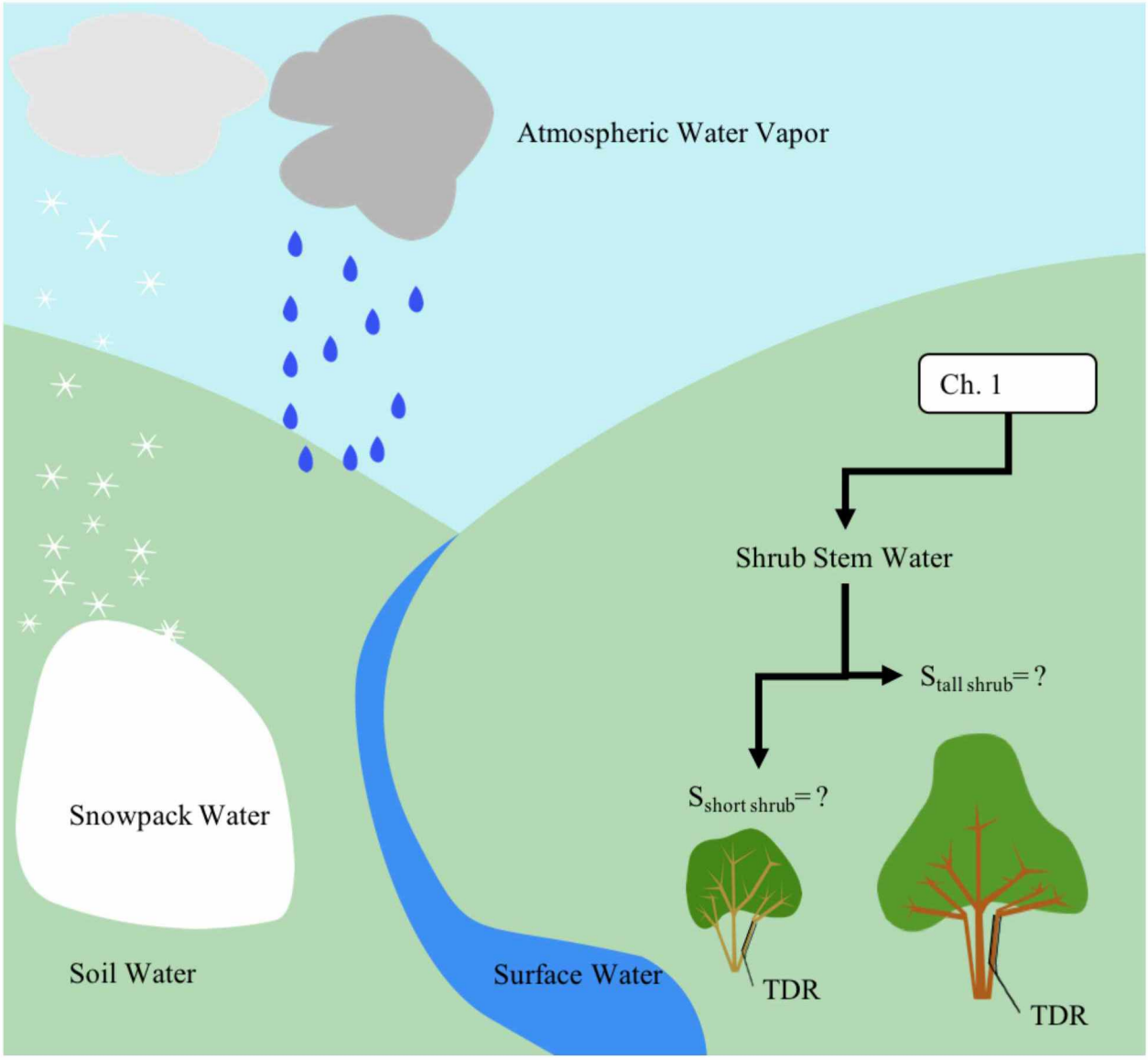

Figure 0.1. Conceptual diagram of Arctic water pools and measurement of shrub stem water content (S) using time-domain reflectometry (TDR).

During much of the year, arctic vegetation is frozen and contains relatively little water. However, during the short (6-12 week) growing season, the vegetation takes up water to support photosynthesis and other cellular processes. In many ecosystems, plants take up water and store it in their stems for later transpiration. The amount of water taken up by deciduous trees in the boreal forest has been found to be a substantial portion of annual precipitation, soil water, and transpiration (Young-Robertson et al., 2016). Although water uptake in boreal deciduous trees has been quantified, woody shrub seasonal water uptake and stem water storage in the Arctic

have not been investigated. Chapter 1 discusses a method by which woody shrub stem water content can be measured *in situ*, and from which seasonal water uptake and stem water storage can be calculated.

In many arctic ecosystems, evapotranspiration (ET, the combined fluxes of evaporation from surfaces and transpiration from vascular plants) is the major flux of water from the terrestrial system (Fig. 2, Jasechko et al., 2013). Vegetation plays a large role in defining the ET flux (Euskirchen et al., 2012; Kane et al., 2004), though the contributions from vegetation types is unknown. Changes to species assemblages or changes to the function of individual species can affect the ET flux (McFadden et al., 2012; Raz-Yaseef et al., 2017). Observations of vegetation change are widespread in the Arctic and many more changes are predicted, including increased shrub density (Tape et al., 2006), increased precipitation (Bring et al., 2016; Haine et al., 2015), and longer growing seasons (Park et al., 2016). Chapter 2 establishes the woody shrub contribution to ET in two foothill tundra communities. Building on Chapter 2, Chapter 3 addresses the respective contributions to ET by mosses, a tussock-forming sedge, and mixed species tundra vegetation communities.

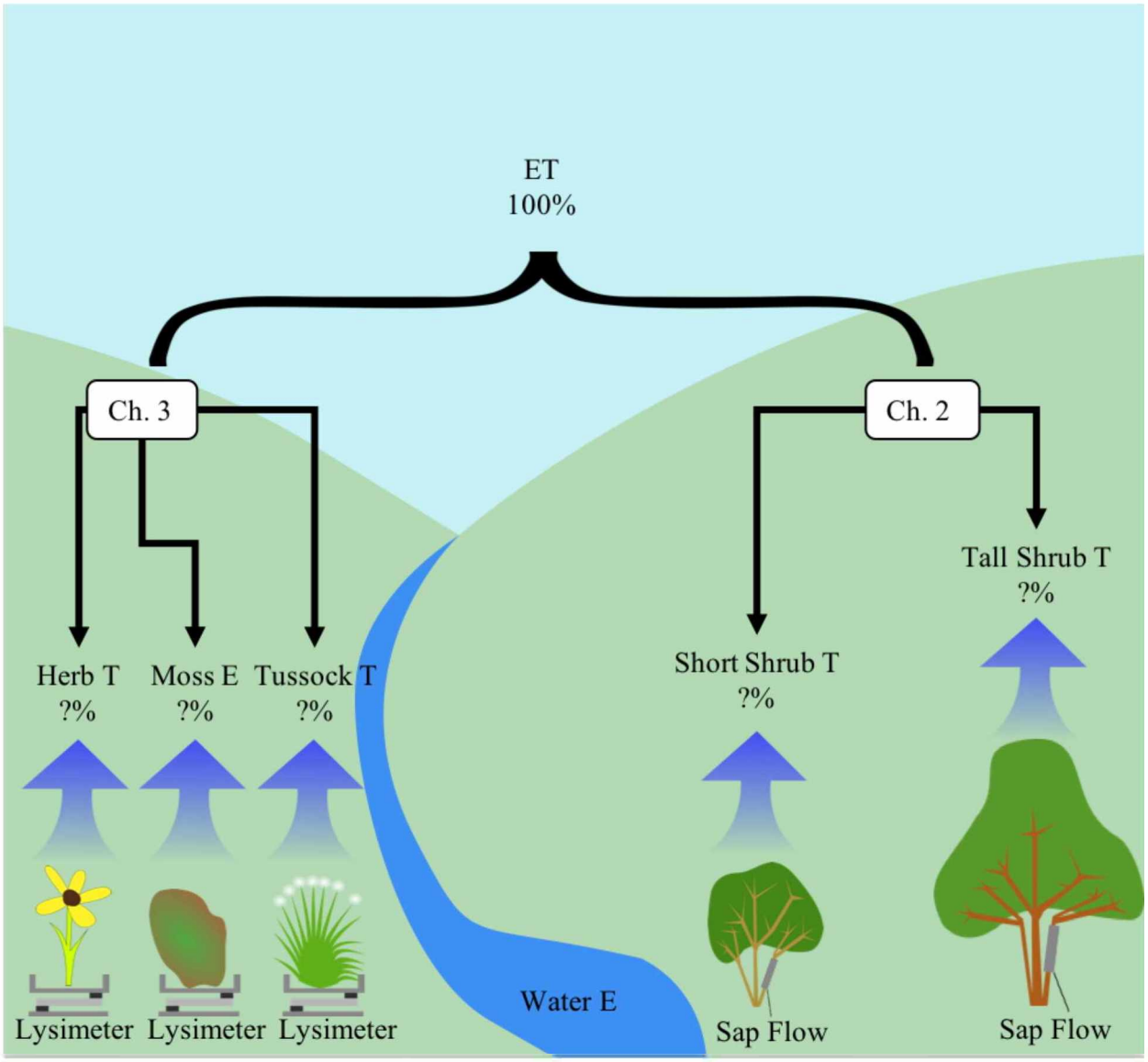

Figure 0.2. Conceptual diagram of Arctic water fluxes (evapotranspiration) from dominant vegetation types including lysimeter and sap flow measurement methods.

References

Bring, A., Fedorova, I., Dibike, Y., Hinzman, L., Mård, J., Mernild, S.H., Prowse, T., Semenova, O., Stuefer, S.L., Woo, M.-K., 2016. Arctic terrestrial hydrology: A synthesis of processes, regional effects, and research challenges. J. Geophys. Res. Biogeosciences 121, 2015JG003131. https://doi.org/10.1002/2015JG003131

Euskirchen, E.S., Bret-Harte, M.S., Scott, G.J., Edgar, C., Shaver, G.R., 2012. Seasonal patterns of carbon dioxide and water fluxes in three representative tundra ecosystems in northern Alaska. Ecosphere 3. https://doi.org/10.1890/ES11-00202.1

Haine, T.W.N., Curry, B., Gerdes, R., Hansen, E., Karcher, M., Lee, C., Rudels, B., Spreen, G., de Steur, L., Stewart, K.D., Woodgate, R., 2015. Arctic freshwater export: Status, mechanisms, and prospects. Glob. Planet. Change 125, 13–35. https://doi.org/10.1016/j.gloplacha.2014.11.013

Jasechko, S., Sharp, Z.D., Gibson, J.J., Birks, S.J., Yi, Y., Fawcett, P.J., 2013. Terrestrial water fluxes dominated by transpiration. Nature 496, 347–350. https://doi.org/10.1038/nature11983

Kane, D.L., Gieck, R.E., Kitover, D.C., Hinzman, L.D., Mcnamara, J.P., Yang, D., 2004. Hydrological cycle on the North Slope of Alaska. North. Res. Basins Water Balance, IAHS Publications 13.

McFadden, J.P., Chapin, F.S., Hollinger, D.Y., 2012. Subgrid-scale variability in the surface energy balance of arctic tundra. J. Geophys. Res. Atmospheres 28947–28961. https://doi.org/10.1029/98JD02400@10.1002/(ISSN)2169-8996.ARCSS1

Park, T., Ganguly, S., Tømmervik, H., Euskirchen, E.S., Høgda, K.-A., Karlsen, S.R., Brovkin, V., Nemani, R.R., Myneni, R.B., 2016. Changes in growing season duration and productivity of northern vegetation inferred from long-term remote sensing data. Environ. Res. Lett. 11, 084001. https://doi.org/10.1088/1748-9326/11/8/084001

Raz-Yaseef, N., Young-Robertson, J., Rahn, T., Sloan, V., Newman, B., Wilson, C., Wullschleger, S.D., Torn, M.S., 2017. Evapotranspiration across plant types and geomorphological units in polygonal Arctic tundra. J. Hydrol. 553, 816–825. https://doi.org/10.1016/j.jhydrol.2017.08.036

Tape, K., Sturm, M., Racine, C., 2006. The evidence for shrub expansion in Northern Alaska and the Pan-Arctic. Glob. Change Biol. 12, 686–702. https://doi.org/10.1111/j.1365-2486.2006.01128.x

Young-Robertson, J.M., Bolton, W.R., Bhatt, U.S., Cristóbal, J., Thoman, R., 2016. Deciduous trees are a large and overlooked sink for snowmelt water in the boreal forest. Sci. Rep. 6. https://doi.org/10.1038/srep29504

Chapter 1: Deciduous Shrub Stem Water Storage in Arctic Alaska

1.1 Abstract

Vegetation water content is a critical aspect of ecosystem water balance and plant physiology, including how plants cope with drought. Yet there is no method to continuously monitor plant water content, particularly for small plants. I developed a method to continuously measure shrub water content using time-domain reflectometry (TDR), a measurement technique commonly used to measure soil moisture. I fabricated TDR probes and installed them in live woody shrubs in Arctic Alaska. I calibrated the TDR measurements to volumetric water content of the shrub stems by controlled drying of stems paired with measurements of gravimetric water content and TDR waveforms. Apparent dielectric constant was derived from TDR waveforms. Gravimetric water content was converted to volumetric water content (VWC) to create calibration equations relating apparent dielectric constant to volumetric water content of shrub stems of felt-leaf willow (*Salix alaxensis*), diamond-leaf willow (*Salix pulchra*) and dwarf birch (*Betula nana*). Automated measurements were made at 30-minute intervals at two field sites over three growing seasons. Our fabricated TDR probes and calibration equations permit continuous, non-destructive, and accurate measurements of stem water content in live shrubs. Our results quantify seasonal patterns of stem water content (40-70% VWC). Spring uptake of snowmelt water and stem water storage was minimal (<2mm). Stem water storage is minor compared to other components of the hydrologic water budget (summer precipitation and end of winter snow water equivalent) and measured shrub transpiration rates.

1.2 Introduction

Many uncertainties remain in the terrestrial arctic water budget, particularly surrounding the storage and efflux of water. Recent findings have highlighted the important role of deciduous trees in the boreal hydrologic budget. Deciduous trees may take up significant portions of early spring snowmelt water for use in transpiration throughout the growing season (Young-Robertson et al., 2016). However, water storage in shrub stems remains unquantified in boreal and arctic tundra ecosystems.

Time-domain reflectometry (TDR) has been used extensively over the last 35 years to measure soil water content and tree stem water content in both in the lab and field (Constantz and Murphy, 1990; Hernández-Santana et al., 2008; Nadler et al., 2006; Sparks et al., 2001; Wullschleger et al., 1996). The technique benefits from minimal tree stem disturbance, accuracy and ease of automation. Despite wide application in soil science and limited use in trees, relatively little work has been done applying the technique to woody shrubs. I developed a method using TDR probes embedded in shrub stems to continuously measure shrub stem water content. Iuse our new technique to measure shrub stem water storage and assess its contribution to the hydrologic budget in the arctic tundra.

1.3 Methods

1.3.1 Probe Development

I fabricated TDR probes using stainless rods 2mm in diameter and 12cm in length. TDR probes were soldered to 15m 50Ω coaxial cable and connected to a multiplexer and a TDR100 time-domain reflectometer (Campbell Scientific, 2007). I inserted the probes into shrub stems by sawing two vertical grooves on opposite sides of a straight section of stem (Fig. 1.1a). The probes were then pressed into the grooves and held in place with silicon tape (Fig. 1.1b). TDR probes were inserted into stems of *Salix alaxensis* (n=22), *Salix pulchra* (n=12), and *Betula nana* (n=10) in early spring of 2016 and 2017 at two field sites in the northern foothills of the Brooks Range, located near Toolik Lake, Alaska.

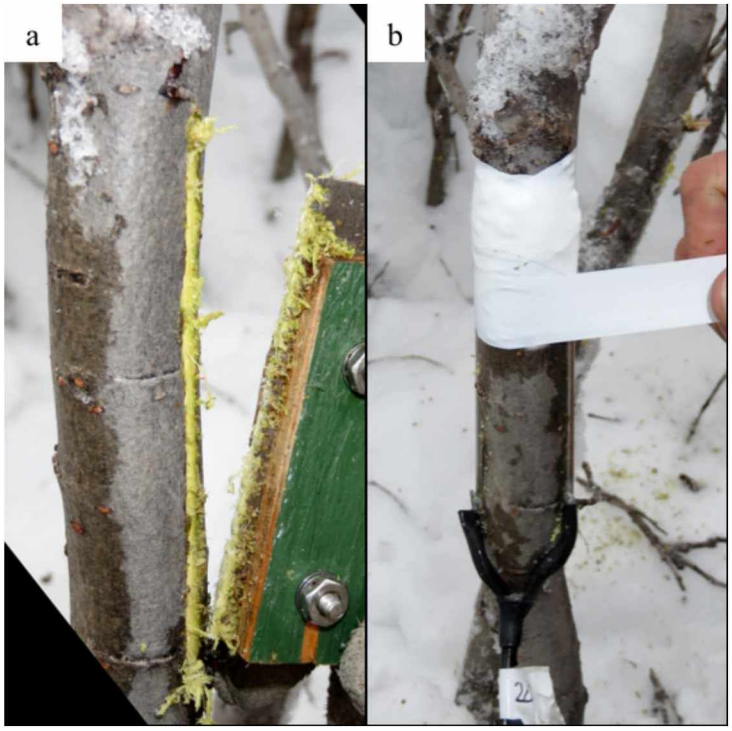

Figure 1.1. Installation of TDR probe on shrub stem for stem water content measurement using a small saw to create grooves in the stem (a); using silicone tape to hold stainless steel TDR probes in place (b).

1.3.2 Principles of Time-Domain Reflectometry (TDR)

The TDR device sends a short electromagnetic pulse through a coaxial cable and into two parallel probes embedded in the test material (i.e. soil or wood); the reflected signal is then recorded. Signal travel time is used with the velocity of the pulse to provide a measure of apparent distance along the probes. The travel time along the probe length is sensitive to the water content of the test material. As water content increases, the travel time of the pulse increases. The reflected waveform is used to determine the apparent probe length (La). The apparent dielectric constant (Ka) of the test material is then calculated as the squared ratio of La to the probe length (L):

$$Ka = \left(\frac{La}{L}\right)^2 \quad (1).$$

1.3.3 Calculation of *La* from TDR Waveform

I used an algorithm to measure *La* from the recorded TDR waveforms (Fig. 1.2, Campbell Scientific, 2007). In each waveform a series of three points are identified (P1, P2, P3). The waveform before P1 is the section of coaxial cable near the probe head with a relatively low reflection coefficient. P1 is the transition from coaxial cable to stainless steel rod proximal end. The change in reflection coefficient between P1 and P2 is related to the difference in impedance between the cable and the probe. P2 corresponds to the rods after the solder joint and P3 is the distal end rods. *La* relates to the difference between P2 and P3 and is obtained by converting waveform data points to distance. The conversion to distance uses the number of waveform data points (2048) and the width of the waveform window (5m).

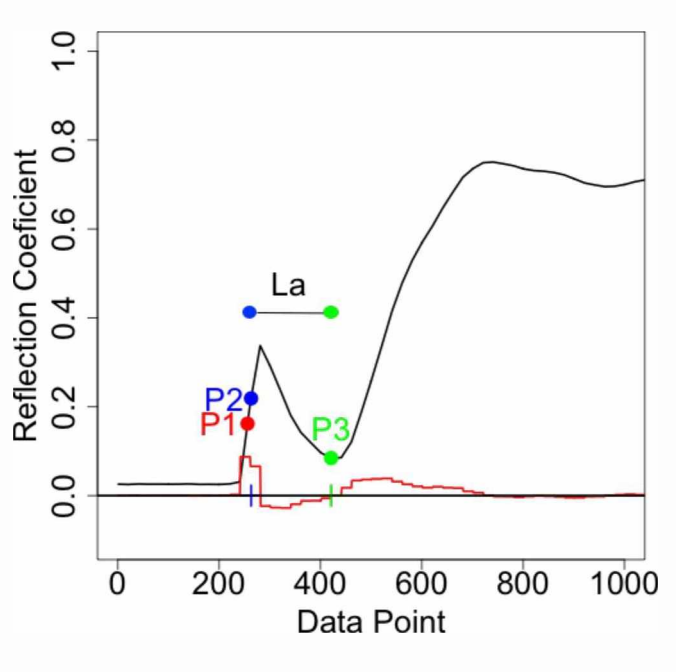

Figure 1.2. Example TDR waveform (black line) and its first derivative (red line), showing water content induced change in signal impedance, and points (P1, P2, P3) for calculating apparent probe length (La) and dielectric constant (Ka).

The waveform and its first derivative are used to calculate *La* (Campbell Scientific, 2007). P1 is identified by searching from the first data point to the point where the first derivative rises above a given threshold. The maximum of the first derivative after P1 is used to define a tangent line through the point of the maximum derivative. P2 is defined by the

intersection of the tangent line and the waveform offset by the distance from the proximal end of the rod to the end of the solder junction. P3 is defined by the next local minima. *La* is defined as the distance between P2 and P3. *Ka* was calculated following Eq. 1.

1.3.4 Water Content Calibration

Calibration of the shrub TDR probes was performed after first drying shrub stems in the laboratory. The TDR stem sections were cut from our field sites for calibration at the end of the growing season in late August 2017. Stem volume was determined using calipers to measure three diameters and length to the nearest 0.1mm. Stems were weighed and then submersed in water for several days to saturate them before the calibration began. Daily TDR measurements and stem masses were recorded. Between measurements, stems were stored in loosely sealed plastic bags to slow drying. After approximately two months, drying slowed, and stems had dried below values recorded in field samples (30% volumetric water content). Samples were placed in a drying oven at 65°C until they dried. Gravimetric water content was calculated and converted to volumetric water content (VWC, % volume) using the stem volume and gravimetric water content. Measurements of shrub stem *Ka* and VWC content were then compared and regression equations for each species were developed to relate TDR measurements of *Ka* to VWC.

1.3.5 Field Measurements of Shrub Stem VWC

Field measurements were conducted over the summers of 2016 and 2017 at two sites—one tundra shrub and one riparian shrub tundra —located in the broad uplands north of the Brooks Range, Alaska (Fig. 1.3). The tundra shrub site was located at the headwaters of Imnaviat Creek, approximately 12 km E of the Toolik Field Station at 884m elevation. Moist acidic shrub tundra, dominated by the woody shrubs *Salix planifolia* ssp. *pulchra* and *Betula nana* and the moss *Sphagnum rubellum*, comprise the vegetation (Walker et al., 2005). The site is on an east-facing slope and the surface geomorphology is poorly-defined water tracks and weakly-developed solifluction lobes. The active layer (e.g. seasonal thaw depth) consists of 10 to 15 cm of peat underlain by 20 to 30 cm of plastic, wet, gravelly sandy clay loam. The site is entirely underlain by near-surface permafrost at a maximum seasonal thaw depth of 35 to 50 cm (Walker and Walker, 1996).

The riparian shrub tundra site is located approximately 18 km south of the Toolik Field Station near a tributary stream of Galbraith Lake at 853m elevation. The vegetation consists of tall riparian shrubs dominated by *Salix alaxensis*. The site is on a stabilized floodplain terrace consisting of glaciofluvial outwash. Bordering the terrace on the north is a toeslope and on the south is an active floodplain. The soils consist of a thin organic layer (< 5 cm) underlain by sandy loam and intermixed with course gravel and cobbles. The presence of permafrost at the riparian site is unknown, but likely deep or absent due to the thin or nonexistent organic layer and location within an active stream floodplain.

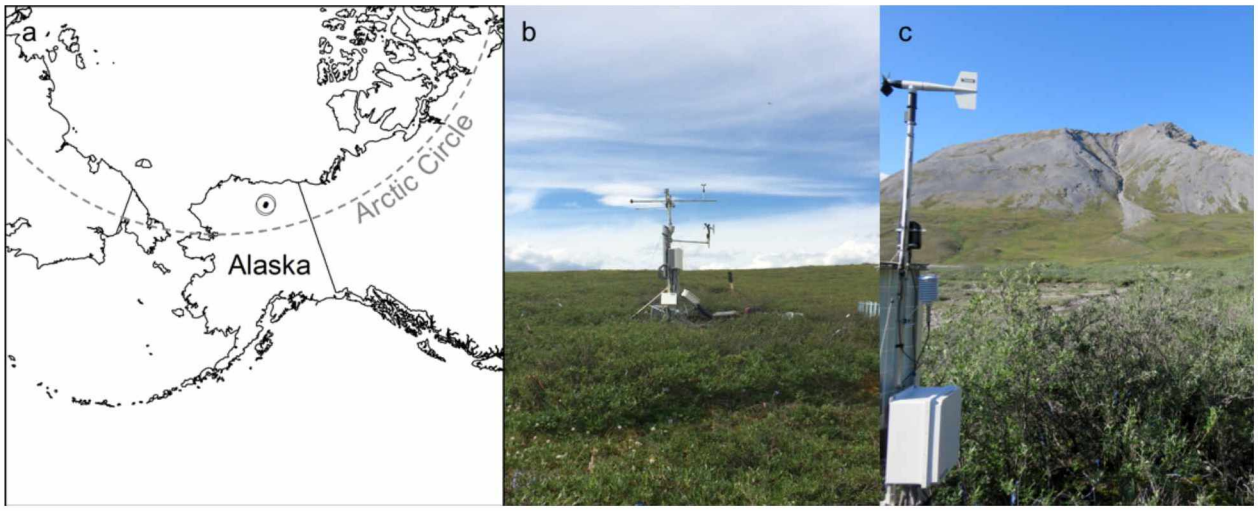

Figure 1.3. Location of study sites (a) in Arctic Alaska, USA, and photographs showing vegetation at the tundra shrub site (b: 68.62°N, 149.32°W) and riparian shrub site (c: 68.47°N, 149.55°W).

1.3.5 Scaling Shrub Stem VWC to Stem Water Storage

Estimates of shrub aboveground biomass (AGB) were taken from Berner et al. (2018) and combined with our measurements of shrub stem density and range of shrub stem VWC to estimate ranges of water stored on the landscape in shrub stems. AGB (kg m^{-2}) was converted to shrub stem volume (V_{stem}, m^{-3}) using shrub stem density by species ($\rho_{species}$, kg m^{-3} m^{-2}):

$$Vs_{species} = AGB/\rho_{species} \quad (2),$$

where ρ was determined from stem volume measurements and stem dry weight. Shrub stem VWC was then used to calculate the volume of water in the shrub stems and converted to mm of water stored in stems (S, mm):

$$S_{species} = (Vs_{species} * VWC) * 1000 \quad (3).$$

A range of AGB (0-2 kg m^{-2}) and shrub stem VWC (30-70%) were used to estimate likely ranges of growing season S for each species. Spring uptake of snowmelt water was estimated from the difference in stem water content during winter dormancy (April) and stem water content at leaf out (early June).

1.4 Results

Preliminary calibration measurements revealed the cut shrub stems quickly dry to below observed live field moisture values (1-3 days). Placing the cut stems in loosely sealed plastic bags slowed the drying process and allowed more data points (30+) to be collected over the range of stem moisture content observed in situ (30-70% VWC). *Ka* showed a linear decline with decreasing stem VWC (Fig. 1.4). However, there was noticeable measurement error for the TDR-derived *Ka* which as not correlated with VWC and had no apparent cause. Possible sources of interference were checked, and the TDR100 and cables were replaced without rectifying the issue. Measurements of soil, water, and larger tree stems using the same calibration setup did not exhibit the same measurement errors.

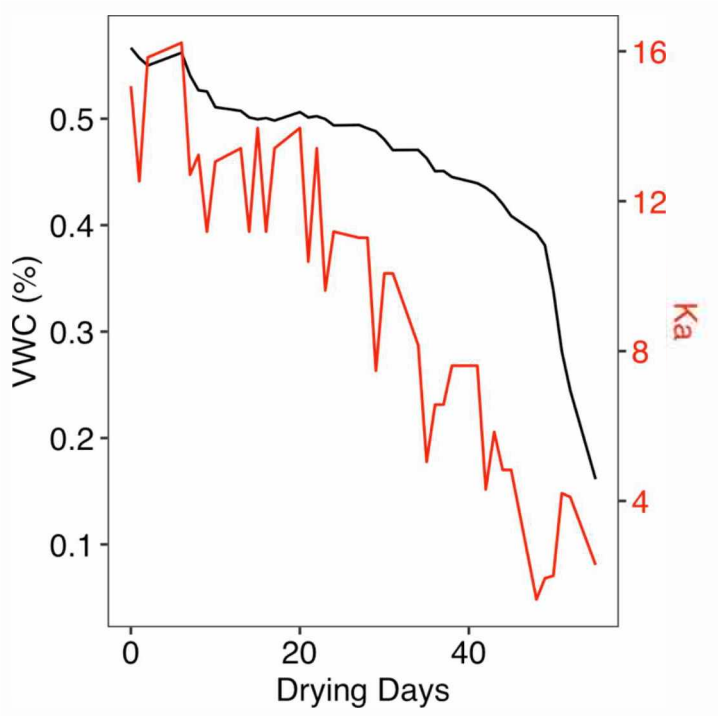

Figure 1.4. Example shrub stem drying curve and corresponding measures of dielectric constant used for calibrating VWC to TDR measurements.

Calibration equations were developed to relate the TDR-derived *Ka* to shrub stem VWC (Fig. 1.5). There was more scatter in the data for *S. alaxensis* than for the other two species. The calibration for both *Salix* species was similar, while that for *B. nana* had a steeper slope and spanned the narrowest range of *Ka* values.

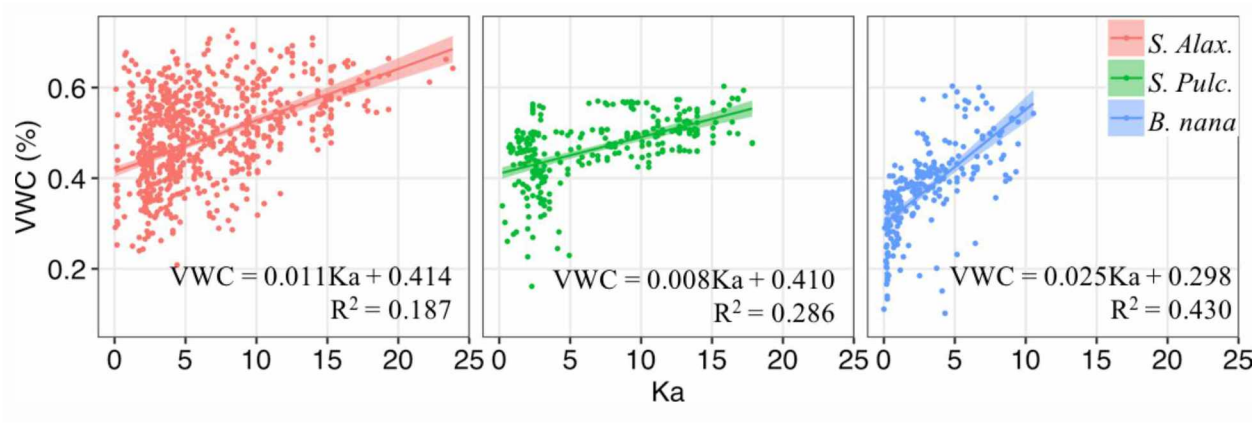

Figure 1.5. Calibration lines for each of the three shrub species. Points represent measures from multiple stems. Solid lines are the best fit linear regression lines and shaded areas are the 95% confidence intervals.

Spring and summer daily average stem VWC from the two field sites reveal early spring wetting of shrub stems, coinciding with snowmelt and above-freezing temperatures approximately six weeks prior to leaf emergence (Fig. 1.6). At the riparian site, stem VWC appeared to increase over the early growing season before leveling out in mid-July. At the tundra site, there was a more apparent wetting period in May and June followed by more constant stem VWC in July and August. Stem VWC was not measured after the growing season in fall or winter.

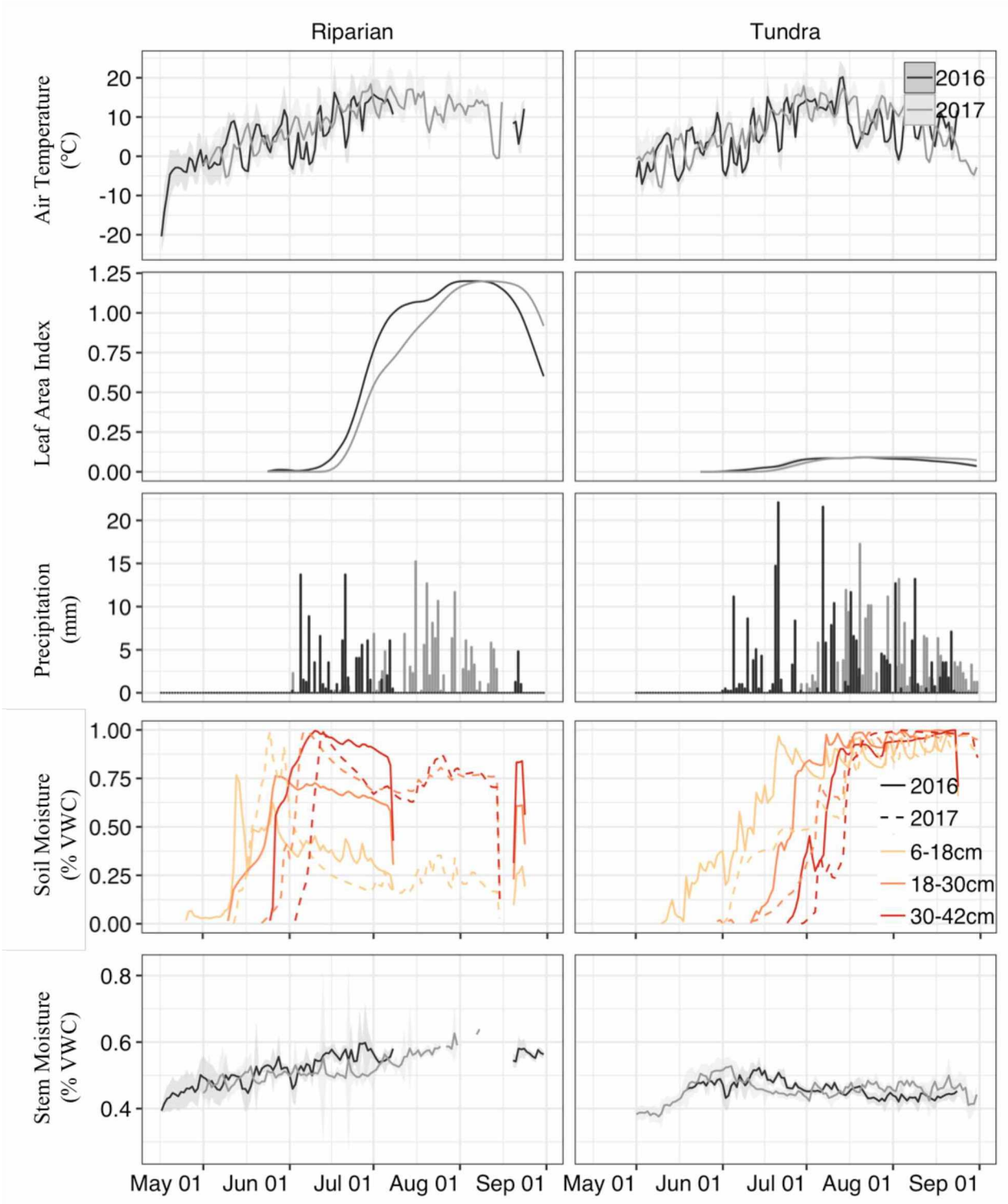

Figure 1.6. Air temperature, leaf area index, precipitation, soil moisture and stem moisture for the riparian and tundra shrub sites for 2016 and 2017.

Scaling the shrub stem VWC over a range of ABG and stem VWC provides an estimate of shrub stem water storage (S) across the tundra landscape (Fig. 1.7). S ranged from 0-3+ mm with *S. alaxensis* having the greatest S capacity due to is lower density and greater biomass. Spring uptake of snowmelt water was found to be minimal (<1mm, Table 1.1).

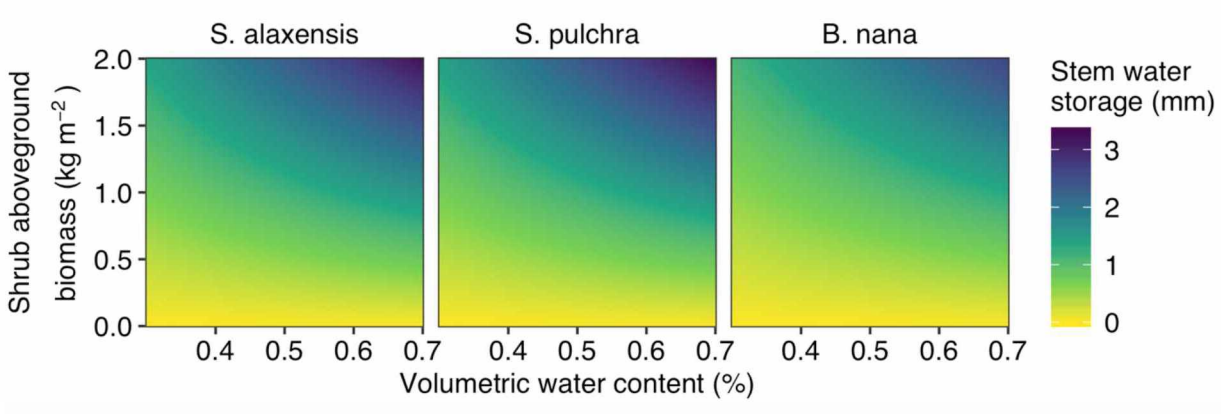

Figure 1.7. Estimated shrub stem water storage for riparian and tundra shrubs.

Table 1.1. Shrub stem density and stem water storage (*S*) over a range of field stem water volumetric water contents (VWC).

Species	n	Density (sd) [kg m^{-3}]	*S* at 40% VWC, 1 kg m^{-2} [mm]	*S* at 60% VWC, 1 kg m^{-2} [mm]	Spring uptake [mm]
S. alaxensis	22	435.7 (33.9)	0.93	1.50	0.57
S. pulchra	12	424.5 (37.2)	0.96	1.54	0.59
B. nana	10	532.0 (50.2)	0.76	1.23	0.47

1.5 Discussion

In this study, I show that stem water storage in arctic shrubs is a trivial portion of the hydrologic budget. Arctic shrub daily transpiration (0-4mm d^{-1}, Ch. 2) is comparable to stem water storage (0-3+ mm). The small amount of stem water storage in arctic shrubs suggests that stem water cannot be used for long-term transpiration and that shrubs are likely taking up soil water on a daily basis to meet transpiration requirements.

Young-Roberston et al. (2016) found that deciduous trees in boreal Alaska uptake large amounts of snowmelt water (21-25%, 30-36mm) in early spring. Furthermore, they found that the deciduous trees appeared to uptake and store the snowmelt water for transpiration needs throughout the growing season. Although there are slight differences in the maximum water content of wood between species, water storage in woody vegetation (trees and shrubs), proportional to biomass, varies by a factor of two (Nobel & Jordan 1983). Deciduous tree water storage is quite large compared to daily transpiration rates. Unlike the boreal deciduous trees, arctic deciduous shrub stem biomass is quite low and is not adequate to store water for later transpiration over weeks to months.

In context of the hydrologic budget, arctic shrub stem water storage is a minor component. For the tundra site, estimates of stem water storage are <3% of winter precipitation, <2% of summer precipitation, <2% of runoff, and <2% of summer ET (Kane et al., 2004). Despite low stem water storage, arctic shrubs still play an important role in the terrestrial water cycle through transpiration (Ch. 2).

The method present here for measuring water content of shrub stems using TDR probes had low accuracy. The calibration equations for each of the three species had poor fit and low R^2 values (0.19 - 0.43). In the controlled calibration drying experiment, the individual TDR measurements were highly variable relative to a stable stem water content. It is possible that the TDR probe and the stem wood physical and electrical connection is weak compared to probes embedded in trees. While other methods of embedding the probes in the shrub stems were not available due to the small size of the stems, the method used here of partially embedding the probes in the stem cambium did result in reduced accuracy.

1.6 References

Berner, L.T., Jantz, P., Tape, K.D., Goetz, S.J., 2018. Tundra plant above-ground biomass and shrub dominance mapped across the North Slope of Alaska. Environ. Res. Lett. 13, 035002. https://doi.org/10.1088/1748-9326/aaaa9a

Campbell Scientific, 2007. TDR100 Time Domain Reflectometry User's Guide. Logan, UT.

Constantz, J., Murphy, F., 1990. Monitoring moisture storage in trees using time domain reflectometry. J. Hydrol. 119, 31–42. https://doi.org/10.1016/0022-1694(90)90032-S

Hernández-Santana, V., Martínez-Fernández, J., Morán, C., 2008. Estimation of tree water stress from stem and soil water monitoring with time-domain reflectometry in two small forested basins in Spain. Hydrol. Process. 22, 2493–2501. https://doi.org/10.1002/hyp.6845

Kane, D.L., Gieck, R.E., Kitover, D.C., Hinzman, L.D., Mcnamara, J.P., Yang, D., 2004. Hydrological cycle on the North Slope of Alaska. North. Res. Basins Water Balance, IAHS Publications 13.

Nadler, A., Raveh, E., Yermiyahu, U., Green, S., 2006. Stress Induced Water Content Variations in Mango Stem by Time Domain Reflectometry. Soil Sci. Soc. Am. J. 70, 510–520. https://doi.org/10.2136/sssaj2005.0127

Nobel, P., & Jordan, W.,1983. Transpiration Stream of Desert Species: Resistances and Capacitances for a C3, a C4, and a CAM Plant. Journal of Experimental Botany, 34, 1379–1391, https://doi.org/10.1093/jxb/34.10.1379

Sparks, J.P., Campbell, G.S., Black, A.R., 2001. Water content, hydraulic conductivity, and ice formation in winter stems of Pinus contorta: a TDR case study. Oecologia 127, 468–475. https://doi.org/10.1007/s004420000587

Walker, D.A., Raynolds, M.K., Daniëls, F.J.A., Einarsson, E., Elvebakk, A., Gould, W.A., Katenin, A.E., Kholod, S.S., Markon, C.J., Melnikov, E.S., Moskalenko, N.G., Talbot, S.S., Yurtsev, B.A.(†), Team, T. other members of the C., 2005. The Circumpolar Arctic vegetation map. J. Veg. Sci. 16, 267–282. https://doi.org/10.1111/j.1654-1103.2005.tb02365.x

Walker, D.A., Walker, M.D., 1996. Terrain and Vegetation of the Imnavait Creek Watershed, in: Reynolds, J.F., Tenhunen, J.D. (Eds.), Landscape Function and Disturbance in Arctic Tundra, Ecological Studies. Springer Berlin Heidelberg, Berlin, Heidelberg, pp. 73–108. https://doi.org/10.1007/978-3-662-01145-4_4

Wullschleger, S.D., Hanson, P.J., Todd, D.E., 1996. Measuring stem water content in four deciduous hardwoods with a time-domain reflectometer. Tree Physiol. 16, 809–815. https://doi.org/10.1093/treephys/16.10.809

Young-Robertson, J.M., Bolton, W.R., Bhatt, U.S., Cristóbal, J., Thoman, R., 2016. Deciduous trees are a large and overlooked sink for snowmelt water in the boreal forest. Sci. Rep. 6. https://doi.org/10.1038/srep29504

Chapter 2: Transpiration and Environmental Controls in Arctic Tundra Shrub Communities

2.1 Abstract

Evapotranspiration (ET) is a major component of the terrestrial arctic hydrologic budget because this process returns large portions of the annual precipitation back to the atmosphere. A better understanding of the partitioning of ET in the Arctic is needed because changes in plant water use may affect permafrost and the carbon stored within it. I conducted measurements of shrub transpiration at two contrasting sites in the arctic tundra of northern Alaska to provide a fundamental understanding of water and energy fluxes in the tundra biome. Total shrub transpiration reflected the 12-fold difference in leaf area between the sites, with much greater total shrub transpiration at the riparian site. Hourly shrub transpiration (T) rates were highly variable but showed strong diurnal patterns and correlations to net radiation (*Rn*) and vapor pressure deficit (*D*). A statistical model was developed using *D*, *Rn*, and leaf area which explained > 80% of the variation in hourly transpiration Shrub transpiration was greatest when *D* and *Rn* were high, suggesting that arctic shrub productivity is energy-limited. Transpiration of three dominant arctic shrub species at the two contrasting sites ranged from approximately 10% of summer ET in a tundra shrub community to a majority of possible summer ET in a riparian shrub community. At the tundra shrub site, the other plant species in that watershed apparently account for a much larger proportion of ET than the measured shrubs. Future increases in shrub abundance and biomass are likely to alter the arctic hydrologic budget.

2.2 Introduction

Evapotranspiration (ET)—a combination of evaporation from surfaces and transpiration from vascular plants—is a major component of the terrestrial arctic hydrologic budget because this process returns large portions of the annual precipitation back to the atmosphere. As in other ecosystems, plants play an important role in the arctic hydrologic cycle via transfer of water vapor to the atmosphere through transpiration, which modifies local temperature and humidity. Transpiration through plants reduces soil moisture, which is paramount in arctic tundra because it controls the soil thermal conductivity and transfer of summer or winter heat to the underlying frozen ground. Tree canopies contribute the majority of transpiration in temperate and boreal forests (Baldocchi et al., 2000; Kelliher et al., 1998; Moore et al., 1996; Oishi et al., 2010;

Wilson et al., 2000), but the arctic tundra lacks trees. Woody shrubs may serve as the tree canopy analog, and sap flow measurements in woody shrubs could quantify their contribution to total evapotranspiration.

Sap flow studies have been conducted primarily in forest ecosystems (e.g. Ewers and Oren, 2000; Oren et al., 1998), with a few from shrub ecosystems (Allen and Grime, 1995; Dawson et al., 2007; Lei et al., 2010; Liu et al., 2011; Naithani et al., 2012), and fewer still from arctic ecosystems (Kropp et al., 2017). Transpiration rates for individual species or functional groups are lacking for specific arctic vegetation communities in part because it is difficult to make continuous sap flow measurements in this remote region. Existing Arctic studies, often derived from eddy covariance measurements of ET, integrate ET over large areas that include mixed vegetation, and thus do not inform how transpiration from functional groups or individual species contribute to ET, nor how ET will change under altered vegetation (Euskirchen et al., 2012; 2009). A better understanding of transpiration in the Arctic is needed because changes in plant water use may affect permafrost and the carbon stored within it.

In the Arctic, widespread environmental change includes increases in air temperature (IPCC, 2013), permafrost temperature (Romanovsky et al., 2010), and thaw depth, and variability in precipitation (Rawlins et al., 2010). Intensification of the freshwater cycle has been reported in arctic tundra: studies have reported increases in precipitation (Pavelsky and Smith, 2006), river discharge (Haine et al., 2015; Peterson et al., 2002; Serreze et al., 2002), groundwater storage (Muskett and Romanovsky, 2009), and ET (Bring et al., 2016; Fernandes et al., 2007; Park et al., 2008). In conjunction with these environmental changes, vegetation composition and increases in plant growth rate and biomass have also been measured (Bjorkman et al., 2019; Hobbie et al., 2017; Myers-Smith et al., 2015; Tape et al., 2006). Shrub expansion has occurred throughout the Arctic (Frost and Epstein, 2014; Myers-Smith, 2011; Sturm et al., 2001; Tape et al., 2006). As shrub cover and productivity continue to increase, transpiration may also increase because they have a relatively larger transpiration surface compared to the smaller leaf surface of the grasses, sedges, and forbs that dominate tundra vegetation communities. Understanding current shrub transpiration rates is critical for establishing the role of shrubs in the

ecosystem water budget, and also is important to predict future scenarios as arctic vegetation changes.

I conducted measurements of shrub sap flow and meteorology in the arctic tundra of northern Alaska to test the idea that shrubs can have a dominant influence on water and energy fluxes in the tundra biome. To provide continuous, species-specific transpiration rates, sap flow was measured on three woody shrub species at two sites in Arctic Alaska over two growing seasons. These rates were combined with meteorological and environmental measurements to determine controls on transpiration at sub-daily and longer time scales (Ewers et al., 2007; Phillips and Oren, 1998). Seasonally-integrated shrub transpiration fluxes were compared to total ecosystem evapotranspiration to determine the role of shrubs in summer water efflux.

2.3 Methods

2.3.1 Study Sites

Research was conducted over the summers of 2016 and 2017 at two sites—one tundra shrub and one riparian shrub—located in the broad uplands north of the Brooks Range, Alaska (Fig. 2.1). The tundra shrub site was located at the headwaters of Imnaviat Creek, approximately 12 km E of the Toolik Field Station at 884m elevation. Moist acidic shrub tundra, dominated by the woody shrubs *Salix planifolia* ssp. *pulchra* and *Betula nana* and the moss *Sphagnum rubellum*, comprise the vegetation (Walker et al., 2005). The site is on an east-facing slope and the surface geomorphology is poorly-defined water tracks and weakly-developed solifluction lobes. The active layer (e.g. seasonal thaw depth) consists of 10 to 15 cm of peat underlain by 20 to 30 cm of plastic, wet, gravelly sandy clay loam. The site is entirely underlain by near-surface permafrost at a maximum seasonal thaw depth of 35 to 50 cm (Walker and Walker, 1996).

The riparian shrub site is located approximately 18 km south of the Toolik Field Station near a tributary stream of Galbraith Lake at 853m elevation. The vegetation consists of tall riparian shrubs dominated by *Salix alaxensis*. The site is on a stabilized floodplain terrace consisting of glaciofluvial outwash. Bordering the terrace on the north is a toeslope and on the south is an active floodplain. The soils consist of a thin organic layer (< 5 cm) underlain by sandy loam and intermixed with course gravel and cobbles. The presence of permafrost at the

riparian site is unknown but likely very deep or absent due to the thin or nonexistent organic layer and location within an active riverine floodplain.

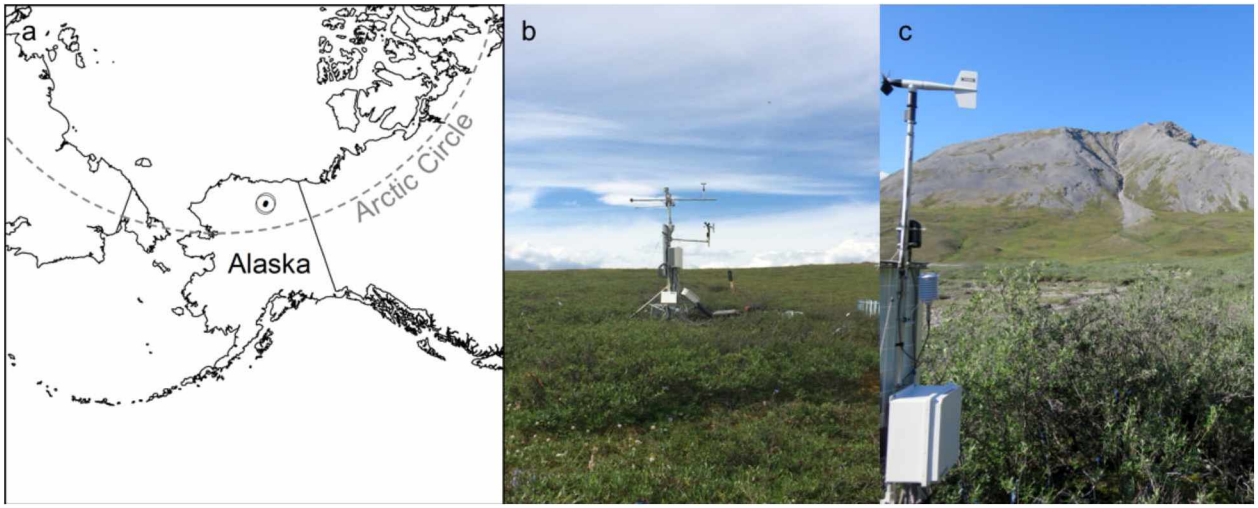

Figure 2.1. Location of study sites (a) in Arctic Alaska, USA, and photographs showing vegetation at the tundra shrub site (b: 68.62°N, 149.32°W) and riparian shrub site (c: 68.47°N, 149.55°W).

2.3.2 Meteorological and Leaf Area Measurements

At each site, measurements of air temperature, relative humidity, vapor pressure deficit (D), net total radiation (R_n), net shortwave radiation, precipitation (P), wind speed and direction, radiometric surface temperature (T_{ir}), soil temperature, and soil moisture were taken at hourly intervals using a data logger (Campbell Scientific, Logan, Utah, USA) from 28 March 2016 to 01 September 2016 and from 28 March 2017 to 01 September 2017. Soil temperature was measured in three locations at 4, 16, and 28 cm depths. Soil moisture sensors were vertically-oriented, with each integrating measurements across 12 cm at three depths (8–20 cm, 20–32 cm, 32–44 cm). Upward-facing photographs were taken every three hours from the ground surface to capture leaf area (LA) development over the growing season. Site leaf area was estimated from the photographs using the LAI package in R (Martin, 2015).

2.3.3 Sap Flow and Canopy Transpiration

Sap flow was measured on shrub stems at both the tundra shrub site (n=16 total, 8 *S. pulchra*, 8 *B. nana*, 1 ramet per plant) and riparian shrub site (n=24 *S. alaxensis*, 1 ramet per plant) using stem heat balance sensors (Dynagage, Dynamax, Houston, Texas, USA).

Measurements were taken hourly from early June through August using a datalogger (CR1000, Campbell Scientific, Logan, Utah, USA). *S. alaxensis.*, *S. planifolia.*, and *B. nana* stems 5–33 mm in diameter were used for sap flow sensors (at the tundra shrub site, sensors were placed on only *S. planifolia* and *B. nana*). Sensors were placed 10–30 cm above the ground and were protected from solar radiation with reflective foil insulation above and below the sensors. Due to the low and sparse canopy at the tundra shrub site, an additional layer of sheet metal flashing was used below the sensors to limit solar radiation influence on sensor performance. The sap flow shrubs at each site were located in a circular footprint of 450 m^2. End-of-winter snow-water-equivalent was measured at each by taking snow depth at 1m intervals and snow density measurements at 10m intervals (and at 10cm depth increments) along a 100m transect.

In 2018, sap flow study plants were harvested during peak leaf area to determine total leaf area for each stem. Additionally, five 1m^2 plots were harvested at each site (10 plots total) to determine average site leaf area, stem density, and stem basal area. All leaves from the sap flow stems and a subset of each of the harvest plot leaves were scanned and leaf area was estimated using the Image-J software (Abramoff et al., 2004). All leaves were dried and weighed to determine relationships between leaf area and mass for calculating total leaf area of the harvested plots.

Sap flow (F, g hr^{-1}) was calculated using formulas and an algorithm provided by the sensor manufacturer (Dynagage, Dynamax, Houston, Texas, USA). Using leaf area of each sap flow stem and leaf area index, sap flow measurements were scaled from individual stems to an aerial measurement (Oren et al., 1998). Transpiration (T, mm hr^{-1}) was calculated by scaling the stem sap flow to the site average leaf area:

$$T = (F * LAI_{site} / LA_{stem}) / 1000 \quad (1),$$

where LAI_{site} (m^2 m^{-2}) is the shrub leaf area index for each site as determined from the harvest plots, and LA_{stem} (m^2) is the leaf area from each sap flow stem.

2.3.4 Canopy Transpiration Model

In preparation for modeling, environmental covariates and sap flow data were manually checked for quality and outliers were removed. No gap-filling was performed. Covariates were scaled by their standard deviation and mean-centered. Stepwise multiple linear regression was used to evaluate the response of sap flow to all possible combinations of an initial set of 15 hourly covariates: air temperature, relative humidity, D, wind speed, Rn, net shortwave radiation, T_{ir}, stem water content, soil volumetric water content at each of three depths, soil temperature at each of three depths, and daily LAI. Some covariate combinations were eliminated because they were correlated (e.g. soil water content, soil temperature, Rn, and T_{ir}). Models were ranked by the Akaike information criterion (AIC) and a top set of ten models was selected for further evaluation within a Bayesian framework.

The transpiration data (T_{obs}) were assumed to follow a normal distribution described by a mean and standard deviation:

$$T_{obs_{t,i}} \sim Normal(\mu_{t,i}, \sigma) \quad (2).$$

The mean hourly T (μ_t) for each observation i was modeled using three approaches: (1) a multiple regression with a random error term for individual stems (Eq. 3); (2) a multiple regression with random slopes for individual stem variation (Eq. 4); and (3) a multiple regression with random slopes for individual stem variation and a time-varying parameter (Eq. 6). The mean hourly T (μ_t) was based on responses to environmental covariates (Var_n) at each observation i, and the parameters describing the response of T did not vary over the season:

$$\mu_{t,i} = \beta_0 + \beta_1 * Var_{1,i} + \beta_2 * Var_{2,i} + \ldots + \beta_n Var_{n,i} + \varepsilon_{s_i} \quad (3),$$

where ε_{s_i} is the random effects associated with individual stems.

A second model formulation was tested to account for variability between plant stems. The multiple regression model (Eq. 3) was modified to include individual shrub effects (*stem* in 1,2,..n) on each model parameter in a hierarchical framework:

$$\mu_{t,i} = \beta_0 + \beta_{1,stem} * Var_{1,i} + \beta_{2,stem} * Var_{2,i} + \ldots + \beta_{n,stem} Var_{n,i} \quad (4),$$

where the parameter estimates ($\beta_{n,stem}$) were considered to be normal with a mean and standard deviation:

$$b_{n,stem} \sim Normal\ (\mu_{b,n}, \tau_{b,n}) \quad (5).$$

Finally, to account for seasonal changes in the response of T to *LAI*, a third model formulation was tested. The random slope model (Eq. 4) was modified to include seasonal estimates of leaf area index (*LAI*) parameter (*season* in 1, 2, 3):

$$\mu_{t,i} = \beta_0 + \beta_{1,stem,season} * LAI_i + \beta_{2,stem} * Var_{2,i} + \ldots + \beta_{n,stem} Var_{n,i} \quad (6).$$

The parameter estimates ($\beta_{1,stem,season}$) were considered to be normal with a mean and standard deviation:

$b_{1,stem,season} \sim Normal\ (\mu_{b,1,season}, \tau_{b,1})$, and
$\mu_{b,stem,season} \sim Normal\ (\mu_{b,1}, \tau_{b,1})$.

The three seasons were defined as early (15 June–9 July), mid (10 July–30 July), and late (31 July–15 August), and are referred to in the text as "early" (leaf out), "mid" (peak), and "late" (senescence).

Non-informative priors were assigned to the multiple regression parameters ($\beta_n, \beta_{n,stem}, \beta_{n,stem,season}$) using normal distribution with a mean of 0 and variance of 10000. The model intercept was given a semi-informative uniform distribution to constrain T_{obs} to positive values. The standard deviation of T_{obs} was given a non-informative gamma distribution. For the individual shrub effects model, shrub-level parameters were given a folded t-distribution with two degrees of freedom. All Bayesian models were coded, run, and evaluated using JAGS (Plummer, 2015), the R package rjags (Plummer et al., 2016), and R (version 3.5). Models were compared using deviance information criteria (DIC), root mean square error (RMSE), and mean

actual error. Three chains were run for a minimum of 100,000 (maximum 8 million) iterations. A total burn-in of 10,000 iterations was excluded and the chains were thinned to obtain 10,000 iteration posterior samples. Model convergence was checked by visual inspection of plots of model parameters and chains (Curtis, 2015), Gelman statistics, and Raftery statistic (Gelman, 2014). The Raftery statistic was used to set the number of iterations for full convergence. Model fit was evaluated by generating replicate data from the posterior predictive distribution and comparing it with observed T (Gelman, 2014). The final set of models was selected based on DIC and parameter parsimony.

The inclusion of shallow soil temperature slightly improved model fit, but it was ultimately excluded due to multiple significant correlations with other covariates and also to reduce the number of model parameters and improve model interpretability. Further model testing, including the effects of antecedent conditions was performed. Antecedent conditions up to 24 hours were evaluated for soil moisture, soil temperature, D, and Rn using the SAM model (Ogle et al., 2015). Weak antecedent effects of D and Rn were found for 1–3 hours antecedent. However, addition of the antecedent effects to the model provided only slight improvements to model fit, indicating little to no lag in plant transpiration response to atmospheric conditions; therefore, these results are not presented.

Data for the 2016 season are incomplete for both sites due to equipment malfunction. At the riparian shrub site, data from 9 July to 27 August are missing; at the tundra shrub site, the data begin on July 12th. To compare model fits between years, a subset of the 2017 data was used that matched the 2016 dates for each site. Therefore, for each site a total of three final models were fit: a 2017 model, a 2017 subset model, and a 2016 subset model.

2.4 Results

2.4.1 Meteorology and Soils

Mean summer air temperature, relative humidity, net radiation (Rn), and precipitation (P) were similar between the two sites in 2017 (Table 2.1, Fig. 2.2). For the tundra shrub site, the summer of 2016 was 3.7°C cooler than 2017, and 2016 had 59 mm more precipitation. Due to equipment malfunction at the riparian shrub site in 2016, environmental data are only available

from 20 April 2016 to 12 July 2016, which prohibits calculation of seasonal means and sums. In early May 2017, air temperature rose above freezing and snowmelt began. The surface soil began thawing on 12 May at the riparian shrub site and 4 June at the tundra shrub site. Peak air temperatures occurred on 30 June (27.5°C at the riparian shrub site and 24°C at the tundra shrub site). End-of-winter snow-water-equivalent in 2017 was 170 mm at the riparian shrub site and 322 mm at the tundra shrub site.

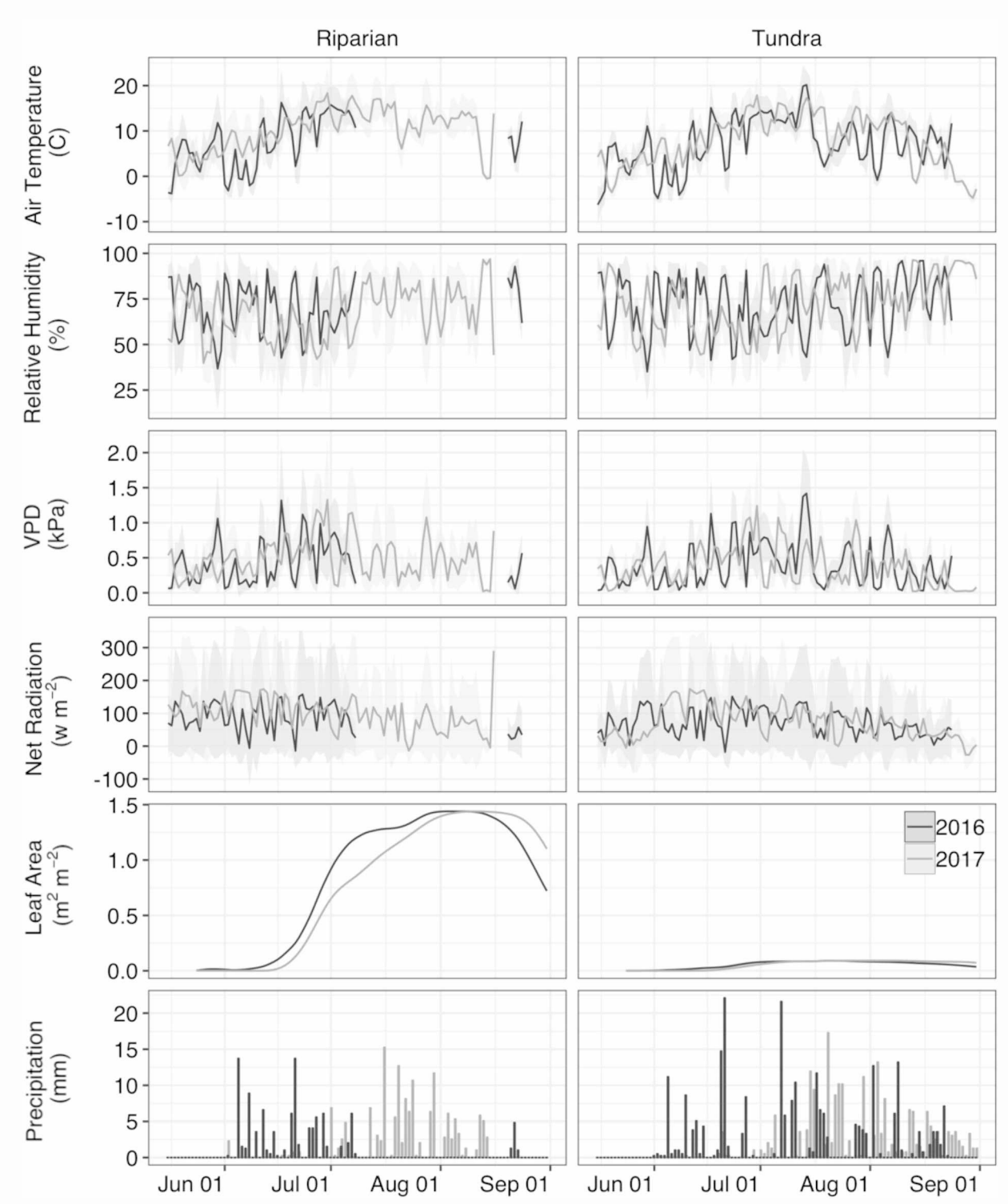

Figure 2.2. Daily meteorology and leaf area index (LAI) from riparian shrub and tundra shrub sites for 2016 and 2017. Solid lines represent daily means of hourly data. Shaded regions represent ± 1 standard deviation of the mean. Precipitation bars are daily sums of hourly data. Equipment malfunction led to meteorology data loss at the riparian shrub site in July & August 2016.

Despite similarities in meteorological conditions, the soils and vegetation were markedly different between the two sites (Fig. 2.3). Soil temperatures were consistently higher at the riparian shrub site, where soils thawed four weeks before leaf out (12 May). Soil moisture at the riparian shrub site was relatively constant and remained high in the deeper soils [(64–77% Volumetric Water Content (VWC)] for the duration of the growing season. Shrub roots at the riparian shrub site extended deep into the alluvium with the majority of roots extending below 15 cm. In contrast, at the tundra shrub site the majority of shrub roots were primarily in the organic layer (<10 cm) and extending into the top of the mineral layer (~15 cm). The riparian shrub site soils thawed earlier (~25 days) than the tundra shrub soils at all depths and were unfrozen for the entire growing season. Soils at the tundra shrub site thawed more slowly and remained colder throughout the growing season (3–7°C colder than the riparian site). Snowmelt water did not penetrate into deeper soils (>10 cm) at the tundra shrub site, presumably because they were frozen and impermeable during the snowmelt period. Precipitation in July increased surface soil moisture after the relatively dry late-May and June period.

Shallow (< 12 cm) soil temperatures increased from near 0°C in early June to 14°C at the riparian shrub site and to 10°C at the tundra shrub site by mid-July before returning to 0°C by September (Fig. 2.3). The tundra shrub site soils were colder (4–6°C) throughout the season at each soil depth compared to the riparian shrub site soils (Fig. 2.3). At the tundra shrub site, shallow (0–12 cm) and intermediate (12–24 cm) soils were unfrozen for the entire growing season, but deep (24–36 cm) soils did not fully thaw until 5 July. Soil moisture was more stable at the riparian shrub site, whereas the tundra shrub site showed moisture increases at all depths over the season.

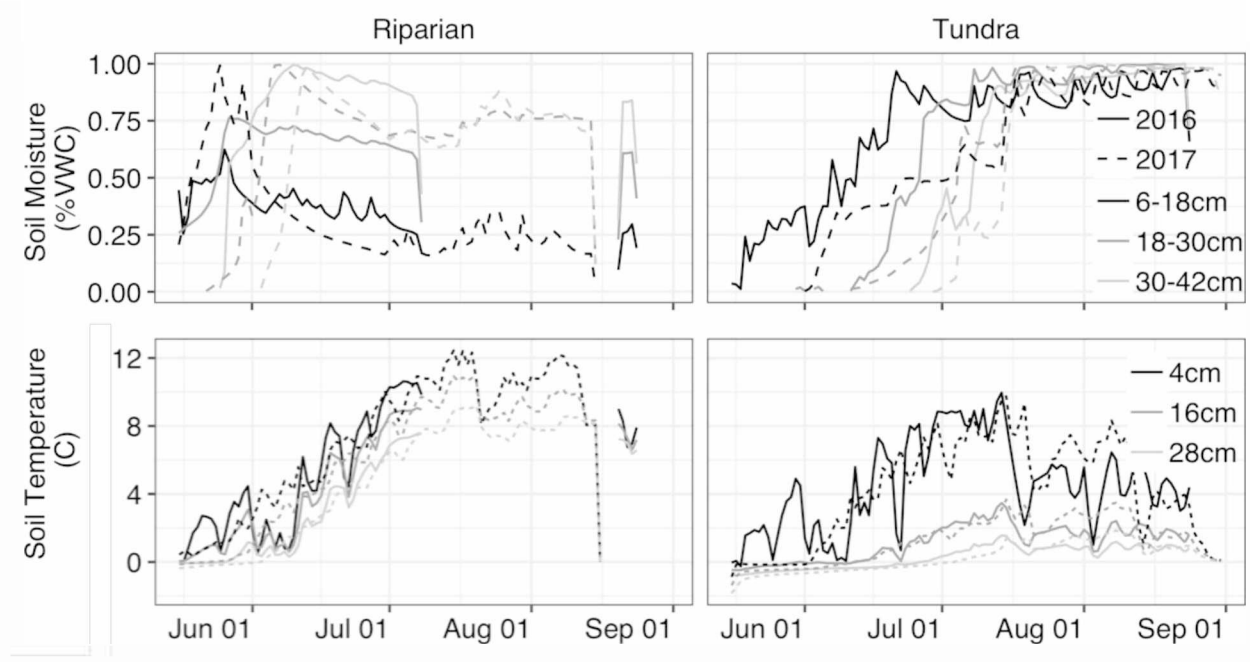

Figure 2.3. Daily soil moisture (% volumetric water content) and temperature data from riparian shrub and tundra shrub sites for 2016 and 2017. Soil moisture is vertically integrated 6-18 cm (black), 18-30 cm (dark grey), and 30-42 cm (light grey). Soil temperature was measured at 4 cm (black), 16 cm (dark grey), and 28 cm (light grey).

2.4.2 Shrub Growth Trends

Following snowmelt in mid-May, leaf area began to increase in mid-June and peaked in mid-July (tundra shrub site) and early August (riparian shrub site) in both years (Fig. 2.2). In mid-August (both sites), leaf area declined in conjunction with leaf senescence. Leaf-out date was the same at both sites (19 June), but maximum leaf area was earlier at the tundra shrub site (24 July) than at the riparian shrub site (7 August) in 2017. Leaf area at the riparian shrub site continued to increase from leaf-out until nearly the end of the growing season, whereas leaf area at the tundra shrub site peaked early in the growing season and maintained peak leaf area until near the end of the season. The riparian shrub site had much greater average LAI (1.20 m^2m^{-2}) than the tundra shrub site (0.092 m^2m^{-2}). In 2016, the tundra shrub site experienced three frost events (21 June, 22–24 July, and 3–5 August) that caused some leaf yellowing, suggesting damage. No growing season frost events or leaf damage were recorded for the riparian site in 2016 or at either site in 2017. Season-ending snowfall and freezing temperatures occurred on 28 August 2016 and 14 August 2017, respectively.

2.4.3 Shrub Transpiration

Seasonal trends in shrub transpiration rates (T) were similar between the sites (Fig. 2.4). Transpiration increased rapidly with increasing LAI in the early season at both sites leading to peak shrub T in the early season (63 mm riparian site; 6.8 mm tundra site). Transpiration at the riparian shrub site declined in mid- and late season (45 mm and 37 mm, respectively) while the tundra shrub site increased slightly in mid-season (6.9mm) and declined in the late season (4.0mm). Season total shrub T and average T rates at the riparian shrub site (107 mm, 0.22 mm hr^{-1}) were an order of magnitude greater than total shrub T and T rates at the tundra shrub site (12 mm, 0.03 mm hr^{-1}; Table 2.2).

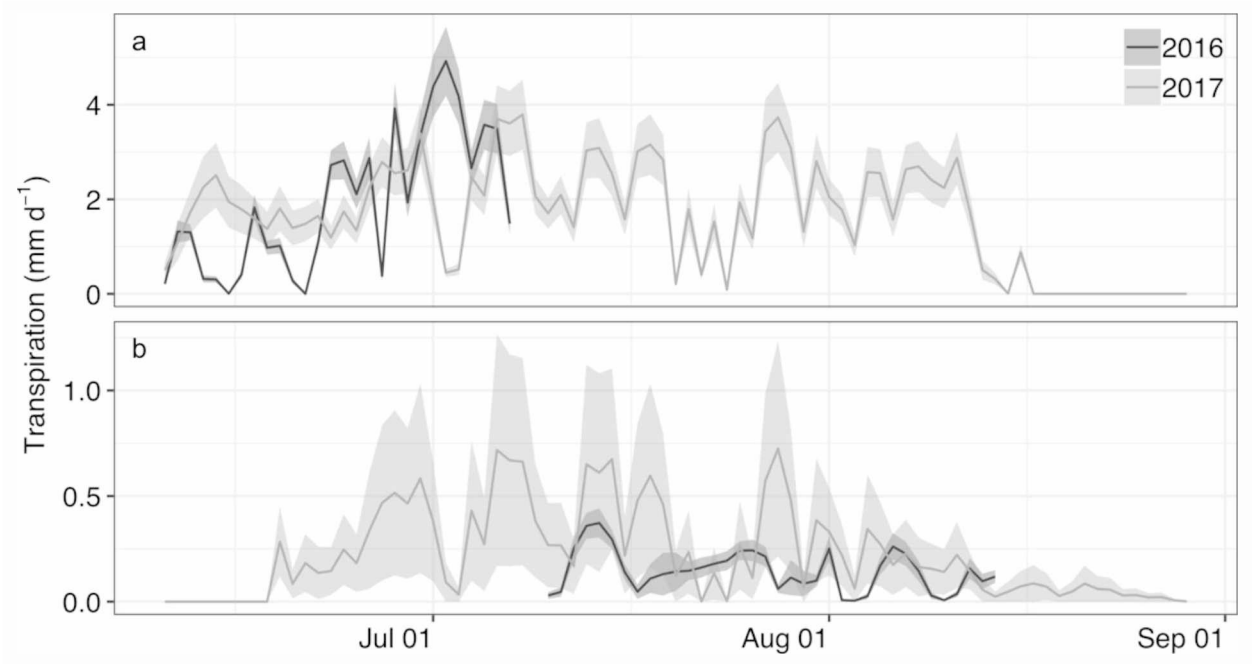

Figure 2.4. Daily shrub transpiration from the (a) riparian shrub and (b) tundra shrub site for 2016 and 2017. Lines are mean transpiration across stems; shaded areas are ± 1 standard error of mean transpiration. Note the differing ranges for the Y axes.

Hourly sap flow showed diurnal, seasonal, and interannual variability but was consistently correlated with air temperature, D, and Rn (Fig. 2.5). The diurnal patterns in T followed the diurnal patterns in the environmental variables (Fig. 2.5). During June and early July, the average shortwave radiation at solar midnight was 16 W m^{-2}, and the average T was 0.005 mm hr^{-1} at the riparian shrub site and 0.0002 mm hr^{-1} at the tundra shrub site. The average

shortwave radiation at solar noon was 495 W m^{-2} and the average *T* was 0.173 mm hr^{-1} at the riparian site and 0.0241 mm hr^{-1} at the tundra shrub site.

Total daily *T* was highly variable, ranging from 0.007 mm d^{-1} to 3.79 mm d^{-1} at the riparian site and from 0.001 mm d^{-1} to 0.72 mm d^{-1} at the tundra shrub site. In 2017, average daily *T* was 1.65 mm d^{-1} at the riparian shrub site and 0.22 mm d^{-1} at the tundra shrub site. The greatest average daily *T* occurred during mid-season for both the riparian shrub site (2.04 mm d^{-1}) and the tundra shrub site (0.35 mm d^{-1}), while the early growing season rates were intermediate (1.98 mm d^{-1}, 0.24 mm d^{-1}) and the late-growing season rates were lowest (1.10 mm d^{-1}, 0.13 mm d^{-1}). Typically, maximum *T* occurred when *Rn* and *D* were high at both sites (Fig. 2.5). At the riparian shrub site, the highest 90th percentile T rates (>0.336 mm hr^{-1}) occurred when *D* was high (1.08 kPa) and *Rn* was high (246 W m^2). At the tundra shrub site, the highest 90th percentile *T* (>0.103 mm hr^{-1}) occurred when both *D* and *Rn* were high (1.13 kPa, 247 W m^2, respectively).

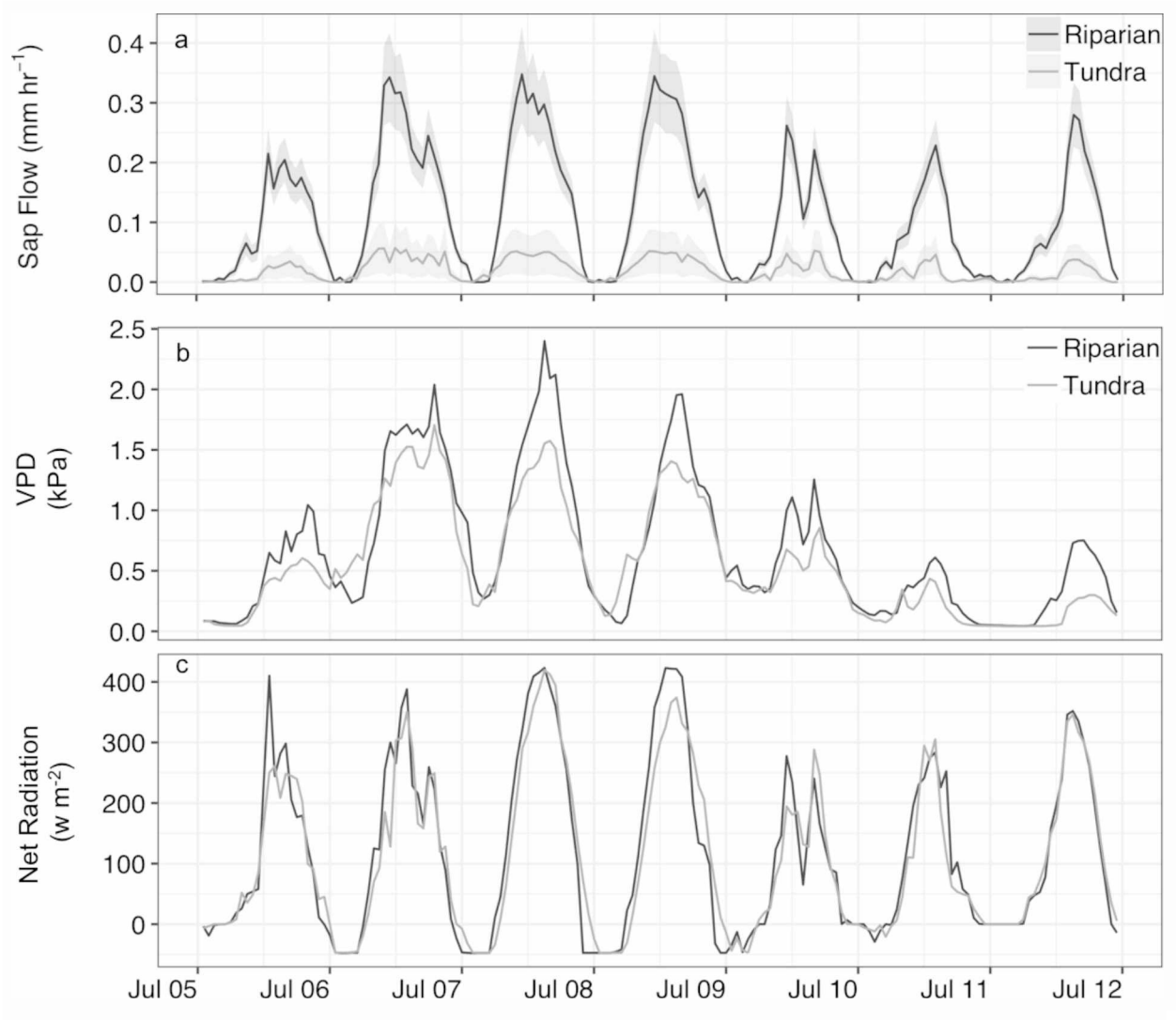

Figure 2.5. One-week subset of hourly (a) sap flow (F), (b) vapor pressure deficit (D), and (c) net radiation (Rn) data from the riparian shrub site and tundra shrub site. The top panel shows mean stem sap flow (lines) and standard error of the mean (shaded).

For 2016, T data were only available for the early season at the riparian site and mid to late season at the tundra shrub site. Early season average daily T and total T at the riparian site were similar in 2016 (1.92 mm d^{-1} and 53.8 mm, respectively) and 2017 (1.98 mm d^{-1} and 57.6 mm, respectively). At the tundra shrub site, both average daily T and total T were lower for the mid-season in 2016 (0.18 mm d^{-1} and 3.36 mm, respectively) than in 2017 (0.35 mm d^{-1} and 6.95 mm, respectively). Average daily T and total T at the tundra shrub site were also lower for the late season in 2016 (0.11 mm d^{-1} and 1.83 mm, respectively) than 2017 (0.13 mm d^{-1} and 4.14 mm, respectively).

2.4.4 Model Development and Selection

The individual effects model with the seasonal parameter for leaf area index (*LAI*) (Eq. 6) consistently performed better than both the individual effects model without the seasonal parameter (Eq. 4) and the random error model (Eq. 3). For both sites and years, the final model contained an intercept term and *D*, *Rn* and *LAI* as covariates:

$$\mu_{t,i} = b_0 + b_{1,stem,season} * LAI_i + b_{2,stem} * D_i + b_{n,stem} R_{n_i} \quad (7).$$

The final model included time-varying effects for leaf area to account for the seasonal changes in leaf area and their effect on *T* (Table 2.3). The leaf area parameter was significant in the early season for both sites and also significant in the mid-season for the tundra shrub site. Shallow soil temperature and radiometric surface temperature increased model fit slightly, but had poor convergence and significant correlations with each other and other model variables. Inclusion of soil moisture (all depths) and *P* did not improve model fit.

2.4.5 Modeling Riparian Shrub Site

In the final model for the riparian shrub site (Table 2.3), *Rn*, *D*, and *LAI* explained 85% of the variability in *T* rates ($\hat{T}$ = 0.07 + 0.85 * *T*, Fig. 2.6). *T* was under-predicted at higher observed rates (> 0.18 mm hr^{-1}) and over-predicted at lower observed rates (≤ 0.18 mm hr^{-1}). Under average *D*, *LAI*, and *Rn* conditions, the mean $\hat{T}$ was 0.26 mm hr^{-1} (Fig. 2.7). Net radiation had a positive effect on *T* and interacted with *D* and *LAI*. A negative interaction between *Rn* and *D* served to attenuate the effects of each parameter at higher values.

The 2016 and 2017 subset model fits were similar for the riparian shrub site. Most model parameters were not significantly different between years (Table 2.3). The effect of *D* and the *D* * *LAI* interaction were significant in the 2017 subset but not the 2016 subset. The estimated $\hat{T}$ under average environmental conditions in the 2016 subset was 33% lower than the 2017 subset (0.18 mm h^{-1} vs. 0.27 mm h^{-1}).

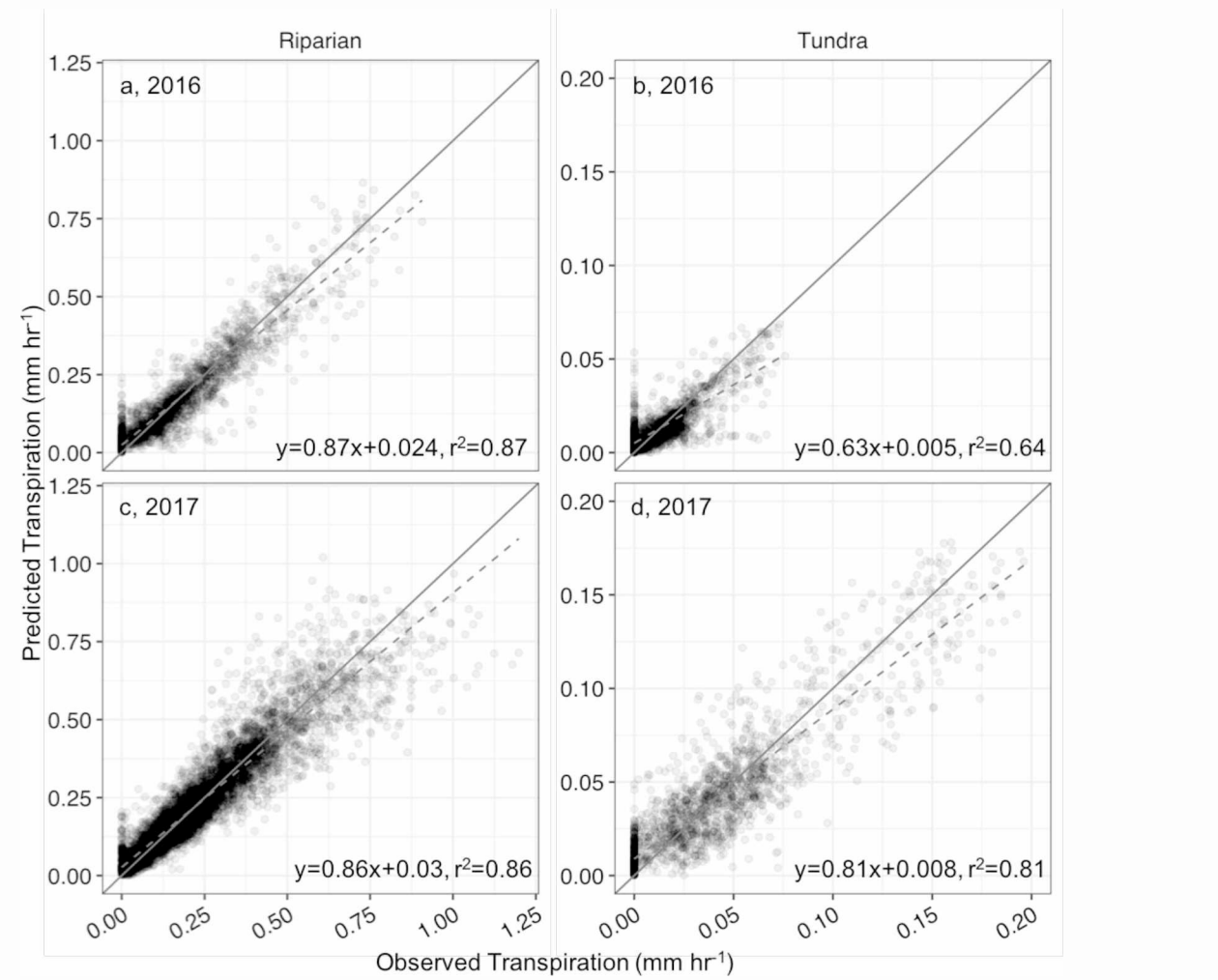

Figure 2.6. Observed T and predicted $\hat{T}$ rate from model for (a) riparian shrub in 2016, (b) tundra shrub in 2016, (c) riparian shrub in 2017, and (d) tundra shrub in 2017. Solid line is 1:1; dashed line is model fit.

2.4.6 Modeling Tundra Shrub Site

In the final model for the tundra shrub site, *Rn*, *D*, and *LAI* (Table 2.4) explained 85% of the variability in T ($\hat{T}$ = 0.007 + 0.846 * T, Fig. 2.6). T was under-predicted at higher values (> 0.028 mm h^{-1}) and over-predicted only at lowest values (≤ 0.028 mm h^{-1}). With average *Rn* and *LAI*, the mean $\hat{T}$ in the 2017 model was 0.050 mm h^{-1} (intercept term; Fig. 2.7). Large variation in transpiration between stems resulted in parameter estimates with wide credible intervals, particularly for the intercept, *Rn*, *D* and *LAI* terms in 2017 (Table 2.4). Net radiation had a positive effect on $\hat{T}$ and interacted with *LAI*.

The 2017 and 2016 subset model fits were similar. Most model parameters were not significantly different between the subset models (Table 2.4). In the 2017 model, the *Rn* parameter was significant while in 2016 the *D* parameter was significant. The estimated $\hat{T}$ under mean conditions in 2016 subset was 78% lower than 2017 subset (0.012 mm h^{-1}, 0.054 mm h^{-1}).

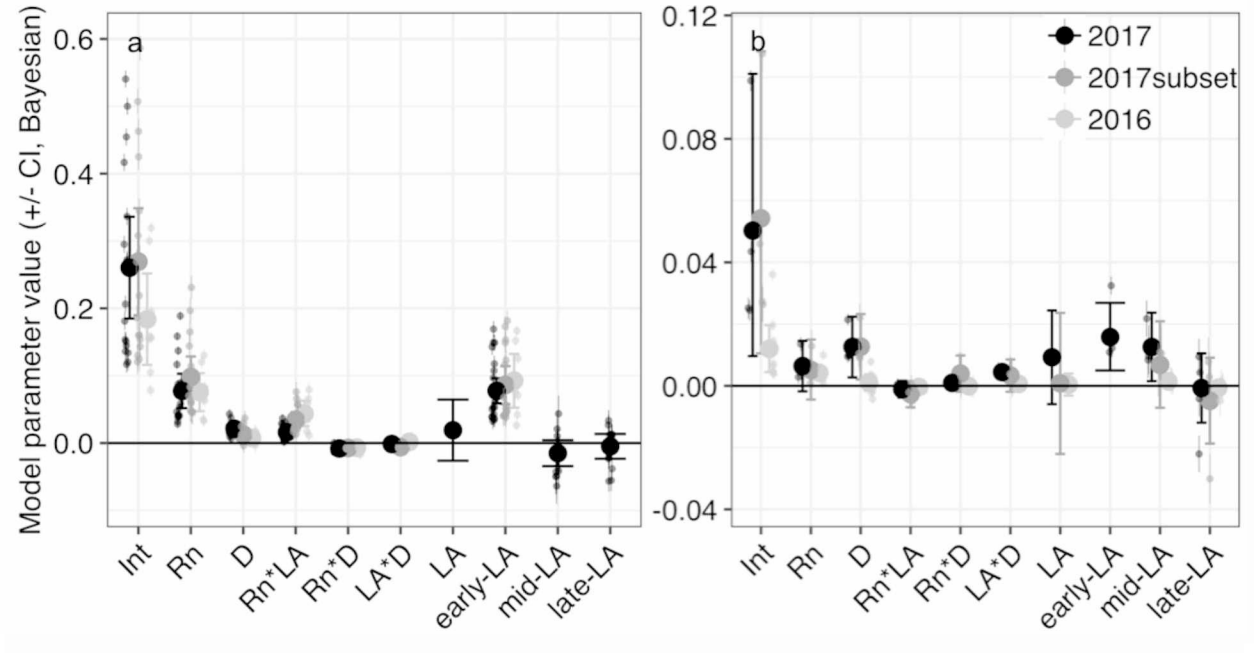

Figure 2.7. Parameters for shrub transpiration model at (a) the riparian shrub site and (b) the tundra shrub site for each time period. Large points and error bars are mean parameter values, and small points and error bars are stem-level parameters. The model intercept (*Int*) represents shrub transpiration rate (mm hr^{-1}) under mean conditions. Net radiation (*Rn*), vapor pressure deficit (*D*), leaf area index (early-, mid-, late-*LAI*), and interaction terms are also shown.

2.5 Discussion

The purpose of this study was to quantify shrub sap flow and transpiration in an arctic ecosystem. I show that arctic shrub transpiration (*T*) in two contrasting shrub communities in Arctic Alaska ranged from approximately 10% of summer ET in a tundra shrub community to a majority of possible summer ET in a riparian shrub community (Fig. 2.8). Transpiration was strongly influenced by *D*, *Rn* and *LAI*, showing limited evidence of transpiration suppression, suggesting that arctic shrub productivity is energy-limited. Consequently, increasing *D*, *Rn*, or growing season length associated with regional climate change should increase shrub productivity, as suggested by experimental and shrub dendrochronological studies (Ackerman et al., 2017; Chapin et al., 1995). Results here also indicate that observed and predicted increases

in deciduous shrubs have potential to increase ET. Shrub expansion has occurred throughout the Arctic (Frost and Epstein, 2014; Myers-Smith, 2011; Sturm et al., 2001; Tape et al., 2006) and is predicted to continue. This phenomenon has been largely attributed to increases in air and soil temperature but is also linked to changes in precipitation, snowpack, soil moisture and nutrient availability (Elmendorf et al., 2012; Myers-Smith et al., 2015; Sturm et al., 2005; Tape et al., 2012; Wrona et al., 2016). Our findings allow us to parse ET into shrub and non-shrub contributions, which will inform future models and predictions of arctic vegetation and water balance responses to climate change.

2.5.1 Role of Shrubs in Arctic Water Balance

The tundra shrub site was situated at Imnaviat Creek watershed, a small arctic watershed with a multi-decadal history of hydrologic (Kane et al., 2004), biogeographic (Walker and Walker, 1996), and, more recently, ecosystem study (Euskirchen et al., 2012). Our measurement of T (12mm) from two dominant erect woody shrub species accounts for 12% of the average estimated summer ET measured previously by eddy covariance (157 mm, Euskirchen et al., 2012), or 10% of the average estimated summer ET (179 mm) from hydrologic studies (Hinzman et al., 1996). The riparian shrub site, in contrast, had very similar weather, but approximately an order-of-magnitude greater LAI and T. The ET at the riparian shrub site is unknown, but the shrub T component at the riparian shrub site (107mm) would constitute 60-68% of the ET measured at the tundra shrub site (157-179 mm).

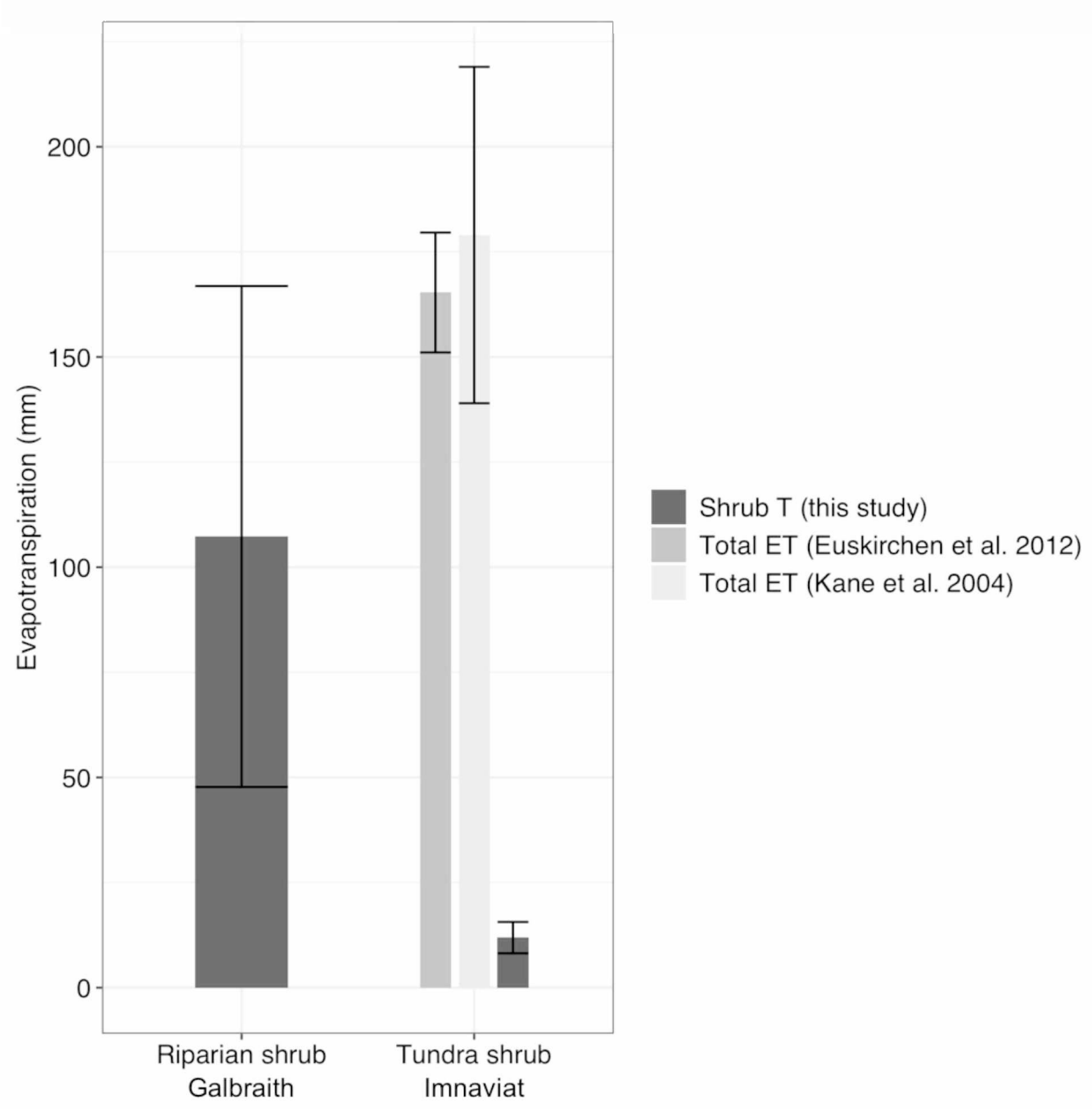

Figure 2.8. Comparison of ET measurements for Imnavait Creek watershed (Euskirchen et al., 2012; Kane et al., 2004) and sap flow derived T from woody shrubs (this study). Error bars are standard deviation. A large range in shrub T, reflected in differences in shrub LAI, is evident.

2.5.2 Stomatal Control in Arctic Shrubs

Many sap flow studies from non-arctic ecosystems have found that stomatal closure limits transpiration at higher D values and under soil water limitation (Oren et al., 1999). Due to stomatal control, the relationship between transpiration and D has been found to be nonlinear and asymptotic. Various thresholds of D (0.6–1.8 kPa) have been proposed as the point at which

stomata begin to limit plant transpiration (Oren et al., 1999; Pataki et al., 2000). In contrast, in our system I found that *T* increases linearly with both *D* and *Rn*, and thus *T* was greatest when *D* was high and peak *D* was greater than 1.8 kPa (Figs. 2.9 & 2.10). Transpiration of the three shrub species (*S. alaxensis, S. planifolia* ssp. *pulchra,* and *B. nana*) growing in the low Arctic of Alaska was limited by available energy (*Rn*) and atmospheric demand (*D*) without evidence of soil water limitation. The tundra shrub site has characteristically wet soils, and though the riparian shrub site has drier soils, the riparian shrubs are likely accessing groundwater or the hyporheic zone. The addition of soil moisture or precipitation to the transpiration model did not contribute significantly to explaining variation in *T*, which is strong evidence that soil water potential is not limiting *T*. Perhaps with reduced soil moisture and longer, drier atmospheric conditions (i.e. reduced *P*, reduced cloudiness, increased air temperature, increased *D*), the tundra shrubs measured in this study would show stomatal closure and reduced *T*. Both the eddy covariance and hydrologic studies near the tundra shrub site measured a positive water balance of 27–100+ mm, offering more evidence for an abundance of soil water for summer transpiration (Euskirchen et al., 2012; Kane et al., 2004).

Dendrochronology work with *S. pulchra* found positive relationships between ring width index and current year summer air temperature at both a riparian and upland site in the adjacent upper Kuparuk watershed; however, this work did not find a significant relationship with current or past precipitation (Ackerman et al., 2017). This supports our findings that *P* (and, in our case, soil moisture) was a not significant factor for predicting tundra shrub growth or *T*. While Idid find positive significant effects of air temperature on shrub hourly *T*, the explanatory power of *Rn* and *D* were much greater. That plants responded more directly to *Rn* and *D* is understandable as both are key physical components of both photosynthesis and transpiration, while air temperature is only related indirectly.

Though many tundra sites have not experienced significant vegetation change in response to ambient or experimental warming, shrub abundance and height have been found to respond positively to warming (Bjorkman et al., 2019; Elmendorf et al., 2012; Myers-Smith et al., 2015). Early tundra warming experiments conducted near the Toolik Field Station recorded large increases in *B. nana* biomass in both controls and in warming treatments (Chapin et al., 1995;

Hobbie and Chapin, 1998). The mechanism for increase in % shrub cover in these warming studies was attributed to temperature- and litter-induced changes in nutrient mineralization, but increased air temperatures still warmed the soil, increased thaw depth, and increased deciduous shrub biomass (Hobbie and Chapin, 1998). The tussock tundra community used in the warming studies had a different species mix from our study; notably, *S. pulchra* was absent from the warming studies. Our study included both *B. nana* and *S. pulchra* and Iwould predict both to increase with warming.

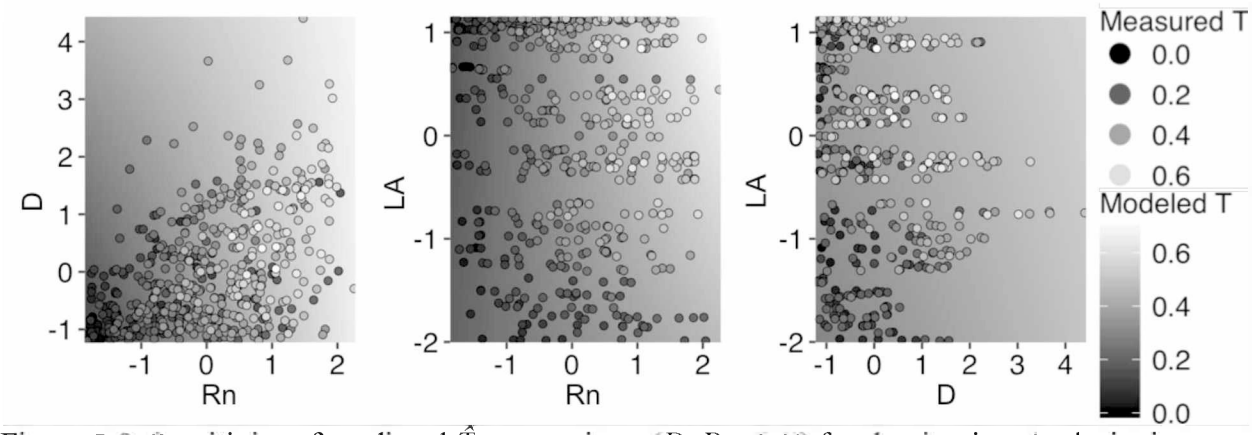

Figure 2.9. Sensitivity of predicted $\hat{T}$ to covariates (*D*, *Rn*, *LAI*) for the riparian shrub site in 2017. Background gradients represent modeled $\hat{T}$ sensitivity to covariates (low $\hat{T}$ to high $\hat{T}$, dark to light). Points represent/show measured T with the same gradient. Covariate values are mean centered and scaled by standard deviation.

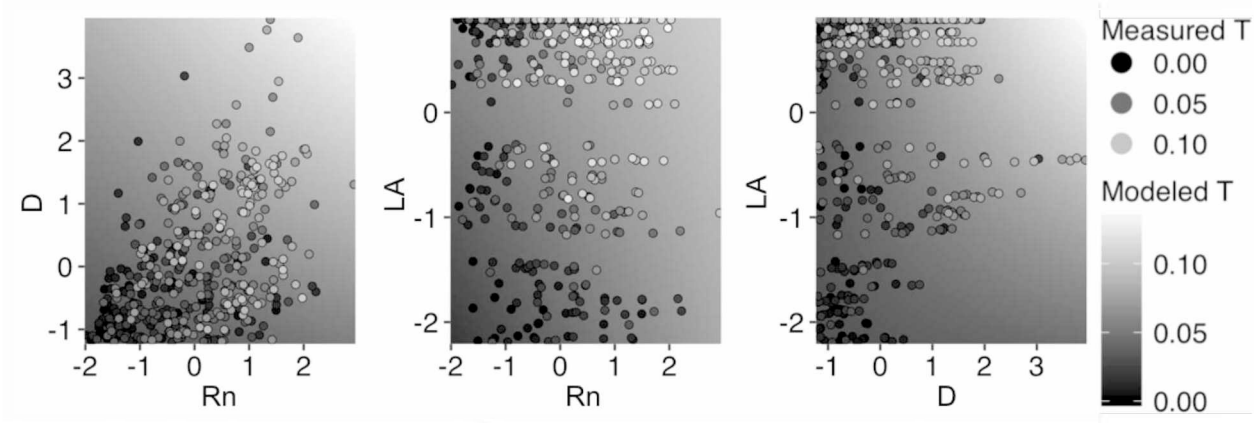

Figure 2.10. Sensitivity of predicted $\hat{T}$ to covariates (*D*, *Rn*, *LAI*) for the tundra shrub site in 2017. Background color gradients represent modeled $\hat{T}$ sensitivity to covariates (low $\hat{T}$ to high $\hat{T}$, dark to light). Points represent measured T with the same gradient. Covariate values are mean centered and scaled by standard deviation.

2.5.3 Shrub Expansion and Intensification of Hydrologic Cycle

Longer growing seasons have likely increased shrub productivity and transpiration in the Arctic. Since shrub T was limited by Rn and D, increasing the number of days (or hours) when Rn and D are sufficient would increase total transpiration. At both sites, a period of 2–4 weeks separates snowmelt and leaf-out dates. During this period shallow soils are thawed, and D, solar radiation, and daytime air temperatures appear to be suitable for transpiration, but freezing nighttime temperatures may be prohibiting leaf development. In our time-lapse leaf area images, swollen leaf buds were visible up to two weeks before leaf-out, but leaves only emerged after a few above-freezing nights. The significance of the leaf area model parameter in the early growing season indicates the reliance of leaf development on T during the early season. Earlier snowmelt is increasing the growing season length by shifting the albedo change and surface energy balance change earlier in the season, leading to warmer air temperature, earlier soil thaw (Hinzman et al., 2013), and earlier leaf-out (Pearson et al., 2013).

The riparian shrub site had much higher LAI and T rates in a very similar atmospheric environment to the tundra shrub site. The riparian shrub site suggests that, given the greater leaf area associated with more or larger shrubs, meteorological conditions in the Arctic exist for much greater transpiration flux than the T measured at the tundra shrub site in this study. As part of the intensification of the hydrologic cycle in arctic tundra, increasing air temperature is predicted to positively affect ET (Bring et al., 2016; Lique et al., 2016; Rawlins et al., 2010). Arctic shrubs are capitalizing on warmer and longer growing conditions, as shown in many studies (e.g. Myers-Smith et al., 2015), by increasing transpiration and contributing to soil drying (Hinzman et al., 2013; Lawrence et al., 2015). Transitions from tundra to shrubland are also predicted to increase ET (Nauta et al., 2015; Pearson et al., 2013), and our results confirm that increasing shrub cover will likely increase transpiration, though the contributions from other species remains unquantified. The profound difference between shrub transpiration at our contrasting shrub sites suggests that the magnitude of increases in ET depends strongly on the size of shrubs.

2.5.4 Interannual Meteorological Differences Affect Model Parameter Estimates

I speculate that the difference in meteorological conditions between years contributed to the differences in the significance of the model parameter estimates. The cooler and wetter conditions of 2016 (i.e. lower *Rn*, lower *D*, higher *P*) led to a 30%–80% decrease in measured *T* compared to the same dates in 2017. Furthermore, at the tundra shrub site in 2016, there were three frost events (one each in the early, middle, and late parts of the growing season) that led to reduced leaf area, leaf yellowing, decreased productivity, and possibly affected hydraulic conductance. Similarly, in 2015 (no data presented here), there was widespread frost damage to leaves from an early frost event after leaf out (mid-June, personal observation). In 2017 there were no frost events that affected leaf area or caused visual damage. Growing season frost events, or the lack thereof, may be a significant factor influencing transpiration fluxes at the decadal scale (Epstein et al., 2004).

2.5.5 Sources of Transpiration Variability

The high variability in *T* rate among stems, even after *T* was normalized by leaf area (Fig. 2.4), indicates that there are microscale factors, such as edaphic or physical disparities between stems, that are driving *T* differences. I measured soil temperature and moisture in three replicate soil pits and at three replicate depths, but the soil pits do not necessarily capture the soil conditions at the base of a given stem. There was also a large range in leaf-area to stem-area ratios and presumably a large range in leaf-to-root ratios and varying levels of browse damage that could explain the observed variability. More direct measures of transpiration and conductance (e.g. leaf porometer, chamber measurements) and hourly leaf and stem water potential would clarify physiological status and stomatal response of the study plants. Furthermore, more accurate measurement of the canopy and leaf environment, rather than at standard measurement heights, may help to better understand transpiration of short-statured tundra plants.

2.5.6 Non-Shrub Species Contributions to ET?

At both sites, I measured *T* for the largest and most conspicuous shrub species; however, each watershed contains many additional species that are contributing to ET. At the tundra shrub site, the other plant growth forms (e.g., graminoids, forbs and evergreen shrubs) in that watershed—including bryophytes—apparently account for a much larger proportion of ET than

the measured shrubs. At the riparian shrub site, where shrub T was an order-of-magnitude greater, it is unclear what the contributions are from other growth forms or land surfaces, because there are no landscape ET measurements for comparison, and the understory is sparse with much soil and gravel exposed. Increasing shrub cover or size and the connected increase leaf area index is likely to increase ET. Further research is needed to better quantify the components of ET in relation to environmental factors since T and E for individual species will respond differently to changing conditions.

2.6 Conclusion

Our study presents continuous hourly transpiration from 40 stems of three tundra shrub species over two growing seasons in the Arctic. Our study sacrificed spatial integration of ET for fine temporal resolution by directly measuring sap flow, calculating transpiration, and modeling individual shrubs at the hourly time scale. Compared to temporally discrete methods of transpiration measurements, the continuous hourly data in this study provide magnitudes more temporal detail from two sites. Furthermore, to begin the process of parsing ET contributions from functional groups, our approach quantifies the shrub component of ET. A better understanding of transpiration in the Arctic is needed because changes in vegetation and transpiration directly affect heat transfer to permafrost and the carbon stored within it.

2.7 References

Abramoff, M.D., Magalhães, P.J., Ram, S.J., 2004. Image processing with ImageJ [WWW Document]. Biophotonics Int. URL http://dspace.library.uu.nl/handle/1874/204900 (accessed 5.21.19).

Ackerman, D., Griffin, D., Hobbie, S.E., Finlay, J.C., 2017. Arctic shrub growth trajectories differ across soil moisture levels. Glob. Change Biol. 23, 4294–4302. https://doi.org/10.1111/gcb.13677

Allen, S.J., Grime, V.L., 1995. Measurements of transpiration from savannah shrubs using sap flow gauges. Agric. For. Meteorol. 75, 23–41. https://doi.org/10.1016/0168-1923(94)02201-T

Baldocchi, D., Kelliher, F.M., Black, T.A., Jarvis, P., 2000. Climate and vegetation controls on boreal zone energy exchange. Glob. Change Biol. 6, 69–83. https://doi.org/10.1046/j.1365-2486.2000.06014.x

Bjorkman, A.D., García Criado, M., Myers-Smith, I.H., Ravolainen, V., Jónsdóttir, I.S., Westergaard, K.B., Lawler, J.P., Aronsson, M., Bennett, B., Gardfjell, H., Heiðmarsson, S., Stewart, L., Normand, S., 2019. Status and trends in Arctic vegetation: Evidence from experimental warming and long-term monitoring. Ambio. https://doi.org/10.1007/s13280-019-01161-6

Bring, A., Fedorova, I., Dibike, Y., Hinzman, L., Mård, J., Mernild, S.H., Prowse, T., Semenova, O., Stuefer, S.L., Woo, M.-K., 2016. Arctic terrestrial hydrology: A synthesis of processes, regional effects, and research challenges. J. Geophys. Res. Biogeosciences 121, 2015JG003131. https://doi.org/10.1002/2015JG003131

Chapin, F.S., Shaver, G.R., Giblin, A.E., Nadelhoffer, K.J., Laundre, J.A., 1995. Responses of Arctic Tundra to Experimental and Observed Changes in Climate. Ecology 76, 694–711. https://doi.org/10.2307/1939337

Curtis, S., 2015. mcmcplots: Create plots from MCMC output. R Package Version 04 2.

Dawson, T.E., Burgess, S.S.O., Tu, K.P., Oliveira, R.S., Santiago, L.S., Fisher, J.B., Simonin, K.A., Ambrose, A.R., 2007. Nighttime transpiration in woody plants from contrasting ecosystems. Tree Physiol. 27, 561–575. https://doi.org/10.1093/treephys/27.4.561

Elmendorf, S.C., Henry, G.H.R., Hollister, R.D., Björk, R.G., Bjorkman, A.D., Callaghan, T.V., Collier, L.S., Cooper, E.J., Cornelissen, J.H.C., Day, T.A., Fosaa, A.M., Gould, W.A., Grétarsdóttir, J., Harte, J., Hermanutz, L., Hik, D.S., Hofgaard, A., Jarrad, F., Jónsdóttir, I.S., Keuper, F., Klanderud, K., Klein, J.A., Koh, S., Kudo, G., Lang, S.I., Loewen, V., May, J.L., Mercado, J., Michelsen, A., Molau, U., Myers-Smith, I.H., Oberbauer, S.F., Pieper, S., Post, E., Rixen, C., Robinson, C.H., Schmidt, N.M., Shaver, G.R., Stenström, A., Tolvanen, A., Totland, Ø., Troxler, T., Wahren, C.-H., Webber, P.J., Welker, J.M., Wookey, P.A., 2012. Global assessment of experimental climate warming on tundra vegetation: heterogeneity over space and time. Ecol. Lett. 15, 164–175. https://doi.org/10.1111/j.1461-0248.2011.01716.x

Epstein, H.E., Calef, M.P., Walker, M.D., Chapin, F.S., Starfield, A.M., 2004. Detecting changes in arctic tundra plant communities in response to warming over decadal time scales. Glob. Change Biol. 10, 1325–1334. https://doi.org/10.1111/j.1529-8817.2003.00810.x

Euskirchen, E.S., Bret-Harte, M.S., Scott, G.J., Edgar, C., Shaver, G.R., 2012. Seasonal patterns of carbon dioxide and water fluxes in three representative tundra ecosystems in northern Alaska. Ecosphere 3. https://doi.org/10.1890/ES11-00202.1

Euskirchen, E.S., McGuire, A.D., Chapin, F.S., Yi, S., Thompson, C.C., 2009. Changes in vegetation in northern Alaska under scenarios of climate change, 2003–2100: implications for climate feedbacks. Ecol. Appl. 19, 1022–1043. https://doi.org/10.1890/08-0806.1

Ewers, B.E., Mackay, D.S., Samanta, S., 2007. Interannual consistency in canopy stomatal conductance control of leaf water potential across seven tree species. Tree Physiol. 27, 11–24. https://doi.org/10.1093/treephys/27.1.11

Ewers, B.E., Oren, R., 2000. Analyses of assumptions and errors in the calculation of stomatal conductance from sap flux measurements. Tree Physiol. 20, 579–589. https://doi.org/10.1093/treephys/20.9.579

Fernandes, R., Korolevych, V., Wang, S., 2007. Trends in Land Evapotranspiration over Canada for the Period 1960–2000 Based on In Situ Climate Observations and a Land Surface Model. J. Hydrometeorol. 8, 1016–1030. https://doi.org/10.1175/JHM619.1

Frost, G.V., Epstein, H.E., 2014. Tall shrub and tree expansion in Siberian tundra ecotones since the 1960s. Glob. Change Biol. 20, 1264–1277. https://doi.org/10.1111/gcb.12406

Gelman, A., Carlin, J.B., Stern, H.S., Dunson, D.B., Vehtari, A., Rubin, D.B., 2013. Bayesian Data Analysis, Third Edition. CRC Press.

Haine, T.W.N., Curry, B., Gerdes, R., Hansen, E., Karcher, M., Lee, C., Rudels, B., Spreen, G., de Steur, L., Stewart, K.D., Woodgate, R., 2015. Arctic freshwater export: Status, mechanisms, and prospects. Glob. Planet. Change 125, 13–35. https://doi.org/10.1016/j.gloplacha.2014.11.013

Hinzman, L.D., Deal, C.J., McGuire, A.D., Mernild, S.H., Polyakov, I.V., Walsh, J.E., 2013. Trajectory of the Arctic as an integrated system. Ecol. Appl. 23, 1837–1868. https://doi.org/10.1890/11-1498.1

Hinzman, L.D., Kane, D.L., Benson, C.S., Everett, K.R., 1996. Energy Balance and Hydrological Processes in an Arctic Watershed, in: Reynolds, J.F., Tenhunen, J.D. (Eds.), Landscape Function and Disturbance in Arctic Tundra, Ecological Studies. Springer Berlin Heidelberg, Berlin, Heidelberg, pp. 131–154. https://doi.org/10.1007/978-3-662-01145-4_6

Hobbie, J.E., Shaver, G.R., Rastetter, E.B., Cherry, J.E., Goetz, S.J., Guay, K.C., Gould, W.A., Kling, G.W., 2017. Ecosystem responses to climate change at a Low Arctic and a High Arctic long-term research site. Ambio 46, 160–173. https://doi.org/10.1007/s13280-016-0870-x

Hobbie, S.E., Chapin, F.S., 1998. The Response of Tundra Plant Biomass, Aboveground Production, Nitrogen, and Co2 Flux to Experimental Warming. Ecology 79, 1526–1544. https://doi.org/10.1890/0012-9658(1998)079[1526:TROTPB]2.0.CO;2

IPCC, 2013. Climate Change 2013: The Physical Science Basis: Working Group I Contribution to the Fifth Assessment Report of the Intergovernmental Panel on Climate Change. Cambridge University Press.

Kane, D.L., Gieck, R.E., Kitover, D.C., Hinzman, L.D., Mcnamara, J.P., Yang, D., 2004. Hydrological cycle on the North Slope of Alaska. North. Res. Basins Water Balance, IAHS Publications 13.

Kelliher, F.M., Lloyd, J., Arneth, A., Byers, J.N., McSeveny, T.M., Milukova, I., Grigoriev, S., Panfyorov, M., Sogatchev, A., Varlargin, A., Ziegler, W., Bauer, G., Schulze, E.-D., 1998. Evaporation from a central Siberian pine forest. J. Hydrol. 205, 279–296. https://doi.org/10.1016/S0022-1694(98)00082-1

Kropp, H., Loranty, M., Alexander, H.D., Berner, L.T., Natali, S.M., Spawn, S.A., 2017. Environmental constraints on transpiration and stomatal conductance in a Siberian Arctic boreal forest. J. Geophys. Res. Biogeosciences 122, 2016JG003709. https://doi.org/10.1002/2016JG003709

Lawrence, D.M., Koven, C.D., Swenson, S.C., Riley, W.J., Slater, A.G., 2015. Permafrost thaw and resulting soil moisture changes regulate projected high-latitude CO2and CH4emissions. Environ. Res. Lett. 10, 094011. https://doi.org/10.1088/1748-9326/10/9/094011

Lei, H., Zhi-Shan, Z., Xin-Rong, L., 2010. Sap flow of Artemisia ordosica and the influence of environmental factors in a revegetated desert area: Tengger Desert, China. Hydrol. Process. 24, 1248–1253. https://doi.org/10.1002/hyp.7584

Lique, C., Holland, M.M., Dibike, Y.B., Lawrence, D.M., Screen, J.A., 2016. Modeling the Arctic freshwater system and its integration in the global system: Lessons learned and future challenges. J. Geophys. Res. Biogeosciences 121, 2015JG003120. https://doi.org/10.1002/2015JG003120

Liu, B., Zhao, W., Jin, B., 2011. The response of sap flow in desert shrubs to environmental variables in an arid region of China. Ecohydrology 4, 448–457. https://doi.org/10.1002/eco.151

Moore, K.E., Fitzjarrald, D.R., Sakai, R.K., Goulden, M.L., Munger, J.W., Wofsy, S.C., 1996. Seasonal Variation in Radiative and Turbulent Exchange at a Deciduous Forest in Central Massachusetts. J. Appl. Meteorol. 35, 122–134. https://doi.org/10.1175/1520-0450(1996)035<0122:SVIRAT>2.0.CO;2

Muskett, R.R., Romanovsky, V.E., 2009. Groundwater storage changes in arctic permafrost watersheds from GRACE and in situ measurements. Environ. Res. Lett. 4, 045009. https://doi.org/10.1088/1748-9326/4/4/045009

Myers-Smith, I.H., Elmendorf, S.C., Beck, P.S.A., Wilmking, M., Hallinger, M., Blok, D., Tape, K.D., Rayback, S.A., Macias-Fauria, M., Forbes, B.C., Speed, J.D.M., Boulanger-Lapointe, N., Rixen, C., Lévesque, E., Schmidt, N.M., Baittinger, C., Trant, A.J., Hermanutz, L., Collier, L.S., Dawes, M.A., Lantz, T.C., Weijers, S., Jørgensen, R.H., Buchwal, A., Buras, A., Naito, A.T., Ravolainen, V., Schaepman-Strub, G., Wheeler, J.A., Wipf, S., Guay, K.C., Hik, D.S., Vellend, M., 2015. Climate sensitivity of shrub growth across the tundra biome. Nat. Clim. Change 5, 887–891. https://doi.org/10.1038/nclimate2697

Myers-Smith, I.H., Forbes, B.C., Wilmking, M., Hallinger, M., Lantz, T., Blok, D., Tape, K.D., Macias-Fauria, M., Sass-Klaassen, U., Lévesque, E., Boudreau, S., Ropars, P., Luise Hermanutz, Trant, A., Collier, L.S., Weijers, S., Rozema, J., Rayback, S.A., Schmidt, N.M., Schaepman-Strub, G., Wipf, S., Rixen, C., Ménard, C.B., Susanna Venn, Goetz, S., Andreu-Hayles, L., Elmendorf, S., Ravolainen, V., Welker, J., Paul Grogan, Epstein, H.E., Hik, D.S., 2011. Shrub expansion in tundra ecosystems: dynamics, impacts and research priorities. Environ. Res. Lett. 6, 045509. https://doi.org/10.1088/1748-9326/6/4/045509

Naithani, K.J., Ewers, B.E., Pendall, E., 2012. Sap flux-scaled transpiration and stomatal conductance response to soil and atmospheric drought in a semi-arid sagebrush ecosystem. J. Hydrol. 464–465, 176–185. https://doi.org/10.1016/j.jhydrol.2012.07.008

Nauta, A.L., Heijmans, M.M.P.D., Blok, D., Limpens, J., Elberling, B., Gallagher, A., Li, B., Petrov, R.E., Maximov, T.C., Huissteden, J. van, Berendse, F., 2015. Permafrost collapse after shrub removal shifts tundra ecosystem to a methane source. Nat. Clim. Change 5, 67. https://doi.org/10.1038/nclimate2446

Ogle, K., Barber, J.J., Barron-Gafford, G.A., Bentley, L.P., Young, J.M., Huxman, T.E., Loik, M.E., Tissue, D.T., 2015. Quantifying ecological memory in plant and ecosystem processes. Ecol. Lett. 18, 221–235. https://doi.org/10.1111/ele.12399

Oishi, A.C., Oren, R., Novick, K.A., Palmroth, S., Katul, G.G., 2010. Interannual Invariability of Forest Evapotranspiration and Its Consequence to Water Flow Downstream. Ecosystems 13, 421–436. https://doi.org/10.1007/s10021-010-9328-3

Oren, R., Phillips, N., Katul, G., Ewers, B.E., Pataki, D.E., 1998. Scaling xylem sap flux and soil water balance and calculating variance: a method for partitioning water flux in forests. Ann. Sci. For. 55, 191–216. https://doi.org/10.1051/forest:19980112

Oren, R., Sperry, J.S., Katul, G.G., Pataki, D.E., Ewers, B.E., Phillips, N., Schäfer, K.V.R., 1999. Survey and synthesis of intra- and interspecific variation in stomatal sensitivity to vapour pressure deficit. Plant Cell Environ. 22, 1515–1526. https://doi.org/10.1046/j.1365-3040.1999.00513.x

Park, H., Yamazaki, T., Yamamoto, K., Ohta, T., 2008. Tempo-spatial characteristics of energy budget and evapotranspiration in the eastern Siberia. Agric. For. Meteorol., Water and energy exchange in East Siberian forest 148, 1990–2005. https://doi.org/10.1016/j.agrformet.2008.06.018

Pataki, D.E., Oren, R., Smith, W.K., 2000. Sap Flux of Co-Occurring Species in a Western Subalpine Forest During Seasonal Soil Drought. Ecology 81, 2557–2566. https://doi.org/10.1890/0012-9658(2000)081[2557:SFOCOS]2.0.CO;2

Pavelsky, T.M., Smith, L.C., 2006. Intercomparison of four global precipitation data sets and their correlation with increased Eurasian river discharge to the Arctic Ocean. J. Geophys. Res. Atmospheres 111. https://doi.org/10.1029/2006JD007230

Pearson, R.G., Phillips, S.J., Loranty, M.M., Beck, P.S.A., Damoulas, T., Knight, S.J., Goetz, S.J., 2013. Shifts in Arctic vegetation and associated feedbacks under climate change. Nat. Clim. Change 3, 673. https://doi.org/10.1038/nclimate1858

Peterson, B.J., Holmes, R.M., McClelland, J.W., Vörösmarty, C.J., Lammers, R.B., Shiklomanov, A.I., Shiklomanov, I.A., Rahmstorf, S., 2002. Increasing River Discharge to the Arctic Ocean. Science 298, 2171–2173. https://doi.org/10.1126/science.1077445

Phillips, N., Oren, R., 1998. A comparison of daily representations of canopy conductance based on two conditional time-averaging methods and the dependence of daily conductance on environmental factors. Ann. Sci. For. 55, 217–235. https://doi.org/10.1051/forest:19980113

Plummer, M., 2003. JAGS: A program for analysis of Bayesian graphical models using Gibbs sampling. Proc. Distrib. Stat. Comput. 8.

Plummer, M., Stukalov, A., Denwood, M., 2016. Package 'rjags': Bayesian graphical models using mcmc. R Package Version 4–6.

Rawlins, M.A., Steele, M., Holland, M.M., Adam, J.C., Cherry, J.E., Francis, J.A., Groisman, P.Y., Hinzman, L.D., Huntington, T.G., Kane, D.L., Kimball, J.S., Kwok, R., Lammers, R.B., Lee, C.M., Lettenmaier, D.P., McDonald, K.C., Podest, E., Pundsack, J.W., Rudels, B., Serreze, M.C., Shiklomanov, A., Skagseth, Ø., Troy, T.J., Vörösmarty, C.J., Wensnahan, M., Wood, E.F., Woodgate, R., Yang, D., Zhang, K., Zhang, T., 2010. Analysis of the Arctic System for Freshwater Cycle Intensification: Observations and Expectations. J. Clim. 23, 5715–5737. https://doi.org/10.1175/2010JCLI3421.1

Romanovsky, V.E., Smith, S.L., Christiansen, H.H., 2010. Permafrost thermal state in the polar Northern Hemisphere during the international polar year 2007–2009: a synthesis. Permafr. Periglac. Process. 21, 106–116. https://doi.org/10.1002/ppp.689

Serreze, M.C., Bromwich, D.H., Clark, M.P., Etringer, A.J., Zhang, T., Lammers, R., 2002. Large-scale hydro-climatology of the terrestrial Arctic drainage system. J. Geophys. Res. Atmospheres 107, 8160. https://doi.org/10.1029/2001JD000919

Sturm, M., Holmgren, J., McFadden, J.P., Liston, G.E., Chapin, F.S., Racine, C.H., 2001. Snow–Shrub Interactions in Arctic Tundra: A Hypothesis with Climatic Implications. J. Clim. 14, 336–344. https://doi.org/10.1175/1520-0442(2001)014<0336:SSIIAT>2.0.CO;2

Sturm, M., Schimel, J., Michaelson, G., Welker, J.M., Oberbauer, S.F., Liston, G.E., Fahnestock, J., Romanovsky, V.E., 2005. Winter Biological Processes Could Help Convert Arctic Tundra to Shrubland. BioScience 55, 17–26. https://doi.org/10.1641/0006-3568(2005)055[0017:WBPCHC]2.0.CO;2

Tape, K., Sturm, M., Racine, C., 2006. The evidence for shrub expansion in Northern Alaska and the Pan-Arctic. Glob. Change Biol. 12, 686–702. https://doi.org/10.1111/j.1365-2486.2006.01128.x

Tape, K.D., Hallinger, M., Welker, J.M., Ruess, R.W., 2012. Landscape Heterogeneity of Shrub Expansion in Arctic Alaska. Ecosystems 15, 711–724. https://doi.org/10.1007/s10021-012-9540-4

Walker, D.A., Raynolds, M.K., Daniëls, F.J.A., Einarsson, E., Elvebakk, A., Gould, W.A., Katenin, A.E., Kholod, S.S., Markon, C.J., Melnikov, E.S., Moskalenko, N.G., Talbot, S.S., Yurtsev, B.A.(†), Team, T. other members of the C., 2005. The Circumpolar Arctic vegetation map. J. Veg. Sci. 16, 267–282. https://doi.org/10.1111/j.1654-1103.2005.tb02365.x

Walker, D.A., Walker, M.D., 1996. Terrain and Vegetation of the Imnavait Creek Watershed, in: Reynolds, J.F., Tenhunen, J.D. (Eds.), Landscape Function and Disturbance in Arctic Tundra, Ecological Studies. Springer Berlin Heidelberg, Berlin, Heidelberg, pp. 73–108. https://doi.org/10.1007/978-3-662-01145-4_4

Wilson, K.B., Hanson, P.J., Baldocchi, D.D., 2000. Factors controlling evaporation and energy partitioning beneath a deciduous forest over an annual cycle. Agric. For. Meteorol. 102, 83–103. https://doi.org/10.1016/S0168-1923(00)00124-6

Wrona, F.J., Johansson, M., Culp, J.M., Jenkins, A., Mård, J., Myers-Smith, I.H., Prowse, T.D., Vincent, W.F., Wookey, P.A., 2016. Transitions in Arctic ecosystems: Ecological implications of a changing hydrological regime. J. Geophys. Res. Biogeosciences 121, 2015JG003133. https://doi.org/10.1002/2015JG003133

Table 2.1. Environmental variables (mean and SD) for the riparian and tundra shrub sites in 2017 summer (June-August).

	Riparian shrub		Tundra shrub	
Variable	Mean	(SD)	Mean	(SD)
Air Temperature (C)	11.57	(5.48)	11.70	(4.73)
Relative Humidity (%)	67.75	(20.55)	71.13	(19.20)
Vapor Pressure Deficit (kPa)	0.54	(0.47)	0.48	(0.42)
Net Radiation (W m^{-2})	94.70	(136.51)	78.42	(115.67)
Precipitation (mm h^{-1})	0.08	(0.41)	0.11	(0.51)
Precipitation Total (mm)	149.86	-	156.46	-
Soil Moisture 1 (%VWC)	0.25	(0.09)	0.71	(0.19)
Soil Moisture 2 (%VWC)	0.76	(0.11)	0.69	(0.33)
Soil Moisture 3 (%VWC)	0.69	(0.22)	0.57	(0.43)
Soil Temperature 1 (°C)	8.63	(3.10)	6.56	(2.53)
Soil Temperature 2 (°C)	7.37	(2.78)	2.21	(0.88)
Soil Temperature 3 (°C)	5.80	(2.82)	0.72	(0.71)

Table 2.2. Summary of measured sap flow for the riparian and tundra shrub sites in 2016 and 2017. "Total hours" reflects the total number of hours the equipment recorded sap flow. "Transpiration (*T*) hours" reflects the total number of hours of sap flow used for summary totals and modeling. "Reported *T*" is scaled by leaf area (see Methods for details).

Site	Year	n stems	Total hours	Sap flow (kg)	T hours	T mm (sd)	T (mm hr^{-1})
Riparian shrub	2016	9	577	77.56	197	42.39 (18.49)	0.178
Riparian shrub	2017	17	1350	467.92	500	107.29 (59.58)	0.215
Tundra shrub	2016	10	1080	6.38	456	2.63 (2.06)	0.013
Tundra shrub	2017	4	1357	5.28	423	11.91 (3.73)	0.032

Table 2.3. Riparian shrub model parameter estimates. Bolded values are significantly different from 0.

	2017		2017 subset		2016 subset		
	mean	95% CI	mean	95% CI	mean	95% CI	
Int	**0.26**	**(0.185, 0.336)**	**0.269**	**(0.190, 0.349)**	**0.184**	**(0.1160, 0.252)**	**aa**
Rn	**0.077**	**(0.052, 0.103)**	**0.098**	**(0.068, 0.129)**	**0.076**	**(0.0473, 0.104)**	**aa**
D	**0.021**	**(0.015, 0.027)**	**0.013**	**(0.005, 0.020)**	0.008	(-0.0007, 0.016)	**aa**
Rn*LAI	**0.016**	**(0.010, 0.022)**	**0.034**	**(0.023, 0.046)**	**0.044**	**(0.0249, 0.063)**	**aa**
Rn*D	**-0.008**	**(-0.011, -0.005)**	**-0.007**	**(-0.010, -0.005)**	**-0.007**	**(-0.0124, -0.001)**	**aa**
LAI*D	-0.001	(-0.004, 0.001)	**-0.006**	**(-0.010, -0.002)**	0.002	(-0.0037, 0.007)	**aa**
LAI	0.019	(-0.026, 0.065)	**0.086**	**(0.058, 0.114)**	**0.093**	**(0.0525, 0.132)**	**aa**
LAI_1	**0.078**	**(0.059, 0.096)**	-	(-, -)	-	(-, -)	
LAI_2	-0.015	(-0.034, 0.004)	-	(-, -)	-	(-, -)	
LAI_3	-0.005	(-0.023, 0.014)	-	(-, -)	-	(-, -)	

Table 2.4. Tundra shrub model parameter estimates. Bolded values are significantly different from 0.

	2017		2017 subset		2016 subset		
	mean	95% CI	mean	95% CI	mean	95% CI	
Int	**0.0503**	**(0.0096, 0.101)**	**0.054**	**(0.011, 0.108)**	**0.012**	**(0.0044, 0.0196)**	aa
Rn	0.0064	(-0.0018, 0.015)	0.005	(-0.004, 0.015)	**0.0042**	**(0.0021, 0.0063)**	-a
D	**0.0126**	**(0.0027, 0.022)**	**0.013**	**(0.002, 0.023)**	0.0011	(-0.0016, 0.0038)	a-
Rn*LAI	**0.0044**	**(0.0024, 0.007)**	0.003	(-0.002, 0.009)	0.0006	(-0.0002, 0.0014)	aa
Rn*D	-0.0011	(-0.0038, 0.002)	-0.003	(-0.007, 0.002)	-0.0004	(-0.0012, 0.0005)	aa
LAI*D	0.0009	(-0.0008, 0.003)	0.004	(-0.002, 0.010)	-0.0001	(-0.0015, 0.0012)	aa
LAI	0.0093	(-0.0059, 0.024)	0.0009	(-0.022, 0.024)	0.0004	(-0.0032, 0.0040)	aa
LAI_1	**0.0158**	**(0.0050, 0.027)**	-	(-, -)	-	(-, -)	--
LAI_2	**0.0126**	**(0.0015, 0.024)**	0.007	(-0.007, 0.021)	0.0014	(-0.0004, 0.0034)	aa
LAI_3	-0.0007	(-0.0119, 0.011)	-0.005	(-0.019, 0.009)	-0.0006	(-0.0028, 0.0014)	aa

Table 2.5. Summer (June-August) environmental variable (air temperature (AT), relative humidity (RH), vapor pressure deficit(D), net radiation (Rn), leaf area index (LAI), and precipitation(P)) means and standard deviation (SD) by season (early, mid, late).

			AT (C)		RH (%)		D (kPa)		Rn (W m-2)	
Site	Year	Season	Mean	(SD)	Mean	(SD)	Mean	(SD)	Mean	(SD)
Riparian	2017	Early 1	11.06	(5.64)	60.78	(20.12)	0.63	(0.50)	120.58	(151.50)
Riparian	2017	Mid 2	12.93	(4.96)	75.72	(18.26)	0.45	(0.46)	75.44	(118.85)
Riparian	2017	Late 3	11.12	(5.43)	73.93	(18.59)	0.43	(0.38)	59.57	(105.89)
Tundra	2017	Early 1	12.73	(4.14)	62.27	(19.58)	0.64	(0.47)	98.86	(126.68)
Tundra	2017	Mid 2	11.89	(4.61)	76.77	(17.40)	0.4	(0.39)	75.28	(113.64)
Tundra	2017	Late 3	10.25	(5.15)	75.02	(16.89)	0.38	(0.32)	57.87	(99.48)
Riparian	2016	Early 1	8.59	(7.43)	69.01	(20.63)	0.48	(0.49)	89.91	(136.54)
Riparian	2016	Mid 2	-	-	-	-	-	-	-	-
Riparian	2016	Late 3	-	-	-	-	-	-	-	-
Tundra	2016	Early 1	7.35	(7.30)	70.17	(19.43)	0.42	(0.40)	82.1	(116.47)
Tundra	2016	Mid 2	10.21	(6.13)	67.88	(20.49)	0.53	(0.52)	82.89	(133.26)
Tundra	2016	Late 3	7.12	(5.37)	77.2	(19.68)	0.31	(0.37)	59.76	(101.57)

			LAI		P (mm)			
Site	Year	Season	Mean	(SD)	Mean	(SD)	Sum	Total
Riparian	2017	Early 1	0.18	(0.21)	0.022	-0.23	20.1	
Riparian	2017	Mid 2	0.78	(0.10)	0.157	-0.6	75.4	
Riparian	2017	Late 3	0.98	(0.02)	0.133	-0.43	54.4	150
Tundra	2017	Early 1	0.51	(0.25)	0.034	-0.21	16.3	
Tundra	2017	Mid 2	0.96	(0.03)	0.17	-0.65	81.5	
Tundra	2017	Late 3	0.99	(0.01)	0.145	-0.55	58.7	156
Riparian	2016	Early 1	0.28	(0.29)	0.106	-0.44	95.3	
Riparian	2016	Mid 2	0.9	(0.04)	-	-	-	
Riparian	2016	Late 3	1	(0.01)	-	-	-	-
Tundra	2016	Early 1	0.45	(0.32)	0.129	-0.55	117	
Tundra	2016	Mid 2	0.96	(0.03)	0.11	-0.36	52.1	
Tundra	2016	Late 3	0.86	(0.05)	0.111	-0.36	45.5	215

Chapter 3: Weighing Micro-Lysimeters Used to Quantify Dominant Vegetation Contributions to Evapotranspiration in the Arctic

3.1 Abstract

The thermal and hydraulic properties of the moss and organic layer regulate energy fluxes, permafrost stability, and future hydrologic function in the arctic tundra. Our goal was to measure evapotranspiration (ET) from dominant vegetation types in the arctic tundra, and thus to partition ET into its primary constituents. I developed and deployed 58 0.06m^2 electronic automated weighing micro-lysimeters. I selectively clipped plants from some lysimeters to isolate ET from moss, tussocks, and mixed vascular plants. A multi-step adaptive window adaptive threshold (AWAT) filtering routine was applied to the sub-hourly lysimeter data to separate real mass changes from measurement noise. The AWAT filter performed well to eliminate noise signals and overcome under-estimation associated with simple thresholding procedures. The high moss E (65mm) and tussock ET (70mm) recorded by the lysimeters (over approximately 22 days) reveal that mosses and sedge tussocks (*Eriophorum vaginatum*), are the major constituents of overall ET. Subtracting moss evaporation (E) from mixed tundra ET provides an estimate of mixed tundra transpiration (T) (10.2 mm) over the recording period (approximately 22 days), indicating that mixed tundra T is minimal, and that moss E dominates tundra water efflux at mossy sites. Summer ET measured using our lysimeters (251mm) was similar to ET measured using a hydrologic water balance approach, as well as using a flux tower at the study area in past years. The ET partitioning shown here will allow us to predict future changes in water flux associated with vegetation change. Changes in the composition and cover of mosses and vascular plants will not only alter tundra ET dynamics, but also affect the significant role that mosses, their thick organic layers, and vascular plants play in the thermodynamics of arctic soils and resilience of permafrost.

3.2 Introduction

Quantifying water fluxes between the land surface and atmosphere is crucial to understanding both the physical and biological components of the arctic system and modeling potential changes. Precipitation (P) is the water flux toward the earth's surface (e.g. rain, snow, dew). Evapotranspiration (ET) is the combination of evaporation (E) from the land surface and transpiration (T) from plants photosynthesizing. ET couples the energy and water cycles and links the land surface to the atmosphere. ET is directly related to plant productivity and energy transfer between the land surface and atmosphere. Water vapor leaving the land surface through ET transports latent heat to the atmosphere. ET flux is typically less than 10 mm d^{-1}, but can contain up to 150 W m^{-2} in latent heat and consume the majority of net radiation (Harazono et al., 1998; Peters et al., 2017). Accurate measurement of ET is needed to understand the exchange of water and energy between the land surface and atmosphere.

Long-term ET measurements are scarce in the Arctic, making it difficult to assess trends. Satellite derived estimates of pan-Arctic ET (1983-2005) show a positive mean trend (0.38mm yr^{-1}; Zhang et al., 2009). Based on a suite of nine global circulation models in the terrestrial pan-Arctic, Rawlins et al. (2010) find a mean increasing trend for ET (0.65 mm yr^{-1}) for the 100 year period 1950-2049. Comparing a 100-year period (1980-2000 vs 2080-2100) Laine et al. (2014) predict a future increase in summer ET (0.25mm d^{-1}). Concurrent with these increases in ET, Pearson et al. (2013), using ecological niche models and climate models for 2050, predict widespread vegetation community shifts and increases in above-ground biomass from 15-68%. There is a lack of understanding of arctic ET despite it being as large or larger than river discharge and a majority of P (Bring et al., 2016; Loranty et al., 2018). The arctic hydrologic response to warming is of great global importance, in part because permafrost is sensitive to soil moisture and contains large quantities of soil carbon (Froese et al., 2008). Shifting hydrologic regimes (drying, wetting) will impact C stored in permafrost, which may act as a positive feedback to climate warming if this C is released to the atmosphere (McGuire et al., 2012; Schuur et al., 2015).

The spatial aggregation or temporal limitation of many techniques for measuring ET integrates out the specific contributions of tundra plants to ET. Weighing lysimeters provide

precise measurements of both ET and P through measuring changes in mass. Decreases in the lysimeter mass are interpreted as ET and increases are interpreted as P. Lysimeters have been used extensively in agricultural studies (e.g. Allen et al., 1998; Meissner et al., 2014; Nolz et al., 2013). Lysimeter scale resolution is dependent on the design and weighing mechanism but can reach 0.01mm (von Unold and Fank, 2008). Lysimeters can provide a range of temporal scales from annual to minute averages of P and ET. A high base temporal scale is required to separate P and ET events, which may occur over very short time intervals. Lysimeter estimates are constrained spatially in heterogeneous vegetation given their limited size (typically ~1m^2).

Our goal was to measure ET from dominant vegetation types in the arctic tundra and to partition ET into its primary constituents. I developed and deployed 58 micro-lysimeters (surface area: 0.06m^2 , combined area: 3.3m^2), and selectively removed plants to isolate ET contributions from moss, *Eriophorum vaginatum* tussocks, shrubs, and mixed small vascular plants. Contrary to vascular plants, the conduction of water in mosses (bryophytes) is predominantly external through capillary action. Mosses photosynthesize and grow during periods of water availability and desiccate during drought. Although some moss species possess limited means of controlling water, they are generally considered to allow unrestricted water loss (Proctor, 1982) and due to their substantial surface area can support high rates of evaporation (Blok et al., 2011). Unlike the canopy of vascular plants, mosses are thermally linked to the ground surface and latent heat transfer during evaporation cools the ground directly. Environmental conditions (solar radiation, wind, vapor pressure deficit) and microclimate play a large role in determining moss E. Shading by overstory (forest canopy) and understory plants has been shown to reduce moss E (Heijmans et al., 2004). The highest-recorded moss E has been in open settings (Kellner, 2001) and can be increased with greater air mixing (Heijmans et al., 2001).

Combining the lysimeter-derived measures of moss E, tussock T, and mixed species ET with our shrub sap flow data (Ch. 2), I were able to deduce the ET contributions from each vegetation type. This clarifies the role of vegetation in the arctic water cycle, and in controlling soil moisture, thermal conductivity, and permafrost. It will allow for improved predictions of landscape water efflux according to future changes in tundra vegetation.

3.3 Methods

I developed and built electronic automated weighing micro-lysimeters (hereafter referred to as lysimeters) for the arctic tundra. I deployed the lysimeters in headwaters of Imnaviat Creek, approximately 12 km E of Toolik Field Station (Fig. 3.1). Moist tussock-sedge, dwarf-shrub tundra, dominated by *Eriophorum vaginatum*, the woody shrubs *Salix planifolia* ssp. *pulchra* and *Betula nana*, and the moss *Sphagnum rubellum*, comprise the vegetation (Walker et al., 2005, 1989). The watershed consists of east-facing and west-facing gentle slopes and the surface geomorphology is poorly-defined water tracks and weakly-developed solifluction lobes. Hydrologic water balance has been measured in the watershed for many years (1985-present). Winter precipitation averages 120mm snow-water equivalent, summer precipitation averages 241mm, runoff averages 181mm, and ET averages 179mm (Kane et al., 2004). I deployed a total of 58 lysimeters in nine spatially-distributed clusters of six to eight lysimeters in early June 2017, prior to leaf out and approximately 10% of the watershed still under snow. A large portion of the moss layer was frozen, and the soil was completely frozen from the top of the organic layer to >40cm.

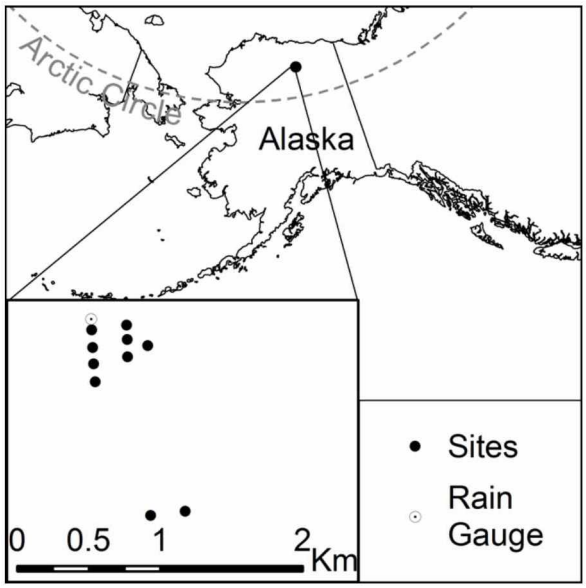

Figure 3.1. Alaska and inset map of spatial distribution of lysimeters in Imnaviat Research Watershed. Sites (dots) represent clusters of 6 lysimeters.

In each cluster the lysimeters were arranged in a circle with a 4m radius. Eighteen lysimeters were placed (three clusters of six lysimeters each) on the east-facing slope, 24 (four clusters) on

the west-facing slope, six (one cluster) in the fen, six (one cluster) near the ridge, and four control lysimeters. The control lysimeters consisted of capped weighing vessels containing 25lb iron weights. The lysimeter placement and removals were designed to quantify the contributions to ET from moss E, tussock ET, and mixed tundra T (not including the erect shrubs *S. pulchra* and *B. nana*).

To isolate and determine moss E, all vascular plants (non-bryophytes) were removed from 18 of the lysimeters (Fig. 3.2). To isolate and determine ET from tussocks, eight of the lysimeters were selected to contain an individual tussock (*E. vaginatum*). The remaining 28 lysimeters contained random communities of tundra vegetation with *B. nana* and *S. pulchra* stems clipped to determine tundra ET without larger stature erect shrubs. Roots of clipped stems were left in place to minimize below-ground disturbance. To determine T from mixed-tundra species, not including *B. nana* and *S. pulchra*, average moss E rates were subtracted from mixed tundra ET rates. Averages of 20 replicate weight measurements were recorded every 10 minutes for each lysimeter during the summer of 2017 along with a measurement of temperature from the load cell thermistor and temperature of the node circuit board (Table 3.3).

Figure 3.2. Micro-lysimeters with mixed tundra vegetation (a) and moss only (b).

The lysimeter consisted of three parts: an outer container, the weighing vessel, and the weighing mechanism (Fig. 3.2). The outer container and the inner container were simple cylindrical buckets. The lysimeter weighing vessels measured 28cm in diameter and 26cm deep. The lysimeters did not have a drainage mechanism in the outer container because the surrounding soil was saturated to supersaturated. Because the outer container lacked drainage,

rain accumulated in the outer container. Sufficient capacity to contain up to a 30mm rain event was incorporated into the lysimeter design. Rain greater than 30mm, or cumulative rain events, required regular removal of excess water from the lysimeter outer container, which limited the operation of the lysimeters to days when personnel were present.

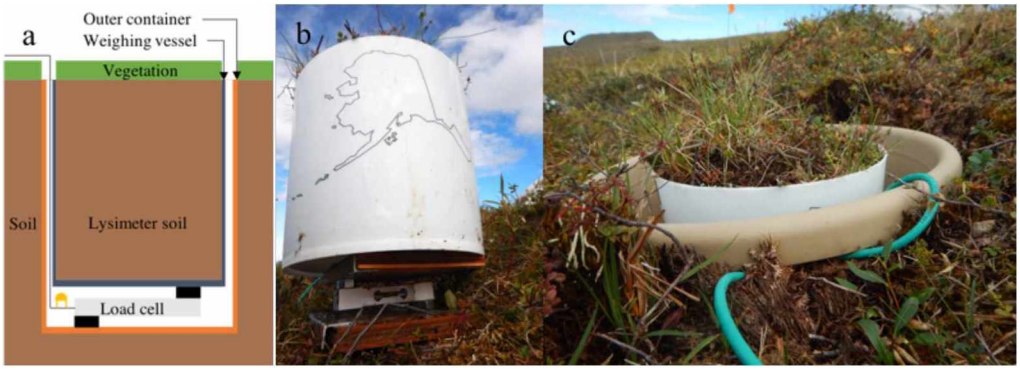

Figure 3.3. (a) Schematic of micro-lysimeter (not to scale). (b) Picture of micro-lysimeter prior to installation, showing the beam load cell weighing mechanism. (c) Installed micro-lysimeter with mixed tundra vegetation.

The weighing mechanism used a beam load cell (50kg capacity, Galoce, GPB100) installed in a Z-shape counter-balance that I constructed of aluminum channel. Weight of the lysimeter applied to one end of the beam load cell creates internal compression and tension forces, which are detected by a Wheatstone bridge strain gauge and converted to electric signals. I designed an electronic circuit (node) to make and record the load cell weight measurements at regular intervals. The circuit consisted of a switching multiplexor to handle up to eight lysimeters, an amplifier circuit to multiply the load cell signal to a suitable measurement range, an analog to digital converter (ADC) to convert the amplified load cell signal to a digital number (SparkFun, SEN-13879), and a programmable microcontroller with an integrated 433MHz radio to transmit weight measurements to a remote logger (LowPowerLab, RFM69HW-433). The microcontroller was programmed to record weight and temperature measurements of each connected lysimeter every 10 minutes, and it also recorded the temperature of the microcontroller and the time of measurement. After each measurement cycle the microcontroller was programmed to transmit the data to the remote logger and then enter a low-power standby mode until the next measurement cycle. The microcontroller was capable of storing data from 12 measurement cycles.

The remote logger consisted of a real-time clock, an SD-card recorder to store the measurement data, and a programmable microcontroller with an integrated radio. A short ping from the node was made to wake the logger and prepare it to receive. Upon receiving the ping, the logger would latch to the ping node, acknowledge the ping with short transmission and prepare to receive data. Upon receiving an acknowledgement from the logger, the node would transmit the data (~100ms). The logger would then write the received data to the SD card and listen for the next transmission. If a node did not receive an acknowledgement to the ping, it would enter a short sleep cycle, before retrying the transmission. This transmission scheme eliminated data loss and unrecorded data transmissions, limited radio transmission time, and limited interfering radio transmissions.

The lysimeter control board (specifically the ADC) showed sensitivity to ambient temperature. A standard temperature correction was developed. After subsets of daily data were detrended, the residuals were fit with the temperature correction and a zero intercept, and the residuals of the temperature corrections were then added back to the trend fit.

Given the frozen soils, a gas-powered jackhammer was used to remove cylinder-shaped blocks of intact tundra vegetation and soil. The frozen, fine-grained, silty soil exhibited a plastic deformation response to the jackhammer force, allowing the intact cylinders to be precisely shaped. Finer shaping and height adjustment of the tundra-soil cylinders was accomplished with a serrated knife and small hatchet. The cylinders were placed immediately into the weighing vessels. A larger ring of soil was then removed from the edge of the lysimeter hole to allow space for the outer container. The outer container was lowered into the hole, raised to the height of the surrounding ground, and leveled. The weighing mechanism was placed in the bottom of the outer container. The weighing vessel, with tundra vegetation and soil inside, was placed atop the weighing mechanism. The lysimeter was positioned so that the lysimeter vegetation was level with surrounding vegetation. A thermistor was placed near the load beam cell to record temperature (accuracy 0.1°C) of the weighing mechanism. Raw data were manually screened for measurement errors. No gap filling was performed. Data records shorter than one day were removed.

A multi-step filtering routine was applied to the lysimeter data to separate real mass changes from measurement noise (e.g. wind-caused mass fluctuation). The adaptive window adaptive threshold (AWAT) filter (Peters et al., 2014) with spline interpolation (Peters et al., 2016) and snap routine (Peters et al., 2017) was applied to each lysimeter dataset (Table 3.1). The AWAT filter was programmed using the R statistical language (R version 3.5). The filter routine first applies a smoothing routine (moving average with window width, w). The filter routine then uses a thresholding approach to remove noise leftover from the smoothing process. The thresholding separates significant weight changes from insignificant changes based on an accuracy threshold parameter (δ), such that changes less than δ are discarded. The value of δ must be greater than the scale resolution.

The adaptive ability of the AWAT filter uses both a time-variable w and δ to overcome over- and under-estimation caused by changes in the amplitude of both the signal and noise over time (i.e. during strong wind events, or calm periods with slow evaporation). To determine w, measures of signal strength and noise are determined by fitting a moving polynomial to the data within a predetermined maximum window width (w_{max}). At each data point (i), polynomials of order 1 to k are fit to the data window of width w_{max}. The optimal order of the polynomial is determined with AIC_c (Hurvich and Tsai, 1989). The coefficient of determination, R^2_i, for each fit is a measure of how much of the data is explained by polynomial and thus also represents signal strength. The polynomial is used solely to gather information about signal strength and noise. A simple linear relationship is then used to determine w_i:

$$w_i = \max\left(w_{min}, \sqrt{1 - R_i^2} * w_{max}\right) \quad (1),$$

where w_{min} and w_{max} are the minimum and maximum window widths (Peters et al., 2014). The adaptive window width, w_i, thus varies between w_{min} and w_{max} based on the signal strength at each data point.

A moving average of width, w_i, is then applied to the data. The adaptive threshold value is then determined by a functional relationship between the data and the 95% confidence interval of the residuals of the polynomial fit (res_i):

$$\delta_i = \begin{cases} \delta_{\max} \text{ for } res_i * t_{97.5,r} \geq \delta_{max} \\ res_i * t_{97.5,r} \text{ for } res_i * t_{97.5,r} < \delta_{min} \\ \delta_{\min} \text{ for } res_i * t_{97.5,r} \leq \delta_{min} \end{cases} \quad (2),$$

where $\delta_{\min}$ and $\delta_{\max}$ are the minimum and maximum accuracy parameters for the weight changes and $t_{97.5,r}$ is the Student t-value for the 95% confidence level (Peters et al., 2014). The adaptive threshold, δ_i, is minimal for low-noise conditions and maximal for high-noise conditions. The thresholding is then applied to the moving average at each i by comparing the difference of the moving average to δ_i such that differences less than δ_i are discarded.

The thresholding process produces a step-like course of fluxes which are unrealistic compared to a continuous process such as ET. To smooth the thresholded data, the points at which the steps occur are used as anchor points between which additional points are interpolated with piecewise Hermitian splines which yield smooth and continuously differentiable curves (Peters et al., 2016). The spline interpolation was only applied to mass decreases (ET) and small mass increases such that only precipitation events like dew fall were smoothed from the threshold stair-steps to continuously differentiable curves ($\Delta M < 1.1\delta$).

At each change in flux direction the thresholding procedure introduces a systematic flux underestimation. A snap routine was used to correct the under-estimation and yield a nearly unbiased representation of the real flux signal (Peters et al., 2017). Where a change in flux direction occurs, two additional anchor points are inserted between the threshold anchor points. The first additional anchor point is determined based on the local maximum (termination of precipitation) or minimum (termination of ET) of the moving average. Rather than using the value of the local maxima or minima, the 75th quantile of the neighboring moving average data is used. The second additional anchor point is placed at the time where the moving average returns to the first threshold anchor point value. Thus, the flux snaps to the moving average when there is a change in flux direction (Peters et al., 2017).

3.4 Results

Bench testing of the lysimeter weighing mechanism revealed an accuracy of 3g, which is equivalent to 0.03mm of water in the weighing vessel. Field testing of the lysimeters was accomplished by adding known weights to the vegetation surface. The average accuracy was 0.32mm (Table 3.3). Due to labor availability and weather, the lysimeters operated periodically throughout the summer, averaging 22 days recorded per lysimeter. Consequently, the lysimeter-measured ET did not capture the entire summer season and is a biased sample of hours and days. The lysimeters recorded 16-33% of the summer days and 4-28% of rain gauge P.

The lysimeters do not represent an unbiased sample of the watershed vegetation, because they were selected not based on their fractional cover, but on replicating measurements of the dominant vegetation types in undisturbed locations. The lysimeters were placed using a systematic random placement scheme on the mid-slopes, but the lowland, riparian, and ridge habitats were underrepresented. Some cover types were not included (e.g. frost boils, water tracks, open water, bedrock, and disturbed areas).

The lysimeter installation and container had potential effects on the contained vegetation and measured ET rates. I did not observe plant stress (yellowing, withering) compared to undisturbed vegetation. While the lysimeter design minimized edge effects, the lysimeter vegetation did experience warmer soil temperatures than surrounding vegetation from the exposure of the sides of the weighing container to ambient air temperature and an air-gap with the underlying thawing active layer and permafrost. Furthermore, because the lysimeter weighing container did not have a drainage mechanism lysimeter, soil moisture was potentially altered relative to the surrounding soil matrix.

For the AWAT filter, parameter values were selected based on the scale resolution (weighing and temporal resolution), and based on qualitative assessment of fit to rain and evaporation events; larger moving average windows were smoothed over small rain events, while shorter windows allowed noise signals to propagate (Table 3.1). The AWAT filter performed well to eliminate noise signals and to overcome under-estimation associated with

simple thresholding procedures (Fig. 3.4). The spline and snap procedures in the AWAT filter produced smooth continuously differentiable curves that are realistic representations of ET without noise.

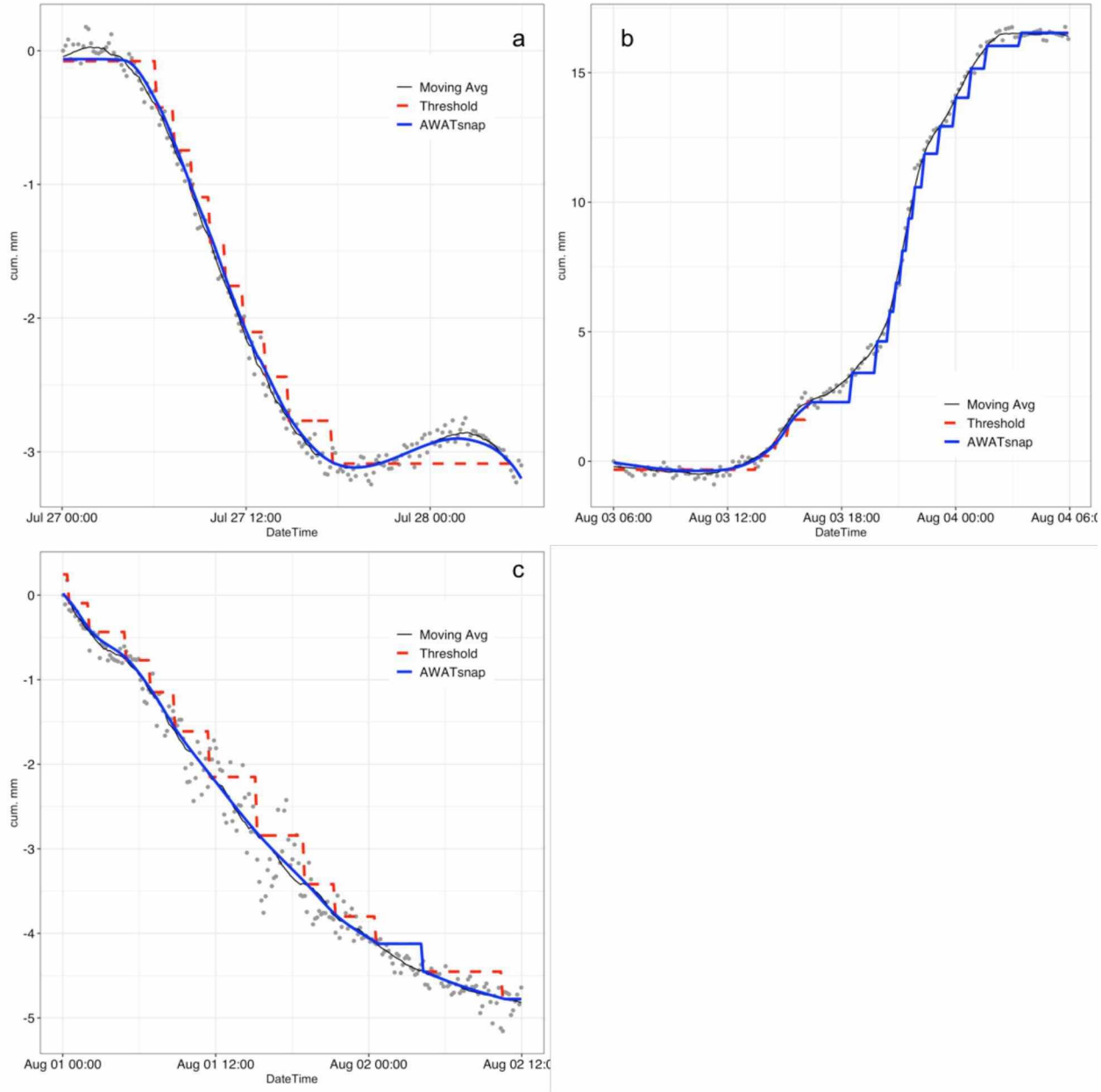

Figure 3.4. Example of AWAT filter applied to lysimeter data for period of strong ET (a), 16mm rain event (b), and strong wind period (c; mean wind speed: 6.8m/s). Grey points are raw lysimeter data. Evaporation event (a) includes overnight dewfall (18:00-03:00; approx. 0.2mm).

The lysimeters and the tipping bucket rain gauge captured rain events, but I did not expect perfect agreement between the gauge and lysimeters, as the rain gauge was not co-located with

the lysimeters (Table 3.3). Individual rain events measured by lysimeters were similar to those measured by the rain gauge (Fig. 3.5). Hourly ET and P results showed strong agreement for specific rain or evapotranspiration events, with small variation between lysimeters (Fig. 3.5). ET rates and totals from the three vegetation types were similar (Table 3.2, Fig. 3.6).

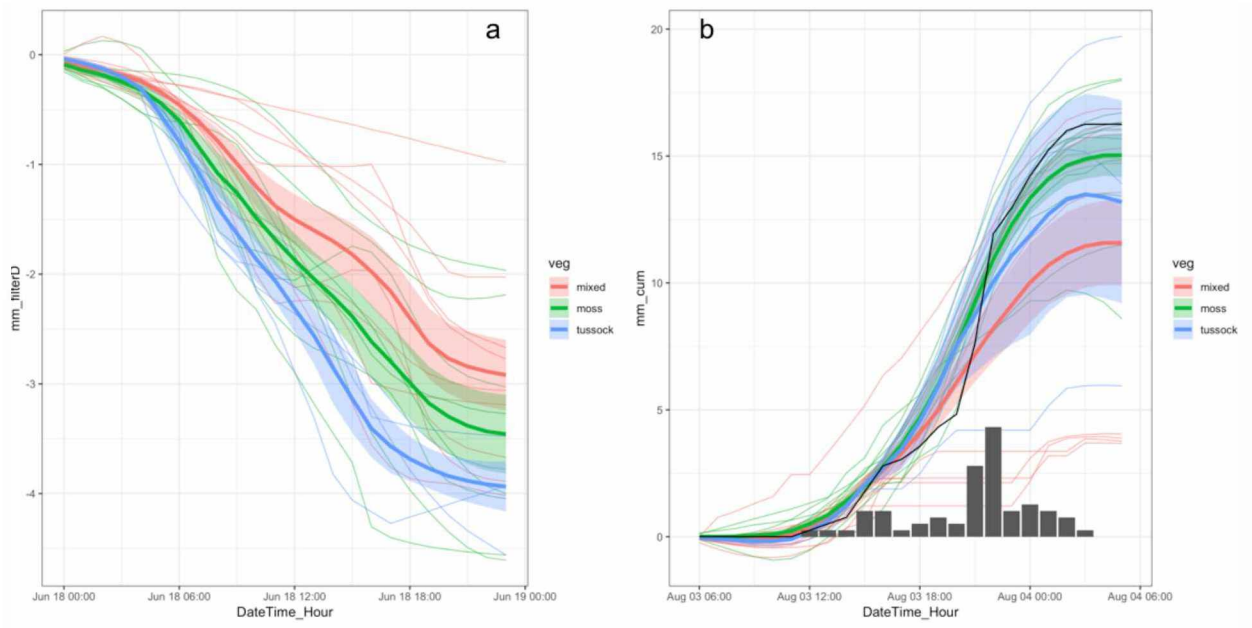

Figure 3.5. Examples of lysimeters recording (a) a daytime evapotranspiration event, and (b) a precipitation event. Individual lysimeters are represented by thin lines, means of each vegetation group are represented by thick lines +-1 SD shaded ribbon. The hourly ET trend (a) shows ET during a single day, with greatest water (mm) lost during the middle of the day. The precipitation event (b) is recorded as water (mm) gained with gauge precipitation shown for reference (hourly as bars and cumulative as solid black line).

Mixed tundra T (as estimated by subtracting moss E from mixed tundra ET) was small compared to moss E. Subtracting moss E from mixed tundra ET yields an estimate of mixed tundra T (10.2 mm, sd 15.9 mm) over the recording period, indicating that mixed tundra T is minimal, and that moss E dominates tundra evapotranspiration at these sites.

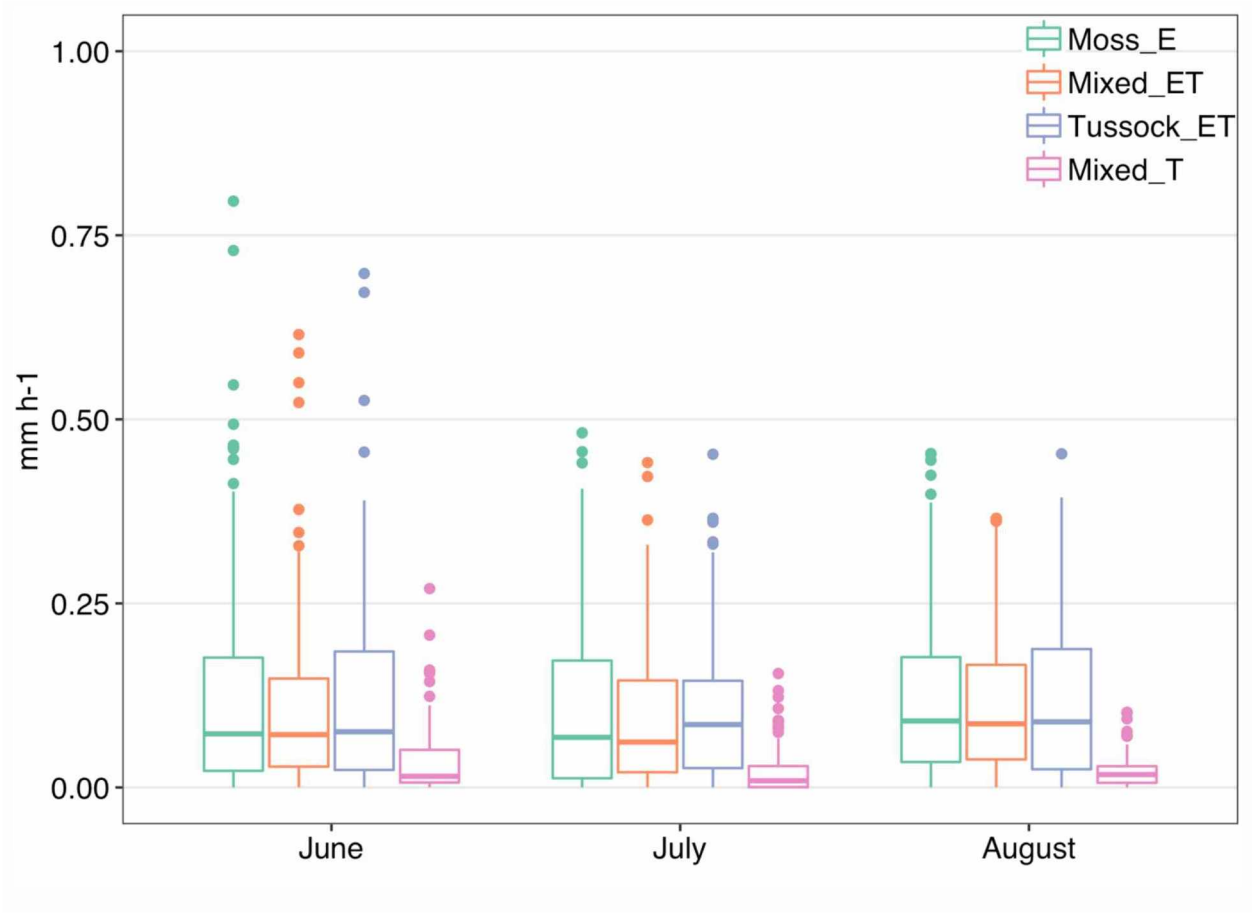

Figure 3.6. Boxplot of hourly E, T, and ET rates by vegetation type and by month.

Seasonal trends in ET were similar between Moss E, Mixed ET and Tussock ET (Fig. 3.7). However, Mixed T had a slower seasonal accumulation and a much-reduced season total (Table 3.2). Given that a majority of the season's rain occurred outside the recording period (Fig. 3.7), I believe the average lysimeter ET rates are likely high and are an overestimation of the summer ET (Fig. 3.8).

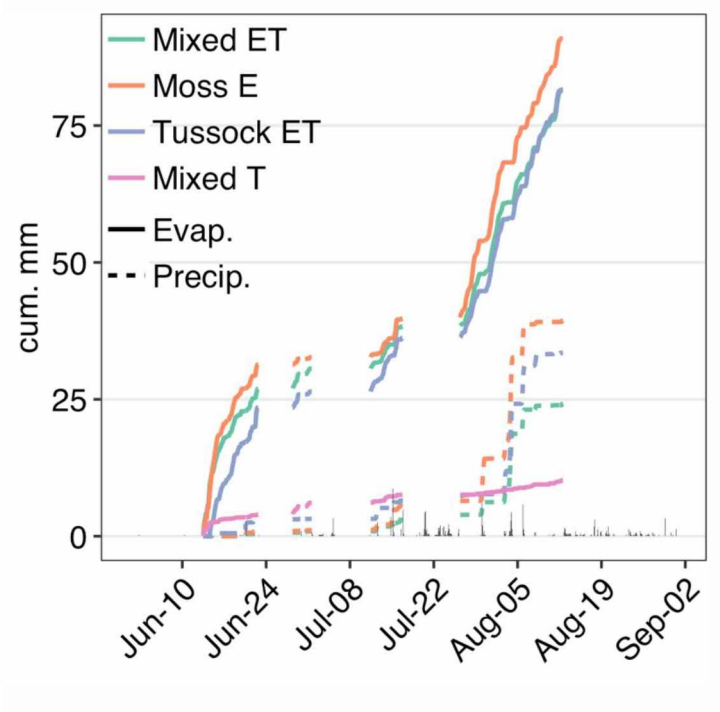

Figure 3.7. Average cumulative ET (solid lines) and P (dashed lines) recorded on lysimeters (n=54) by vegetation type (colors). Breaks in the ET and P lines occur during periods when the lysimeters were not recording. Thin vertical black lines are hourly rain events captured by the rain gauge.

3.5 Discussion

Overall, the lysimeters performed well, capturing ~22 days of arctic tundra sub-hourly ET and P across a small (2.2 km^2) watershed. While the lysimeter ET estimates (moss E, mixed tundra ET, and tussock ET) are representative of the vegetation components in the watershed, the variation of the estimates is a measure of variation in the vegetation composition and productivity across the landscape. Our manipulative removal of vascular plants in the moss E lysimeters increased the incident solar radiation at the moss surface and possibly both wind speed and boundary layer mixing. The micro-lysimeters employed in this study are well-suited for the small stature vascular plants and bryophytes that make up a majority of the tundra vegetation. Additionally, the replication of the micro-lysimeters and wireless data transmission allowed us to achieve much more distributed spatial coverage (54 lysimeters, totaling 3.3 m^2, over 2.2 km^2 watershed, instead of 1 lysimeter 1m^2) and high temporal resolution. Furthermore, the inexpensive cost of construction and reasonable installation labor allowed for easy replication for comparing vegetation types and capturing variability in landscape ET.

These results describe an important first attempt to partition arctic tundra ET into its constituent parts on the landscape. Summer ET measured using our lysimeters (251 mm) was similar to total ET measured using a hydrologic water balance approach (179mm; Kane et al., 2004) and using a flux tower (165mm; (Euskirchen et al., 2012)) at the study area in past years (Fig 3.8). The high moss E and tussock ET reveal that bryophytes and *E. vaginatum,* where abundant, are the major constituents of overall ET. Transpiration from the small shrubs *B. nana* and *S. pulchra* contribute a small fraction of total ET (12 mm, ~12%), while taller shrubs with greater leaf area at a nearby site efflux an order of magnitude greater T (107 mm) (Ch. 2). Mixed-tundra vascular plants contribute a very small fraction of total ET (28 mm) but have relatively large variability.

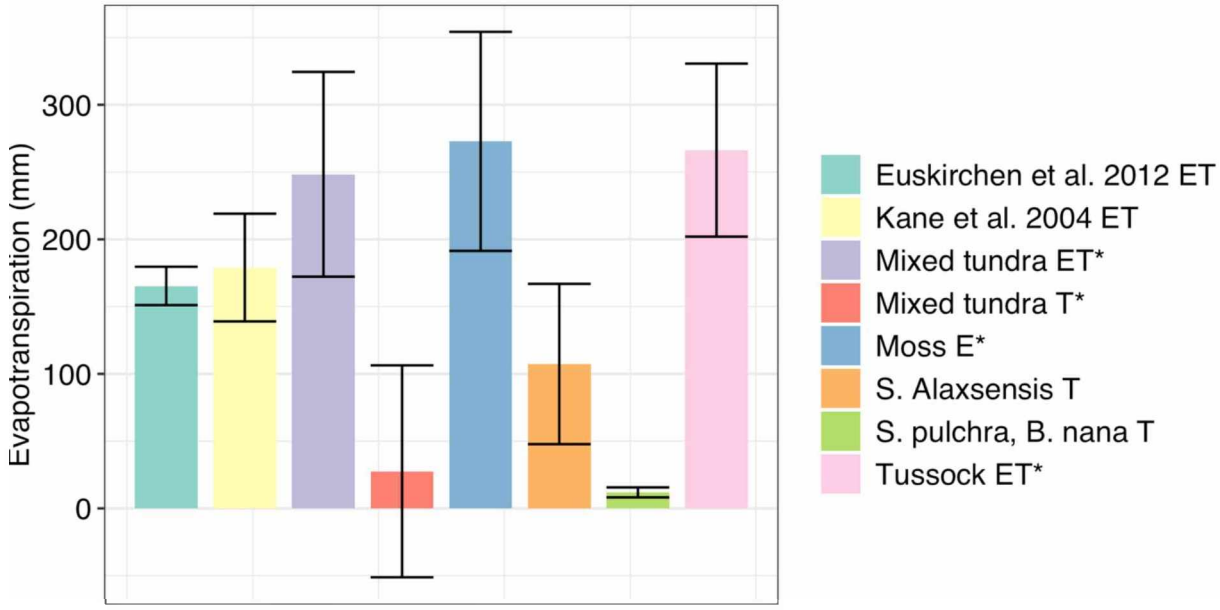

Figure 3.8. Comparison of summer (June, July, August) ET measurements for Imnavait Creek watershed (Euskirchen et al., 2012; Kane et al., 2004, Ch. 2) and lysimeter-derived ET (this study, denoted by *). Error bars are standard deviation.

Woody shrubs (Ch. 2, Chapin and Shaver, 1996), tussocks (this study, Oberbauer and Miller, 1981; Stuart et al., 1982) and moss E (this study, Blok et al., 2011; Heijmans et al., 2004; Stoy et al., 2012) are the major components of tussock tundra ET. Tussocks are a common component of vegetation composition at Imnavait, but occur with varying density in tundra ecosystems (Walker et al., 2005). While a small portion of the recorded tussock ET is

evaporation of intercepted P (including dewfall), the majority is T due to their dense growth habit and correspondingly high leaf area and high rate of stomatal conductance (Oberbauer and Miller, 1981).

Considering sap flow measurements of the dominant woody shrubs in the watershed (Ch. 2) along with these lysimeter ET measurements gives a detailed picture of the various vegetation contributions to total ET. Sap flow measurements indicated that shrubs *S. pulchra* and *B. nana* combined transpiration comprised 10-12% of summer ET in the Imnavait watershed, indicating that other species contributions must comprise the majority of ET (Ch. 2). However, in a nearby riparian area with much greater leaf area (1.2 vs 0.09m^2m^{-2}), the shrub *S. alaxensis* summer total transpiration was nine times greater (107 mm vs 12 mm). These results show that transitions from short shrubs with low LAI to tall shrubs with high LAI, as predicted by models (Pearson et al., 2013), would increase the shrub contribution to ET by an order of magnitude, making it comparable to moss E and tussock ET.

Numerous dewfall events were captured by the lysimeters (0.1-0.3 mm), but are not analyzed here. While total season dewfall is unknown, it constitutes a measurable portion of summer P not captured by tipping bucket rain gauges. When dewfall occurred, the lysimeters measured it twice nightly, once as P during deposition and again as E during upward flux. When dewfall is regular (e.g. nightly), it may constitute a sizable part of moss E, particularly if the additional water from dewfall helps to maintain moss moisture above desiccation levels. The evaporation of dew from moss plays a further role in the ecosystem by drawing additional latent heat from the ground surface into the atmosphere.

Moss has several physical effects on the tundra ecosystem. Live moss and thick mats of decaying moss serve to insulate the underlying soil from solar radiation and can facilitate permafrost development and protect existing permafrost by lowering soil temperatures by up to 2dC (Jorgenson et al., 2010). Kade & Walker (2008) found that soil temperatures beneath transplanted moss were significantly reduced (~3°C) relative to controls, bare soil and transplanted tussocks. Mosses, unlike vascular plant canopies, are thermally connected to the soil and also transfer heat into and out of the ground via conduction (O'Donnell et al.,

2009). The experimental removal of green mosses below intact shrub canopies has been found to increase ET (moss E, and latent heat) and ground heat flux (Blok et al., 2011). These studies highlight the important role live moss and the underlying peat layer play in surface energy and water fluxes.

Tussock forming sedges (*E. vaginatum*) alter their microclimate through their distinctive shape. The vegetative reproductive pattern of *E. vaginatum* tillers creates a hemispherical- to mushroom-shaped clump that raises the base plant 10-40 cm above the surrounding low-lying vegetation and soil surface (Mark and Chapin, 1989). The raised height of the tussock alters its microclimate by lengthening the growing season 5-10% and increasing the tussock temperature 6-8°C relative to the underlying soil through increased exposure to solar radiation during the snowmelt period and at low sun angles (Chapin et al., 1979). Despite elevated soil temperatures within the tussock, the temperature of the soil beneath the tussock and active layer depths are similar to the soil of the inter-tussock spaces (Chapin et al., 1979). However Kade & Walker (2008), found soil temperatures beneath transplanted tussocks were not different from bare soil temperatures.

Mosses and organic soil (including peat and tussock cores), have lower thermal conductivity than mineral soils due to their low bulk density and high porosity. Moisture content plays a large role in determining soil thermal dynamics as thermal conductivity is strongly related to moisture content. Mosses and soils have lower thermal conductivity when dry than when saturated (Hinzman et al., 1991). Furthermore, thermal conductivity is increased in winter as soil freezes, and also with higher ice content (Hinzman et al., 1991). In general, moss and thick organic layers serve to insulate soil from summer heat transfer and promote shallow active layers and cooler soil temperatures, while also allowing winter heat loss through high thermal conductivity when saturated and frozen.

During evapotranspiration, energy is conducted from the soil surface to the air and creates a negative ground heat flux, thereby cooling the soil. This loss of soil water through evaporation further decreases the thermal conductivity of the moss and underlying layers (Hinzman et al., 1991). In the Arctic, ground heat flux is relatively large compared to more

temperate biomes because of the large temperature gradient from the ground surface and permafrost (Langer et al., 2011a, 2011b). The magnitude of arctic ground heat flux is comparable to the other major atmospheric heat fluxes: sensible heat and latent heat (Loranty et al., 2018). The combination effects of ET, surface cooling and reduced thermal conductivity through drying, serve to reduce two of the major factors controlling ground heat flux: the temperature gradient between the permafrost and the soil surface and the thermal conductivity of the organic soil and moss.

Continuous field measurements of ET remain difficult and costly in the Arctic. Hydrologic water balance estimates of ET require in-river equipment that is vulnerable to damage and disturbance by seasonal freezing and spring breakup. Hydrologic water balance estimates of ET have coarse temporal resolution (i.e. seasonal or annual), large spatial scale (i.e. watershed), and large error in the Arctic due to the effects of ice on discharge and precipitation measurements, wind effects on precipitation gauges, and infrequent and difficult measurement validation (Kane et al., 2004; Michelson, 2004; Yang et al., 1998). Energy balance flux tower measures capture high frequency continuous estimates of ET, but require substantial equipment and power and only measure ET at a coarse spatial scale (100-1000m^2, Berger et al., 2001; Oren et al., 2006). Satellite-based energy balance methods require little on the ground equipment, but are limited to the scale of the data both spatially (10-1000m^2) and temporally (instantaneous acquisition, 1-14+ day intervals) (Chávez et al., 2008; Kustas and Norman, 1996). Gas chambers and leaf porometry that measure T on a fine scale (<1cm^2 - 1m^2) are typically limited to short duration measurements and are predominantly manual (Garcia et al., 1990; Oberbauer and Miller, 1981; Wheeler, 1992).

Measurement of ET at scales finer than the landscape or watershed scale allows us to understand ecosystem components which may be useful for assessing future change, making predictions, ongoing monitoring and targeting future research. Changes in climate are changing arctic vegetation composition and structure, and these transitions will likely have strong effects on arctic ET. Furthermore, changes in the composition and cover of mosses and vascular plants will not only alter tundra ET dynamics, but also affect the significant role mosses, their thick organic layers, and vascular plants play in the thermodynamics of arctic soils and resilience of

permafrost. Shrub expansion could reduce moss cover, as observed by experimental warming (Chapin et al., 1995), by reducing surface albedo and increasing sensible heat flux (Sturm et al., 2005), thus contributing to regional warming. Although increases in shrub canopy density and shading may lead to soil cooling and reduce permafrost thaw (Blok et al., 2010). Increased shrub biomass has also been correlated with warmer soils and deeper active layers in latitudinal and temperature gradient studies (Walker et al., 2003), but understanding of casualty is still lacking.

This improved understanding of the constituents of tundra ET allows for predictions of how hydrologic fluxes may change, but the interactions of climate, vegetation, hydrology and soil thermal dynamics are complex and remain uncertain. The energy fluxes, thermal properties, and hydraulic properties of the active layer and vegetation are of great importance for permafrost stability and future arctic hydrologic function.

Table 3.1. AWAT filter parameters.

Parameter	Value
k	5
w_{max}	73 (12 hr)
w_{min}	3 (0.5 hr)
δ_{max}	1.0 (mm)
δ_{min}	0.32 (mm)
Q_{ma}	0.75

Table 3.2. Lysimeter ET components, recording period, hourly rates, and seasonal total ET.

ET component	n	Mean recording period [d]	Mean recording period [h]	ET recorded (sd) [mm]	ET recorded (sd) [mm h^{-1}]	Season ET (sd) [mm]
Mixed ET	28	21.1	507.5	57.88 (19.34)	0.11 (0.04)	251.81 (84.15)
Moss E	18	22.4	537.8	64.76 (18.39)	0.12 (0.03)	265.89 (75.52)
Tussock ET	8	23.5	565.1	70.03 (18.94)	0.12 (0.03)	273.63 (74.00)
Mixed T	-	-	-	10.23 (15.90)	0.01 (0.03)	27.53 (74.60)

Table 3.3. Rain gauge and lysimeter recording period, measured precipitation and accuracy.

Site	Recording period [d]	Recording period [h]	Distance from Rain Gauge [m]	Lysimeter P (sd) [mm]	Gauge P [mm]	Accuracy (sd) [mm]
Rain Gauge	92.0	2208.0	0.0	-	196.3	0.254
1	26.3	630.0	75.4	40.11 (5.64)	50.6	0.31 (0.21)
2	23.5	564.3	198.2	35.51 (1.87)	40.4	0.42 (0.11)
3	19.0	457.0	313.8	31.27 (6.41)	38.5	0.42 (0.10)
5	15.2	363.7	1437.2	6.56 (1.21)	8.4	0.07 (0.06)
6	15.0	361.0	1497.7	7.81 (1.84)	8.8	0.34 (0.09)
7	26.8	643.0	366.8	29.66 (2.97)	43.9	0.20 (0.10)
8	29.8	714.5	291.0	49.92 (3.4)	54.4	0.67 (0.21)
9	24.0	577.0	252.4	36.6 (3.07)	42.7	0.16 (0.13)
10	17.7	424.7	437.7	25.44 (2.64)	37.2	0.58 (0.32)

3.6 References

Allen, R.G., Pereira, L.S., Raes, D., Smith, M., 1998. FAO Irrigation and drainage paper No. 56. Rome Food Agric. Organ. U. N. 56, e156.

Berger, B.W., Davis, K.J., Yi, C., Bakwin, P.S., Zhao, C.L., 2001. Long-Term Carbon Dioxide Fluxes from a Very Tall Tower in a Northern Forest: Flux Measurement Methodology. J. Atmospheric Ocean. Technol. 18, 529–542. https://doi.org/10.1175/1520-0426

Blok, D., Heijmans, M.M.P.D., Schaepman-Strub, G., Kononov, A.V., Maximov, T.C., Berendse, F., 2010. Shrub expansion may reduce summer permafrost thaw in Siberian tundra. Glob. Change Biol. 16, 1296–1305. https://doi.org/10.1111/j.1365-2486.2009.02110.x

Blok, D., Heijmans, M.M.P.D., Schaepman-Strub, G., van Ruijven, J., Parmentier, F.J.W., Maximov, T.C., Berendse, F., 2011. The Cooling Capacity of Mosses: Controls on Water and Energy Fluxes in a Siberian Tundra Site. Ecosystems 14, 1055–1065. https://doi.org/10.1007/s10021-011-9463-5

Bring, A., Fedorova, I., Dibike, Y., Hinzman, L., Mård, J., Mernild, S.H., Prowse, T., Semenova, O., Stuefer, S.L., Woo, M.-K., 2016. Arctic terrestrial hydrology: A synthesis of processes, regional effects, and research challenges. J. Geophys. Res. Biogeosciences 121, 2015JG003131. https://doi.org/10.1002/2015JG003131

Chapin, F.S., Shaver, G.R., 1996. Physiological and Growth Responses of Arctic Plants to a Field Experiment Simulating Climatic Change. Ecology 77, 822–840. https://doi.org/10.2307/2265504

Chapin, F.S., Shaver, G.R., Giblin, A.E., Nadelhoffer, K.J., Laundre, J.A., 1995. Responses of Arctic Tundra to Experimental and Observed Changes in Climate. Ecology 76, 694–711. https://doi.org/10.2307/1939337

Chapin, F.S., van Cleve, K., Chapin, M.C., 1979. Soil Temperature and Nutrient Cycling in the Tussock Growth Form of Eriophorum Vaginatum. J. Ecol. 67, 169–189. https://doi.org/10.2307/2259343

Chávez, J.L., Neale, C.M.U., Prueger, J.H., Kustas, W.P., 2008. Daily evapotranspiration estimates from extrapolating instantaneous airborne remote sensing ET values. Irrig. Sci. 27, 67–81. https://doi.org/10.1007/s00271-008-0122-3

Euskirchen, E.S., Bret-Harte, M.S., Scott, G.J., Edgar, C., Shaver, G.R., 2012. Seasonal patterns of carbon dioxide and water fluxes in three representative tundra ecosystems in northern Alaska. Ecosphere 3. https://doi.org/10.1890/ES11-00202.1

Froese, D.G., Westgate, J.A., Reyes, A.V., Enkin, R.J., Preece, S.J., 2008. Ancient Permafrost and a Future, Warmer Arctic. Science 321, 1648–1648. https://doi.org/10.1126/science.1157525

Garcia, R.L., Norman, J.M., McDermitt, D.K., 1990. Measurements of canopy gas exchange using an open chamber system. Remote Sens. Rev. 5, 141–162. https://doi.org/10.1080/02757259009532126

Harazono, Y., Yoshimoto, M., Mano, M., Vourlitis, G.L., Oechel, W.C., 1998. Characteristics of energy and water budgets over wet sedge and tussock tundra ecosystems at North Slope in Alaska. Hydrol. Process. 12, 2163–2183. https://doi.org/10.1002/19981030

Heijmans, M.M., Arp, W.J., Berendse, F., 2001. Effects of elevated CO2 and vascular plants on evapotranspiration in bog vegetation. Glob. Change Biol. 7, 817–827.

Heijmans, M.M.P.D., Arp, W.J., Chapin, F.S., 2004. Controls on moss evaporation in a boreal black spruce forest. Glob. Biogeochem. Cycles 18. https://doi.org/10.1029/2003GB002128

Hinzman, L.D., Kane, D.L., Gieck, R.E., Everett, K.R., 1991. Hydrologic and thermal properties of the active layer in the Alaskan Arctic. Cold Reg. Sci. Technol. 19, 95–110. https://doi.org/10.1016/0165-232X

Hurvich, C.M., Tsai, C.-L., 1989. Regression and time series model selection in small samples. Biometrika 76, 297–307. https://doi.org/10.1093/biomet/76.2.297

Jorgenson, M.T., Romanovsky, V., Harden, J., Shur, Y., O'Donnell, J., Schuur, E.A.G., Kanevskiy, M., Marchenko, S., 2010. Resilience and vulnerability of permafrost to climate change. Can. J. For. Res. 40, 1219–1236. https://doi.org/10.1139/X10-060

Kade, A., Walker, D.A., 2008. Experimental Alteration of Vegetation on Nonsorted Circles: Effects on Cryogenic Activity and Implications for Climate Change in The Arctic. Arct. Antarct. Alp. Res. 40, 96–103. https://doi.org/10.1657/1523-0430

Kane, D.L., Gieck, R.E., Kitover, D.C., Hinzman, L.D., Mcnamara, J.P., Yang, D., 2004. Hydrological cycle on the North Slope of Alaska. North. Res. Basins Water Balance, IAHS Publications 13.

Kellner, E., 2001. Surface energy fluxes and control of evapotranspiration from a Swedish Sphagnum mire. Agric. For. Meteorol. 110, 101–123. https://doi.org/10.1016/S0168-1923(01)00283-0

Kustas, W.P., Norman, J.M., 1996. Use of remote sensing for evapotranspiration monitoring over land surfaces. Hydrol. Sci. J. 41, 495–516. https://doi.org/10.1080/02626669609491522

Laîné, A., Nakamura, H., Nishii, K., Miyasaka, T., 2014. A diagnostic study of future evaporation changes projected in CMIP5 climate models. Clim. Dyn. 42, 2745–2761. https://doi.org/10.1007/s00382-014-2087-7

Langer, M., Westermann, S., Muster, S., Piel, K., Boike, J., 2011a. The surface energy balance of a polygonal tundra site in northern Siberia – Part 1: Spring to fall. The Cryosphere 5, 151–171. https://doi.org/10.5194/tc-5-151-2011

Langer, M., Westermann, S., Muster, S., Piel, K., Boike, J., 2011b. The surface energy balance of a polygonal tundra site in northern Siberia – Part 2: Winter. The Cryosphere 5, 509–524. https://doi.org/10.5194/tc-5-509-2011

Loranty, M.M., Abbott, B.W., Blok, D., Douglas, T.A., Epstein, H.E., Forbes, B.C., Jones, B.M., Kholodov, A.L., Kropp, H., Malhotra, A., Mamet, S.D., Myers-Smith, I.H., Natali, S.M., O'Donnell, J.A., Phoenix, G.K., Rocha, A.V., Sonnentag, O., Tape, K.D., Walker, D.A., 2018. Reviews and syntheses: Changing ecosystem influences on soil thermal regimes in northern high-latitude permafrost regions. Biogeosciences 15, 5287–5313. https://doi.org/10.5194/bg-15-5287-2018

Mark, A.F., Chapin, F.S., 1989. Seasonal control over allocation to reproduction in a tussock-forming and a rhizomatous species of *Eriophorum* in central Alaska. Oecologia 78, 27–34. https://doi.org/10.1007/BF00377194

McGuire, A.D., Christensen, T.R., Hayes, D., Heroult, A., Euskirchen, E., Kimball, J.S., Koven, C., Lafleur, P., Miller, P.A., Oechel, W., Peylin, P., Williams, M., Yi, Y., 2012. An assessment of the carbon balance of Arctic tundra: comparisons among observations, process models, and atmospheric inversions. Biogeosciences 9, 3185–3204. https://doi.org/10.5194/bg-9-3185-2012

Meissner, R., Rupp, H., Seyfarth, M., 2014. Advanced Technologies in Lysimetry, in: Mueller, L., Saparov, A., Lischeid, G. (Eds.), Novel Measurement and Assessment Tools for Monitoring and Management of Land and Water Resources in Agricultural Landscapes of Central Asia, Environmental Science and Engineering. Springer International Publishing, Cham, pp. 159–173. https://doi.org/10.1007/978-3-319-01017-5_8

Michelson, D.B., 2004. Systematic correction of precipitation gauge observations using analyzed meteorological variables. J. Hydrol. 290, 161–177. https://doi.org/10.1016/j.jhydrol.2003.10.005

Nolz, R., Kammerer, G., Cepuder, P., 2013. Interpretation of lysimeter weighing data affected by wind. J. Plant Nutr. Soil Sci. 176, 200–208. https://doi.org/10.1002/jpln.201200342

Oberbauer, S., Miller, P.C., 1981. Some Aspects of Plant Water Relations in Alaskan Arctic Tundra Species. Arct. Alp. Res. 13, 205–218. https://doi.org/10.2307/1551196

O'Donnell, J.A., Romanovsky, V.E., Harden, J.W., McGuire, A.D., 2009. The effect of moisture content on the thermal conductivity of moss and organic soil horizons from black spruce ecosystems in interior Alaska. Soil Sci. 17412 646-651 174, 646–651.

Oren, R., Hsieh, C.-I., Stoy, P., Albertson, J., Mccarthy, H.R., Harrell, P., Katul, G.G., 2006. Estimating the uncertainty in annual net ecosystem carbon exchange: spatial variation in turbulent fluxes and sampling errors in eddy-covariance measurements. Glob. Change Biol. 12, 883–896. https://doi.org/10.1111/j.1365-2486.2006.01131.x

Pearson, R.G., Phillips, S.J., Loranty, M.M., Beck, P.S.A., Damoulas, T., Knight, S.J., Goetz, S.J., 2013. Shifts in Arctic vegetation and associated feedbacks under climate change. Nat. Clim. Change 3, 673. https://doi.org/10.1038/nclimate1858

Peters, A., Groh, J., Schrader, F., Durner, W., Vereecken, H., Pütz, T., 2017. Towards an unbiased filter routine to determine precipitation and evapotranspiration from high precision lysimeter measurements. J. Hydrol. 549, 731–740. https://doi.org/10.1016/j.jhydrol.2017.04.015

Peters, A., Nehls, T., Schonsky, H., Wessolek, G., 2014. Separating precipitation and evapotranspiration from noise – a new filter routine for high-resolution lysimeter data. Hydrol Earth Syst Sci 18, 1189–1198. https://doi.org/10.5194/hess-18-1189-2014

Peters, A., Nehls, T., Wessolek, G., 2016. Technical note: Improving the AWAT filter with interpolation schemes for advanced processing of high resolution data. Hydrol Earth Syst Sci 20, 2309–2315. https://doi.org/10.5194/hess-20-2309-2016

Proctor, M., 1982. Physiological ecology: water relations, light and temperature responses, carbon balance, in: Bryophyte Ecology. Chapman and Hall, New York, pp. 333–381.

Rawlins, M.A., Steele, M., Holland, M.M., Adam, J.C., Cherry, J.E., Francis, J.A., Groisman, P.Y., Hinzman, L.D., Huntington, T.G., Kane, D.L., Kimball, J.S., Kwok, R., Lammers, R.B., Lee, C.M., Lettenmaier, D.P., McDonald, K.C., Podest, E., Pundsack, J.W., Rudels, B., Serreze, M.C., Shiklomanov, A., Skagseth, Ø., Troy, T.J., Vörösmarty, C.J., Wensnahan, M., Wood, E.F., Woodgate, R., Yang, D., Zhang, K., Zhang, T., 2010. Analysis of the Arctic System for Freshwater Cycle Intensification: Observations and Expectations. J. Clim. 23, 5715–5737. https://doi.org/10.1175/2010JCLI3421.1

Schuur, E. a. G., McGuire, A.D., Schädel, C., Grosse, G., Harden, J.W., Hayes, D.J., Hugelius, G., Koven, C.D., Kuhry, P., Lawrence, D.M., Natali, S.M., Olefeldt, D., Romanovsky, V.E., Schaefer, K., Turetsky, M.R., Treat, C.C., Vonk, J.E., 2015. Climate change and the permafrost carbon feedback. Nature 520, 171–179. https://doi.org/10.1038/nature14338

Stoy, P.C., Street, L.E., Johnson, A.V., Prieto-Blanco, A., Ewing, S.A., 2012. Temperature, Heat Flux, and Reflectance of Common Subarctic Mosses and Lichens under Field Conditions: Might Changes to Community Composition Impact Climate-Relevant Surface Fluxes? Arct. Antarct. Alp. Res. 44, 500–508. https://doi.org/10.1657/1938-4246-44.4.500

Stuart, L., Oberbauer, S., Miller, P.C., 1982. Evapotranspiration measurements in Eriophorum vaginatum tussock tundra in Alaska. Ecography 5, 145–149. https://doi.org/10.1111/j.1600-0587.1982.tb01029.x

Sturm, M., Schimel, J., Michaelson, G., Welker, J.M., Oberbauer, S.F., Liston, G.E., Fahnestock, J., Romanovsky, V.E., 2005. Winter Biological Processes Could Help Convert Arctic Tundra to Shrubland. BioScience 55, 17–26. https://doi.org/10.1641/0006-3568(2005)055[0017:WBPCHC]2.0.CO;2

von Unold, G., Fank, J., 2008. Modular Design of Field Lysimeters for Specific Application Needs. Water Air Soil Pollut. Focus 8, 233–242. https://doi.org/10.1007/s11267-007-9172-4

Walker, D.A., Binnian, E., Evans, B.M., Lederer, N.D., Nordstrand, E., Webber, P.J., 1989. Terrain, vegetation and landscape evolution of the R4D research site, Brooks Range Foothills, Alaska. Ecography 12, 238–261. https://doi.org/10.1111/j.1600-0587.1989.tb00844.x

Walker, D.A., Epstein, H.E., Jia, G.J., Balser, A., Copass, C., Edwards, E.J., Gould, W.A., Hollingsworth, J., Knudson, J., Maier, H.A., Moody, A., Raynolds, M.K., 2003. Phytomass, LAI, and NDVI in northern Alaska: Relationships to summer warmth, soil pH, plant functional types, and extrapolation to the circumpolar Arctic. J. Geophys. Res. Atmospheres 108, 8169. https://doi.org/10.1029/2001JD000986

Walker, D.A., Raynolds, M.K., Daniëls, F.J.A., Einarsson, E., Elvebakk, A., Gould, W.A., Katenin, A.E., Kholod, S.S., Markon, C.J., Melnikov, E.S., Moskalenko, N.G., Talbot, S.S., Yurtsev, B.A.(†), Team, T. other members of the C., 2005. The Circumpolar Arctic vegetation map. J. Veg. Sci. 16, 267–282. https://doi.org/10.1111/j.1654-1103.2005.tb02365.x

Wheeler, R.M., 1992. Gas-exchange measurements using a large, closed plant growth chamber. HortScience 27, 777–780.

Yang, D., Goodison, B.E., Ishida, S., Benson, C.S., 1998. Adjustment of daily precipitation data at 10 climate stations in Alaska: Application of World Meteorological Organization intercomparison results. Water Resour. Res. 34, 241–256. https://doi.org/10.1029/97WR02681

Zhang, K., Kimball, J.S., Mu, Q., Jones, L.A., Goetz, S.J., Running, S.W., 2009. Satellite based analysis of northern ET trends and associated changes in the regional water balance from 1983 to 2005. J. Hydrol. 379, 92–110. https://doi.org/10.1016/j.jhydrol.2009.09.047

General Conclusion

In this dissertation, I investigated and described the role of vegetation in the arctic water cycle. In Chapter 1, spring water uptake and summer water storage in woody shrub stems was quantified and compared to other water storage pools. Unlike previous work in the boreal forest that found large uptake of spring snowmelt water and subsequent storage for summer transpiration by deciduous trees (Young-Robertson et al., 2016), arctic shrubs take up relatively little water during snowmelt and do not have a large storage capacity due to their relatively small biomass. Because of their limited storage capacity, arctic shrubs must rely on daily uptake of soil water throughout the growing season.

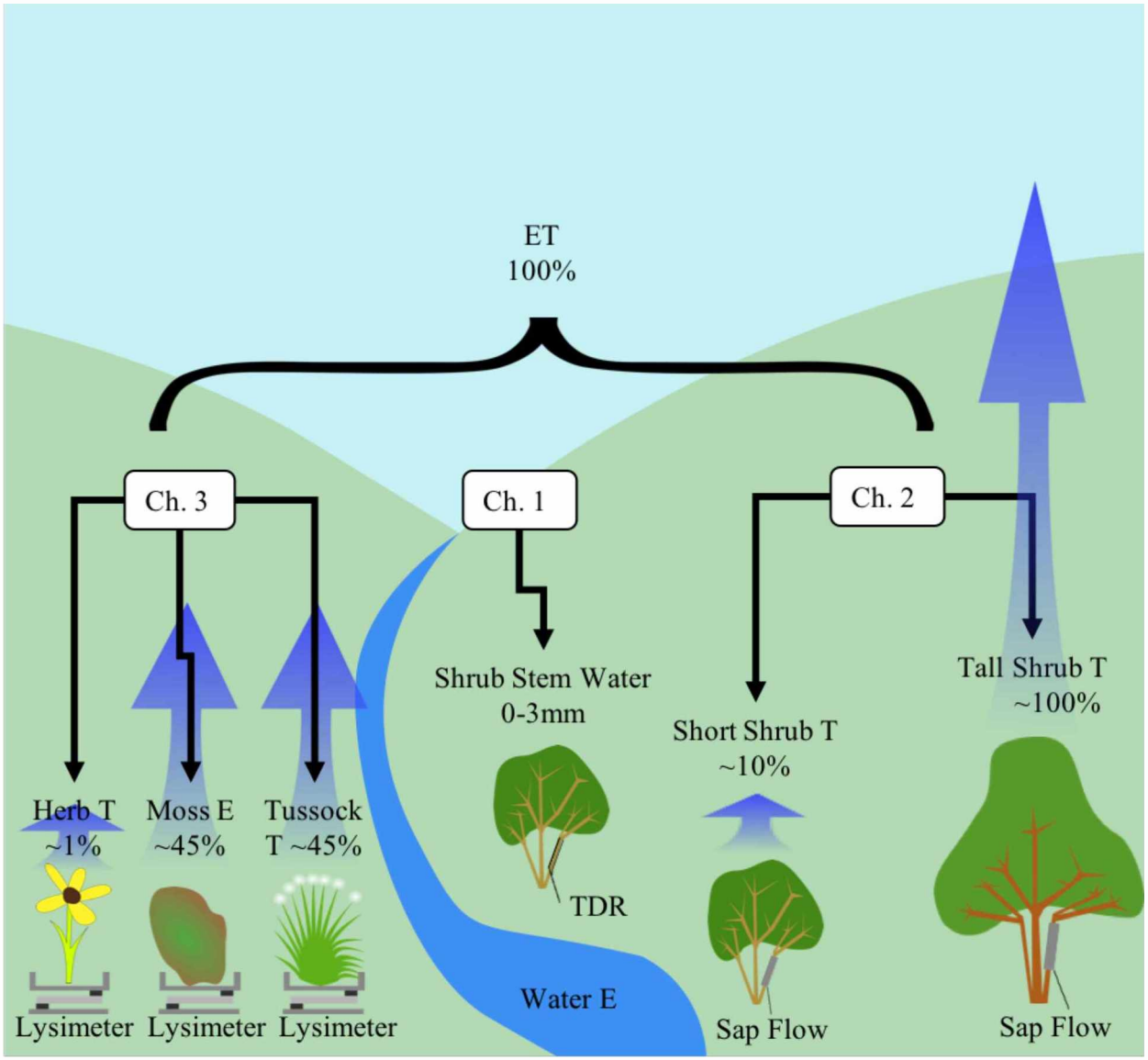

Figure 4.1. Conceptual diagram depicting findings of this dissertation and measurement methods.

In Chapter 2, transpiration flux from three dominant woody shrub species was quantified, a statistical model of transpiration was developed, and woody shrub transpiration was compared to summer ET flux. The riparian shrub site had an order of magnitude greater transpiration than the shrub tundra site. The statistical model revealed that net radiation, vapor pressure deficit, and leaf area index were the greatest predictors of shrub transpiration, while soil moisture was not a significant predictor. The lack of power in predicting transpiration using soil moisture indicates that soil moisture is adequate for woody shrub transpiration throughout the growing season. In contrast to more arid ecosystems, the lack of water limitation is largely due to the perched water

table and wet soils in the shallow thawed active layer, the relatively short growing season, and low evaporative demand.

The two dominant low shrub species at the shrub tundra site contributed only a small fraction to total ET flux, while at the riparian site the dominant tall shrub species likely contributed a majority to total ET flux. Although the two sites are characteristically different, the large discrepancies in site-specific shrub biomass and leaf area largely account for the order-of-magnitude differences in transpiration flux. Continued climate change is predicted to increase shrub biomass (Bjorkman et al., 2019) and shrub transpiration, also affecting other components of ET (Nauta et al., 2015; Pearson et al., 2013), and this thesis supports those predictions with actual measurements. The two sites and contrasting water fluxes can be thought of as members on a spectrum of current and future arctic shrub biomass: the tundra shrub site represents the low end of shrub biomass in low shrub and tussock tundra, whereas the riparian shrub site represents a future level of biomass (and transpiration) for the same low shrub and tussock tundra vegetation sites.

While Chapter 2 focused on a single ET component, Chapter 3 expanded that focus to include a full complement of species and growth forms over a spatially diverse small watershed. The use of weighing lysimeters allowed individual components of ET to be assessed and compared in combination (mixed species tundra) and in isolation (sedge tussocks & mosses). The high ET rates and extrapolated seasonal ET totals of both the sedge tussocks and mosses highlight the importance of these two vegetation types composing the majority of the watershed ET flux, and of vegetation community composition in controlling ET fluxes.

This dissertation describes the roles of major vegetation components in the arctic water cycle of the Alaskan arctic tundra. Prior to this work, little was known about how the efflux of water from the terrestrial system to the atmosphere was partitioned among dominant tundra species. To further our understanding of this process, I have partitioned water efflux by quantifying the amount of water that passes through specific vegetation types. This work shows that vegetation—specifically woody shrubs, sedge tussocks, and mosses—will play an important role in the water cycle as climate-induced changes continue to manifest in the Arctic.

References

Bjorkman, A.D., García Criado, M., Myers-Smith, I.H., Ravolainen, V., Jónsdóttir, I.S., Westergaard, K.B., Lawler, J.P., Aronsson, M., Bennett, B., Gardfjell, H., Heiðmarsson, S., Stewart, L., Normand, S., 2019. Status and trends in Arctic vegetation: Evidence from experimental warming and long-term monitoring. Ambio. https://doi.org/10.1007/s13280-019-01161-6

Nauta, A.L., Heijmans, M.M.P.D., Blok, D., Limpens, J., Elberling, B., Gallagher, A., Li, B., Petrov, R.E., Maximov, T.C., Huissteden, J. van, Berendse, F., 2015. Permafrost collapse after shrub removal shifts tundra ecosystem to a methane source. Nat. Clim. Change 5, 67. https://doi.org/10.1038/nclimate2446

Pearson, R.G., Phillips, S.J., Loranty, M.M., Beck, P.S.A., Damoulas, T., Knight, S.J., Goetz, S.J., 2013. Shifts in Arctic vegetation and associated feedbacks under climate change. Nat. Clim. Change 3, 673. https://doi.org/10.1038/nclimate1858

Young-Robertson, J.M., Bolton, W.R., Bhatt, U.S., Cristóbal, J., Thoman, R., 2016. Deciduous trees are a large and overlooked sink for snowmelt water in the boreal forest. Sci. Rep. 6. https://doi.org/10.1038/srep29504